INVESTIGATING THE NEUROBIOLOGICAL CHANGES ASSOCIATED WITH CEREBELLAR TRANSCRANIAL DIRECT CURRENT STIMULATION (tDCS) USING MAGNETIC RESONANCE IMAGING (MRI)

Roya Jalali

A thesis submitted to the University of Birmingham for the degree of
DOCTOR OF PHILOSOPHY

Physical Sciences of Imaging in the Biomedical Sciences
College of Engineering and Physical Sciences
University of Birmingham

July 2017

ABSTRACT

Anodal cerebellar transcranial direct current stimulation (tDCS) is known to enhance motor learning and it is suggested to hold promise as a therapeutic intervention. However, the neural mechanisms underpinning the effects of cerebellar tDCS are unknown. In addition, it is unclear whether this effect is robust across varying task parameters as if cerebellar tDCS is to be used clinically it must have a consistent effect across a relatively wide range of behaviours. Therefore, I performed four studies to address these questions. In the first three studies, I investigated the neural changes associated with cerebellar tDCS using magnetic resonance spectroscopy (MRS) and resting state functional magnetic resonance imaging (fMRI). My goal was to understand how cerebellar tDCS affected the metabolites within the cerebellum and functional connectivity between the cerebellum and distant brain areas. In addition, I wanted to understand if individual differences in how cerebellar tDCS influenced visuomotor adaptation could be explained by the effect tDCS had on neurobiology. Therefore, healthy participants underwent 3 sessions in which they received concurrent anodal cerebellar tDCS during visuomotor adaptation, MRS and resting state fMRI. I found that in 21% of participants cerebellar tDCS caused enhanced visuomotor adaptation, a decrease in GABA and increase in functional connectivity between the cerebellum and parietal cortex. This work suggests an 'all-or-nothing' type effect of cerebellar tDCS. In my final study, I examined the consistency of the cerebellar tDCS effect on visuomotor adaptation across a wide range of task parameters which were systematically varied. Each experiment examined whether cerebellar tDCS had a positive effect on adaptation when a unique feature of the task was altered. I found cerebellar tDCS to have an inconsistent effect on visuomotor adaptation. I conclude that such inconsistencies could be dependent on the amount of participants in each group that are receptive to cerebellar tDCS and suggest that at the very least it warrants substantially large sample size in cerebellar tDCS studies.

This thesis is dedicated to my parents

Mr. M. Jalali and Mrs. P. Safa

ACKNOWLEDGEMENTS

I would like to express my sincere gratitude to both of my supervisors Professor Chris Miall and Dr. Joseph Galea for their helps during my PhD. They have been very supportive and kind and I would like to heartfelt thank them for their dedicated guidance, inspiration and enthusiasm. They made my PhD study an enjoyable experience.

I am fortunate to have had the opportunity to collaborate with academics from a wide range of departments. I thank Dr. Alimul Chawdhury for his patient help in teaching me operating MR imaging and spectroscopy. I acknowledge Dr. Stephen Mayhew for his great assistance in fMRI analysis and his patience for answering all of my questions. I thank Dr. Martin Wilson for his help and support in MRS analysis.

This work would not have been possible without the help of the technical staff in the PRISM lab. I am much obliged to Jonathan Winter for all his support in the lab.

I would like to thank my mentor Dr Hamid Dehghani and my friends in the PRISM lab during my PhD. Angel, Antonis, Nick, and Orna: it has been a great pleasure to know you and thanks for your company. I would also like to thank Trevor Smith, Remi Gau and Nina Vyas, and everyone in the PSIBS centre.

I wish to acknowledge the financial support of my father, Mr. M. Jalali during these years. I acknowledge fFWG for the main grant for my last year. I thank Professor Michael Hannon for admitting me to the PSIBS program and enabling me to begin my PhD journey.

Finally, I heartfelt thanks my beloved family members, Edris, and my friends for their assistance, support, and all of their encouragement. I am profoundly grateful to my parents in particular for their infinite loving encouragement and support.

CONTENTS

LIST OF TABLES

LIST OF FIGURES

LIST OF APPENDICES

1 INTRODUCTION

1.1 Overview

The purpose of the present thesis is to investigate the effect of transcranial direct current stimulation (tDCS) on the cerebellum and cerebellar function in the healthy human brain. This investigation has been carried out by behavioural assessment, magnetic resonance spectroscopy (MRS), and functional magnetic resonance imaging (fMRI). This work has been performed to deliver novel information regarding not only the neurobiological basis of cerebellar tDCS, but also novel insights into cerebellar function and connectivity between the cerebellum and distant brain regions.

I start this chapter with an overview of motor control and the role of the cerebellum in motor control. This is followed by a brief summary on where tDCS stands in research. Then, I describe the physiology of the cerebellum and cerebellar learning including the methods that have been utilised in this thesis. In chapter 2, I explain the MRS pulse

sequence that has been tailored for this piece of research and corresponding data analysis.

In chapter 3, I explain how I have assessed individual's learning via a common visuomotor task. Then with MRS, the changes in gamma-aminobutyric acid (GABA) and other metabolites have been quantified within the right cerebellar cortex directly underneath the anodal electrode. I have also examined whether they have been able to predict individual differences in the effect cerebellar tDCS has on visuomotor adaptation.

In chapter 4, I use the behavioural data from chapter 3 and performed resting state fMRI to examine how cerebellar tDCS alters connectivity between the cerebellum and other visuomotor-related networks. To understand the functional significance of these neural changes, I examined whether they could predict individual differences in the effect cerebellar tDCS had on visuomotor adaptation.

In chapter 5, I examine the effect of cerebellar tDCS on visuomotor adaptation across a wide range of task parameters, which were systematically varied. In my final chapter, I discuss the results achieved in my thesis in relation to the current literature and their importance for future studies.

1.2 Motor control

Motor control is the study of how we make precise goal-oriented movement (Shadmehr et al., 2010, Sherrington, 1924). In order to move and interact with an ever-changing and unpredictable environment, it is essential for our motor system to be able to adapt in a fast and efficient manner. However, there are inherent delays in our motor and sensory systems that make such adaptability impossible if it were based on purely sensory-feedback processes. Instead, it has been suggested that our brain forms an adaptive internal model of the body and environment which can be used to overcome these

inherent delays by making predictive changes in our movements (Kawato et al., 1987). These internal models are proposed to consist of both forward and inverse models:

1.2.1 Forward model

Forward models predict the sensory consequences of a motor command (Jordan and Rumelhart, 1992) and is proposed to be located in the cerebellum and used to overcome the delay associated with sensory feedback control (Miall and Wolpert, 1996, Wolpert et al., 1998). A forward model, as inputs, takes the current state of the body using proprioception (from sensory endings in joints, muscles and the skin) plus an efference copy of a motor command (signal from the brain to the muscle) and as an output, produces a prediction of the new state estimate of the body (Jordan & Rumelhart, 1992; Miall and Wolpert, 1996). After the body changes, a reafference (sensory consequences of self-movement) informs the brain of the sensory outcome of the motor commands. The inverse model transforms the error between the desired and actual output into the motor command in order to update and create a new motor command (Miall and Wolpert, 1996).

Therefore, feedforward motor control transforms a set of motor commands into a prediction of their outcome in terms of the sensory reafference of the movement will generate. As such, it can rapidly predict whether a motor programme will achieve its goals before it is carried out, and adjust if it is unlikely to do so (Miall et al., 1993, Wolpert et al., 1998).

1.2.2 Motor adaptation

Feedforward movement control can be investigated through motor adaptation tasks. Motor adaptation is a specific form of motor learning (also called error-based learning)

which refers to error reduction occurring in response to a novel perturbation (Krakauer, 2009, Shadmehr and Mussaivaldi, 1994). When we make a movement with a specific goal, i.e. reaching to a visual target, the brain compares the actual and predicted sensory outcome of the executed movement. A sensory prediction error can be induced by a systematic perturbation such as a visual displacement or force applied to the arm. This prediction error informs the brain of a movement error (Miall and Wolpert, 1996, Wolpert et al., 1998). To return to accurate performance, the brain gradually updates its prediction, and resulting motor commands, so that it accounts for the new dynamics of the environment (Yamamoto et al., 2006, Tseng et al., 2007).

The two very well-studied paradigms of motor adaptation are visuomotor adaptation and force field adaptation. In visuomotor adaptation, the visual consequences of a motor command are distorted, while proprioceptive consequences remain intact. This can be achieved by wearing prism goggles or having participants move a cursor on the screen where cursor and hand movement are incongruent (Krakauer, 2009, Krakauer et al., 1999). In force-field adaptation, neither proprioception nor vision consequences are perturbed, but the forces needed to overcome an external perturbation must be adapted (Shadmehr and Mussaivaldi, 1994).

One of the common visuomotor adaptation tasks, which highlights the crucial role of sensory prediction errors, was introduced decades ago and used by, for example, Mazzoni and Krauker in 2006 (Mazzoni and Krakauer, 2006). In their task, participants controlled a cursor on the screen by moving their finger on the table without direct vision of their arm. Participants were instructed to make a fast ‘shooting’ movement through the target such that online corrections were effectively prevented. Participants were reminded that spatial accuracy was the main goal of the task. The task started with a familiarisation period called baseline (Figure 1.1A), when cursor and hand are congruent, and then the experimenter applied a $\Theta = 45°$ counter clockwise (CCW) rotation onto the cursor. Therefore the cursor and hand were not congruent anymore and the subject experienced a large error between what they predicted and what they observed (sensory feedback) (Figure 1.1B). Then they had to generate a motor command that brought the cursor to the target again. Depending on the subjects’

learning, after about 80 trials, this error reduced until they could again hit the target accurately.

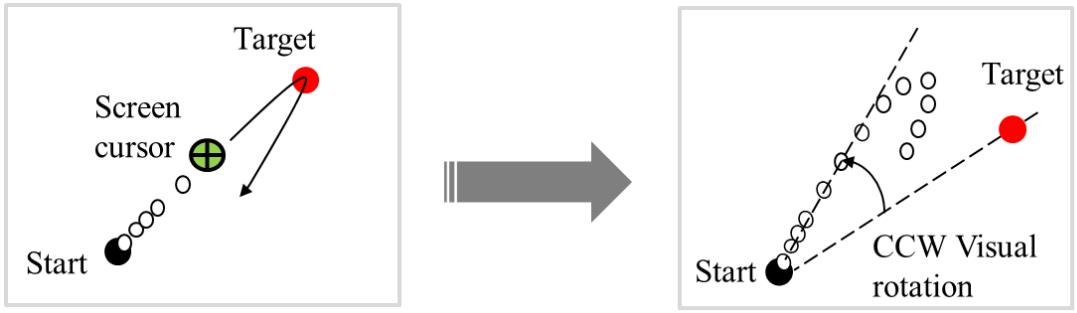

Figure 1.1 A sample data from a visuomotor adaptation task. A target is shown in red and subject hits the target with a cursor on the screen. (A) Baseline: subject hit the target accurately. (B) Adapt: subject is introduced to a counter-clock wise visual rotation and made big errors initially. In order to hit the target accurately, they have to adapt or compensate for the visual rotation.

1.2.3 Timescale of motor adaptation

Explicit vs. implicit adaptation (fast vs. slow learning)

The state of the body can be simultaneously sensed through both intrinsic coordination via proprioception and extrinsic coordination via vision (Rossetti et al., 1995). The initial idea that learning and memory have different time scales dates back to 1996, when Rubin and Wenzel modelled a double exponential function to their data (Rubin

and Wenzel, 1996) and it was also shown later for an adaptation motor task (Scheidt et al., 2000, Smith et al., 2006).

It was shown by Smith et al. in 2006 that during force field adaptation task, at least two distinguished processes are involved: one process responds to the error strongly and fast but retains less and the other responds slowly but retains more (Smith et al., 2006). Later on, Taylor supported these findings with a visuomotor task and demonstrated that there are two distinct processes, which simultaneously occur during a sensorimotor learning task: explicit and implicit learning (Taylor et al., 2014). They tested the proportion of these two processes during both force field and visuomotor adaptation tasks. They explicitly asked participants about their aiming strategy during a visuomotor task and subtracted this from their actual performance in order to measure implicit learning. The timecourse of explicit and implicit learning was similar to the fast and slow processes suggested by Smith et al., (2006). Therefore, they suggested explicit and implicit learning approximately corresponds to the fast and slow process of learning and provided evidence that these two processes are temporally distinctive. Later on in 2015, McDougle and colleagues also confirmed this result by using a motor task and modelling. They argued that explicit learning was driven by target error (difference between the target and feedback location) and reflected the fast process of learning, while implicit learning of a forward model was driven by prediction error (difference between aiming and feedback location) and reflected the slow process of learning (McDougle et al., 2015).

Hwang et al. in 2006 also studied the contribution of two distinct implicit and explicit components of learning in dynamic adaptation by manipulating the relative value of proprioceptive and visual information in a force-field task (Hwang et al., 2006). They found that both proprioception and vision form, in a different way, an internal model to update motor commands that can compensate for the perturbation; however, those who had only proprioceptive cues got more benefit than those with only visual cues. With visual cues, participants could verbally report the patterns of perturbation and thus showed awareness; proprioceptive cues, however, did not lead to awareness. Therefore, their results suggested that the implicit process is mainly developed via proprioception

and that it strongly influences performance but not awareness; while the explicit process mainly influences the probability of awareness, yet has a smaller effect on performance.

1.3 The cerebellum

1.3.1 Role of the cerebellum in motor control

The cerebellum is a key component of motor control through its interactions with the cerebral cortex and brainstem and can be damaged through different neurological diseases, stroke, or tumours. Consensus holds that the cerebellum is critical in behaviours requiring real time prediction (for review see (Manto et al., 2012)) and acts as a forward model during motor control (Miall and Wolpert, 1996).

The cerebellum predicts the future state of the limbs by using a copy of the motor command (delay of 50 ms for neural processing). Such feedforward control enables the secondary (mid-movement) motor commands to be sent in a time frame not possible with feedback control (takes 200-300 ms), ensuring a smooth and accurate reaching movement (Shadmehr and Krakauer, 2008).

Damage to the cerebellum can result in disruption of feedforward control. Cerebellar patients (e.g ataxia patients) have difficulty in coordination and overcome their problems by moving slowly so that their sensory feedback has enough time to catch up with their actual body state (Gazzaniga et al., 2014). It has been shown that patients who exhibit deficits during fast and complicated movements can overcome their deficiencies by breaking their movements into simple and slow steps (Holmes, 1939, Diedrichsen, 2014).

Patients with cerebellar lesions also show a pronounced impairment in their ability to adapt to novel perturbations (Yamamoto et al., 2006, Criscimagna-Hemminger et al.,

2010, Diedrichsen et al., 2005, Martin et al., 1996, Maschke et al., 2004, Rabe et al., 2009, Smith and Shadmehr, 2005, Weiner et al., 1983, Donchin et al., 2012). For example, Martin et al. in 1996 compared the performance of two groups of healthy and cerebellar patients in throwing a ball at a visual target while wearing prism glasses. Healthy subjects initially threw the balls towards the prism-bent gaze; however, by repeating the task they learnt to overcome this displacement and adapted to hit the target again. In contrast, cerebellar patients were unable to adapt to this prismatic displacement (Martin et al., 1996).

Patient studies has been shown that different cerebellar areas may be involved in different tasks, for example, patients with lesions in interior cerebellum showed deficiency in force-field and posterior lesion showed deficiency in visuomotor task. This suggest that

The contribution of the cerebellum to abrupt and gradual perturbation paradigms is an area of continued interest within the motor adaptation literature. For example, Criscimagna-Hemminger et al., (2013) showed ataxia patients were unable to adapt to abrupt perturbations but preserved the capacity to adapt to gradual perturbations. Similarly, Schlerf et al., (2012) using transcranial magnetic stimulation (TMS) reported modulation of cerebellar excitability for abrupt, but not gradual, visuomotor adaptation (Schlerf et al., 2012). However, Gibo et al., in 2013 showed that cerebellar ataxia might use non-cerebellar strategic learning to successfully adapt (Gibo et al., 2013). In line with this argument, other recent work suggests that large abrupt visual rotations reduce cerebellar-dependent sensory-prediction error learning and enhance strategic learning, whilst smaller visual rotations bias learning towards sensory-prediction error learning (McDougle et al., 2015, Bond and Taylor, 2015, Taylor et al., 2014). These contradictory results suggest further investigation is required, and one alternative approach is using brain simulation to perturb cerebellar function, which is the subject of this thesis.

1.3.2 Physiology of the cerebellum

The cerebellar cortex has regular cytoarchitecture in all regions, consisting of one output cell type, the inhibitory Purkinje cells and at least six types of interneurons- Molecular layer (basket cell and stellate cell), Golgi cells, Granule cells, Lugaro cells, and unipolar brush cells. The cerebellar cortex receives sensory feedback inputs from mossy fibres and climbing fibres. Mossy fibres are excitatory and transfer information from the neocortex, the brain stem, or from the spinal cord to Purkinje cells. These axons synapse on granule cells or cerebellar nuclear cells (Azevedo et al., 2009). Climbing fibres are also excitatory, which transfer the sensory motor signal directly from the limb to the Purkinje cells through the olivo-cortico-nuclear pathway (Figure 1.2).

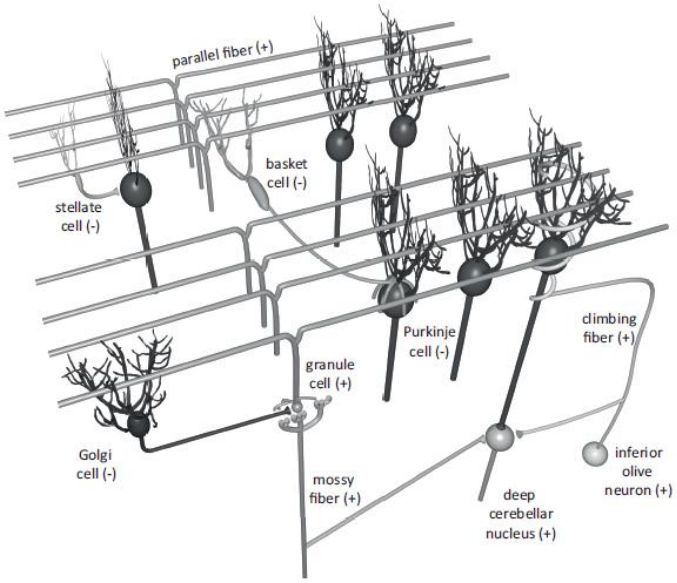

Figure 1.2 Microstructure layout of cerebellar cortex. The sign (+) shows excitatory and (-) inhibitory connections (figure adapted from Gazzaniga et al., 2014).

Purkinje cells receive excitatory input via granule cells and project inhibition to the cerebral cells via the deep cerebellar nuclei. The dentate nucleus, the largest cerebellar nucleus, receives input from lateral hemisphere of the cerebellar cortex and sends the

output to contra-lateral premotor, prefrontal and parietal regions through the thalamus (Gazzaniga et al., 2014). The excitatory cells are mainly driven by Glutamate (Glu) and inhibitory cells are driven by gamma-amino butyric acid (GABA).

During motor learning, it is proposed that the mossy fibre-parallel fibre system transmit the current state of the body plus an efference copy of the motor command to Purkinje cells and cause simple spikes (SS). The error signals, which induce learning, are carried by climbing fibres to Purkinje cells (Marr, 1969, Albus, 1971). It is proposed that climbing fibres response during unexpected sensory events, with this causing a complex spike (CS) in the Purkinje cells (De Zeeuw et al., 1998) due to strong input. This excitatory input from climbing fibres reduces the parallel fibre input to the Purkinje cells and cause long term depression (LTD) - reduction in the efficacy of neuronal synapses and it is proposed to be involved in motor learning.

1.4 Transcranial direct current stimulation (tDCS)

Patient studies can provide us with a good insight regarding cerebellar function (Yamamoto et al., 2006, Criscimagna-Hemminger et al., 2010, Diedrichsen et al., 2005, Martin et al., 1996, Maschke et al., 2004, Rabe et al., 2009, Smith and Shadmehr, 2005, Weiner et al., 1983, Donchin et al., 2012); however, there is a scarcity of patients with isolated cerebellar lesions. In addition, testing patients leaves the possibility that some changes, or a lack of them, are due to long-term compensation by other brain areas (Diedrichsen, 2014). An alternative approach to investigate cerebellar function is to use non-invasive brain stimulation such as transcranial direct current stimulation (tDCS) in healthy participants.

Anodal cerebellar tDCS has been reported to induce different levels of excitability that has been shown to improve cognitive functions such as alertness, mood, reaction to acoustic stimulus and motor activity, while cathode tDCS has the opposite, or no effect (Lippold and Redfearn, 1964, Hall et al., 1970). As for the cerebellum, transcranial magnetic stimulation (TMS) was used to demonstrate the effect of tDCS on cerebellar function. Ugawa in 1995 applied a single pulse TMS over the cerebellum, and it inhibited the motor evoked response from the next TMS delivered on the contralateral motor cortex (motor evoked response is peripheral muscle response to the electrical stimulation of the motor cortex). This inhibition is called cerebellar brain inhibition (CBI) and showed the cerebellum exerted an inhibitory tone over the M1.

Later, in 2009, Galea and colleagues applied TMS on M1 before and after 25 minutes of cerebellar tDCS. They showed that cathodal tDCS decreased CBI (increasing MEP), while anodal had the opposite effect, relative to sham tDCS. Their findings also confirmed the inhibitory output of the cerebellum over M1. Two years later, they applied tDCS over the cerebellum during a visuomotor adaptation task and found that anodal cerebellar tDCS led to faster adaptation, relative to either primary motor cortex (M1) anodal tDCS or sham tDCS (Galea et al., 2011). This cerebellar tDCS effect on adaptation has been replicated in visuomotor adaptation (Block and Celnik, 2013, Cantarero et al., 2015, Hardwick and Celnik, 2014), force-field adaptation (Herzfeld et al., 2014), locomotor adaptation (Jayaram et al., 2012) and saccade adaptation (Panouilleres et al., 2015). As a result, it has been suggested that cerebellar tDCS is not only a useful tool to understand cerebellar function in humans but also as a possible clinical technique to restore cerebellar function in patients suffering cerebellar-based disorders (Grimaldi et al., 2014). However, in order for cerebellar tDCS to be applied in a clinical context, we must first understand the neurobiological changes associated with cerebellar tDCS. To address this question in more detail, magnetic resonance techniques can be used to measure cerebellar metabolites and its functional connectivity between the cerebellum and other brain areas, which is the focus of this thesis.

1.5 Neurotransmitters and Neuroplasticity; Magnetic resonance spectroscopy (MRS)

Magnetic resonance spectroscopy (MRS) has been used for several decades in many basic physics, chemistry, and bioscience research areas and recently has drawn the attention of neuroscientist. MRS is similar to MRI and works based on nuclear magnetic resonance, but provides us with the molecular components of an object instead of an image. Using in-vivo MRS in the brain, dozens of metabolites can be measured including N-acetyl-aspartate (NAA), creatine (Cr), choline (Cho), lactate, myoinositol (MI), glutamate (Glu) / glutamine (Gln), lipids and gamma-amino butyric acid (GABA).

Although the focus of this thesis is mostly on GABA, due to the cerebellar structure, I also provide a brief overview of other metabolites measured by MRS.

NAA is one of the most concentrated metabolites in human brain. Although the role of NAA is not understood completely, based on MRS studies on different diseases, NAA is known to be a the most reliable marker for recognising the neuronal disease as its concentration changes in neurological disorders (Savic et al., 2000, Watanabe et al., 2010, Edden et al., 2007). NAA can be used as a reference in MRS for measuring other low concentrated metabolites in healthy brain (Stagg et al., 2011). However, there is some evidence that NAA concentration modulates in response to tDCS (Hone-Blanchet et al., 2016), therefore using NAA as a reference in tDCS studies may not be the best option.

Creatine (Cr) plays a significant role in storing, transporting, and regulating the cellular energy. Cr is mostly consumed through our diet and assumed to be constant within different brain areas. In MRS, Cr has been another alternative to be utilised as a reference for measuring lower concentrated metabolites. However, some studies have shown that Cr can be modulated by tDCS (Rae et al., 2013).

Choline (Cho) has a varied and complex role in the human brain. For example, it can be used as a marker for cellular density and membrane turnover. The concentration of Cho is associated with the degree of membrane proliferation and is useful to detect

abnormalities such as cancer (Miller et al., 1996). Cho has a high concentration in the human brain and changes significantly due to some neurodegenerative disease and psychiatric conditions such as Alzheimer's disease (Nitsch et al., 1992) or multiple sclerosis (Bitsch et al., 1999), and also in response to electrical stimulation (Yoon et al., 2016).

Myo-Inositol (Ins) was initially considered as a marker for glial cell proliferation due to its higher concentration in glial cells than neurons (Brand et al., 1993); this, however, is recently in doubt. Ins concentration is thought to be changed in several neurodegenerative disorders and through electrical brain stimulation. (Xu et al., 2005, Bitsch et al., 1999, Castillo et al., 2000, Duarte et al., 2012)

Glutamate (Glu) or glutamic acid, with the highest concentration in neurons is the main excitatory neurotransmitter in CNS and also is an important component in the biosynthesis of some other molecules such as NAA, glutathione and proteins (Hertz, 2004). Glutamatergic pathways are not only involved in different processes and disorders, but also in learning and memory through long term potentiation (LTP) (Shepherd, 1994). Glu in the human brain can be modulated by tDCS depending on the polarity of tDCS (Stagg et al., 2009).

GABA is the primary inhibitory neurotransmitter in the human brain (Roberts, 1956) and GABAergic interneurons play a major role in long-term depression and plasticity in the cerebellum (Hirano, 2013), which is the base of motor learning. GABA measure by MRS is proposed to be from extracellular pool (Stagg and Nitsche, 2011). Glutamate and GABA have a strong bio-chemically link due to their metabolism and inhibition-excitation balance in a healthy brain (Sumner et al., 2010b). GABA has recently been quantified to assess the inter-individual differences in both cognitive and motor control functions. Levels of localised GABA have been related to the quality of performance in a range of motor tasks (Stagg et al., 2011, Kim et al., 2014, Sumner et al., 2010a).

The link between metabolites and performance has been shown in a wide range of tasks. For example, it has been shown that a higher concentration of GABA in the frontal eye fields was associated with a greater ability to suppress the influence of a visual

distracter (Sumner et al., 2010a). Another study in the sensorimotor area showed a higher level of GABA was correlated with better performance in a tactile frequency discrimination task (Puts et al., 2011a). In contrast, in the visual cortex, it has been shown that the baseline level of GABA was inversely correlated with a change in visual-stimulus task-related blood-oxygen-level-dependant (BOLD) (Muthukumaraswamy et al., 2009). In 2011, Stagg and colleagues measured GABA in the primary motor cortex (M1) of healthy individuals and demonstrated that the amount of M1 tDCS-induced change in GABA was positively correlated with the change in reaction times due to learning in a sequence-learning task. These results were only specific to M1 and not the control region (visual cortex) (Stagg et al., 2011). Similarly, Kim et al. in 2014 showed anodal M1 tDCS, significantly decreased the level of GABA and the degree of tDCS-induced reduction in GABA could predict individual differences in learning and memory of a force-field motor task (Kim et al 2014). However, all these studies were carried out on different brain areas and not on the cerebellum. Therefore, in chapter 3, I expanded this measurement for the cerebellum and cerebellar tDCS.

1.6 Functional anatomy and connectivity: Functional magnetic resonance imaging (fMRI)

Anatomically, the cerebellar cortex can be divided into several regions according to its microscopic anatomy and lobule division. In the anterior- posterior direction, the cerebellum is divided into lobules I to X (Jansen, 1972) and each lobule is linked to different regions in the cerebral cortex through both inputs and outputs, making several closed neural circuits. Every individual neural pathway appears to be involved in distinct behavioural functions. For example, damage to the neuronal circuit linking the cerebellum with motor areas causes deficits in movement, while damage to the neuronal

circuit between the cerebellum and prefrontal cortex causes higher order deficiencies (cognitive function) (Middleton and Strick, 2000).

Different imaging methods have been utilised to distilenct these neural pathways. One of the most common techniques is functional MRI (fMRI). fMRI is a non-invasive method of imaging that is based on a haemodynamic response to neural activity through oxygenated blood flow. Oxygen is the fuel for active neurons in the brain, and when different areas in the brain activate together, the BOLD signal synchronously fluctuates and shows a corresponding functional connectivity. These areas are directly or indirectly connected through axons. However, these connections are not a simple one-to-one relationship. The activation of one area can arise from different conditions as shown in figure 1.3: a) direct influence, b) indirect influence via another region, c) shared influence of a common input region. Therefore, the results from functional connectivity have to be interpreted cautiously, because the activity of a region 2 might not be the consequence of direct efferent connection of region 1, yet reflect the effect of 3 via 2, or both 1 and 2 might reflect of activity 3 simultaneously (Poldrack et al., 2011)
.

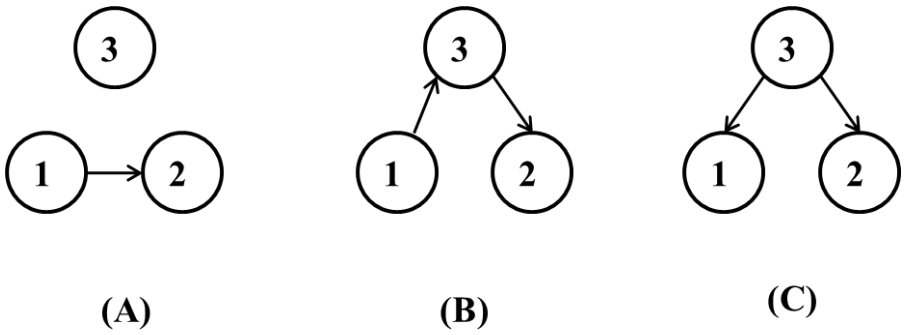

Figure 1.3 Three different ways in which correlated activity between two brain areas 1 and 2. (a) direct influence, (b) indirect influence via another region, (c) shared influence of a common input region. modified from (Poldrack et al., 2011).

The role of cerebellar circuitry in motor control, motor learning, and automation have been studied through different imaging techniques such as fMRI (for review see (Manto et al., 2012)). It is proposed that learning and retention of visual rotation (kinematic) and force-field (dynamic) perturbation both occur in the cerebellum, but they are processed separately and rely on different cerebellar structures (Rabe et al., 2009). The anterior lobe has shown activation in most kinds of movement; however, the amount of cerebellar activation and involvement of dentate nuclei depends on the difficulty of the task. For example, the dentate nucleus activates more when a tactile discrimination task becomes more demanding (Habas, 2010). By increasing the activation of the dentate nucleus, cerebellar activity reduces and it is proposed that plasticity transfers from the cerebellar cortex to the deep nuclei (Jenkins et al., 1994, Floyer-Lea and Matthews, 2005). In the over-learning phase of motor learning, activation of the dentate nucleus diminished, and the cerebellar motor activation is partly replaced by activity within basal ganglia. Although lobule VII was also engaged during the late phase of the motor performance, it is thought that this activation might be associated with executive requirements rather than motor control per se (Manto et al., 2012).

The interaction of the cerebellum with both cortical and sub-cortical brain areas has recently been investigated through resting state-fMRI (Krienen and Buckner, 2009, O'Reilly et al., 2010, Buckner et al., 2011, Bernard et al., 2012). The cerebellar-cerebral motor network is functionally connected in order to optimise performance in many motor and cognitive functions such as kinematic, dynamic, and temporal planning and error-driven online correction (Manto et al., 2012). Based on resting state functional connectivity, two parts of the cerebellum are functionally connected with the sensorimotor parts of the cortex (Figure 1.4; shown in blue). Other regions of the cerebellum are more connected to non-motor cerebral areas, such as frontal lobes (in orange), which are associated with more cognitive functions of the brain (Buckner et al., 2011). It has also been shown that sensory prediction errors happen in the cerebellum regardless of this error resulting from unexpected presence or unexpected absence of sensory information (Schlerf et al., 2012, Diedrichsen et al., 2005, Rabe et al., 2009). Lehericy in 2005 reported that the activation of lobules V and VI is positively correlated

with error in motor sequence learning, suggesting that the anterior cerebellum intervenes in error-driven motor adjustments and learning (Lehericy et al., 2005).

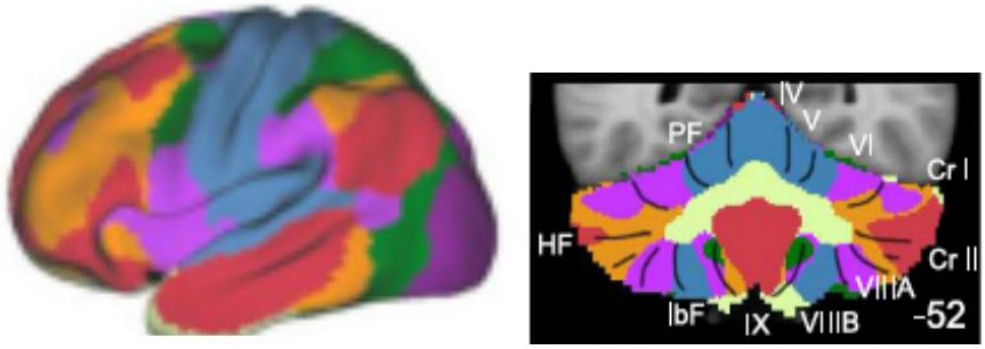

Figure 1.4 The connectivity between the cerebrum (left) and the cerebellum. Colours show the areas that are functionally connected through correlated patterns of oxygen utilization. Almost two parts of the cerebellum (in blue) are functionally connected with the sensorimotor parts of the cortex. Other regions of the cerebellum are more connected to non-motor cerebral areas, such as frontal lobes (in orange), which are associated with more cognitive functions of the brain (adapted from (Buckner et al., 2011)).

The combination of resting state fMRI with transcranial magnetic stimulation (TMS) has also provided an insight into the cerebellum. For example, targeting the lateral cerebellum affects the default mode network, while targeting the midline cerebellum (vermis) affects the dorsal attention network (parietal and dorsal), while neither of them affects the motor network (Halko et al., 2014). This highlights the importance of stimulation resolution in modulating different networks through one node. Although TMS and tDCS induce current in different ways, both can give an insight into cerebellar connectivities and function. Until now, the effect of tDCS on the cerebellum is largely unknown, which is the target of this thesis.

1.7 Conclusion

As discussed in this literature review, the cerebellum plays a major role in motor learning and its function can be enhanced by anodal cerebellar tDCS. Although promising as a therapeutic intervention, the neural mechanisms underneath cerebellar tDCS have to be investigated. Therefore, in this work I addressed this question by measuring the neural changes associated with cerebellar tDCS using MRS and resting state fMRI. My goal was to understand how cerebellar tDCS affected the metabolites within the cerebellum and functional connectivity between the cerebellum and distant brain areas. In addition, I wanted to understand if individual differences in how cerebellar tDCS influenced visuomotor adaptation could be explained by the effect that cerebellar tDCS had on neurobiology. Finally, I examined the consistency of the cerebellar tDCS effect on visuomotor adaptation across a wide range of task parameters.

2 MAGNETIC RESONANCE SPECTROSCOPY (MRS) METHOD

2.1 Introduction

Magnetic resonance spectroscopy (MRS) has been used over several decades in many basic physics, chemistry, and bioscience research areas and recently has drawn the attention of neuroscientists. MRS is similar to MRI and works based on nuclear magnetic resonance, but provides us with the molecular components of an object instead of an image. Using in-vivo MRS in brain, dozens of metabolites can be measured including N-acetyl-aspartate (NAA), creatine (Cr), choline (Cho), lactate, myoinositol (MI), glutamate (Glu) / glutamine (Gln), lipids and gamma-amino butyric acid (GABA). Among these metabolites, detecting GABA is quite challenging due to its small concentration and its overlapped spectrum from molecules with the same resonance frequency and/or higher concentration metabolites such as Cr. In order to measure GABA in this study, despite utilising a well-developed technique (MEGA-PRESS), several scanner parameters had to be optimised for this study. Therefore, I start this

section with a brief summary of the theory of NMR and MRS (a more complete explanation about NMR, MRI, MRS theory can be found in text book (Harris, 1985, Haacke et al., 1999)), and then continue by discussing the brain phantom study that was carried out to detect and optimise scanner parameters prior to the in vivo MRS study.

2.2 Physics of Nuclear Magnetic Resonance (NMR)

NMR works based on the absorption and emission of radio frequency electromagnetic energy. Hydrogen atoms are the most abundant atoms in the human body. Therefore, ^{1}H MRI is the most common technique utilised for different tissues. Quantum mechanics can be used to correctly describe the NMR phenomenon because each hydrogen atom nucleus has a quantum mechanical property called "spin" that is either in a "spin up" or a "spin down" state, associated with the nuclear spin is a quantizes magnetic dipole moment **μ**, which is a fundamental vector quantity. On the other hand, for describing a macroscopic sample of nuclei a classical mechanics NMR model is often useful, particularly to develop experimental ideas; In the absence of an external magnetic field, B_0, the magnetic dipole moments associated with the nuclei in the macroscopic sample are randomly orientated and the magnetic dipole moments cancel each other out. When an external magnetic field B_0 is applied, there is a precession of **μ** about the direction of B_0, with two possible orientations that have discreet energy levels, called "Zeeman splitting" (Haacke et al., 1999). The lower energy level is associated with a component of **μ** parallel to B_0 and the higher energy level occurs when the component of **μ** is anti-parallel to B_0. The difference in energy, ΔE, between the two spin states is given by:

$$\Delta E = h\nu_0$$

Where h is Planck's constant. The resonance frequency ν_0 is expressed by the Larmor equation, given by:

$$\nu_0 = \left(\gamma/_{2\pi}\right)B_0$$

Where, γ is the gyromagnetic ratio and the value of $\gamma/2\pi$ is equal to 42.6 MHz/T for hydrogen nuclei, which means at 3T the Larmor frequency is approximately 128 MHz which is within the radio-frequency range.

According to the Bloch equation (McRobbie et al., 2003), applying an oscillating magnetic field at the Larmor frequency pulse perpendicular to B_0 for a specific amount of time, the net magnetization can be flipped into the transverse (x-y) plane. After ceasing RF pulse, the net magnetization will tend to relax back to the thermal equilibrium state.

Spin-lattice relaxation (also called the longitudinal relaxation) is characterised by the spin-lattice relaxation time constant, T1, and it occurs because the nuclear spins exchange energy with the lattice. The longitudinal component of the net magnetization as a function of time (t) can be described by:

$$M_z(t) = M_o\left(1 - e^{-\left(\frac{t}{T_1}\right)}\right)$$

Where M_0 is the net magnetic moment at thermal equilibrium, which is the summation of the magnetic moment of each nucleus, μ_i given by:

$$M_0 = \sum_i \mu_i$$

Depending on the rate of dissipation of the thermal energy to lattice, T1 can vary in different tissue.

Due to inhomogeneity of magnetic field, different nuclei have different Larmor frequencies so they lose phase coherency with increasing time and the transverse component of the net magnetization decays to zero. This is characterised by the time constant, T2*. T2* shows dephasing from both B_0 inhomogeneity (T2') and spin-spin relaxation T2 and can be described by:

$$\frac{1}{T_2^*} = \frac{1}{T_2} + \frac{1}{T_2'}$$

The effect of B_0 inhomogeneity can be improved by shimming. T2, similar to T1 varies depending on the material and the structure of the tissue. The time between the 90 degree RF excitation and the "spin-echo" signal from the sample after application of a 180 degree refocusing RF pulse is known as echo-time (TE) and the time between two excitation RF pulses is called repetition Time (TR).

According to Faraday's law of electromagnetic induction, change in the magnetic flux, can induce a current in the RF coils surrounding the participant. The NMR signal received by the RF coil includes all the information required to produce the image or spectrum. The NMR signal decays with time by the phenomenon called "Free Induction Decay (FID)". FID happens due to different factors; inhomogeneity in magnetic fields, spin-lattice relaxation, and spin-spin relaxation. These are some of the main parameters that need to be optimised in developing an RF pulse sequence and are fundamental to NMR techniques such as MR spectroscopy and MR imaging. The next section explains the basics and application of MRS and its importance to this project.

2.3 Basics of Magnetic Resonance Spectroscopy (MRS)

Magnetic Resonance Spectroscopy (MRS) is a non-invasive technique using the NMR phenomenon to detect and quantify the biochemical compounds in different living tissues and in our case, brain metabolites. Different nuclei can be studied using MRS such as 13C, 15N, 1H, and 31P, but from among them, 1H is the most common nucleus that is used in MRS because first, 1H is abundant in the human brain and in most metabolite structures. Second, it has a higher gyromagnetic ratio compared to other stable isotopes and therefore making MR experiments is more sensitive to it.

2.3.1 Chemical shifts

Chemical shift and J-coupling are the basis for MRS and are dependant on the molecules' chemical composition (Proctor and Yu, 1950). When atoms are exposed to an external magnetic field (B0), the atomic electrons produce a small magnetic field in opposition of B0. Therefore, nuclear spins depending on their bonds to other spins, which is called J-coupling, feel different effective magnetic field, B_{eff}, and causes NMR signal frequncy shifts. B_{eff} is expressed by:

$$B_{eff} = B_0(1 - \sigma)$$

Where σ is called the shielding constant and is dependant on the position of each nucleus in the molecule. For example nuclei in high electron density region are more shielded from B0 than those which are in the lower electron density region (Figure 2.1).

The Larmor frequency can then be expressed as:

$$\nu_0 = \left(\gamma/_{2\pi}\right)\mathrm{B}_0(1 - \sigma)$$

The chemical shift, δ, is defined by:

$$\delta = \frac{\nu_0 - \nu_{ref}}{\nu_{ref}}$$

By assigning ν_0 relative to a reference frequency ν_{ref}, chemical shift is independent of B_0 and because it is very small for protons; therefore it is conventionally expressed in parts per million. Protons with n equivalent nearest neighbours will split into n+1 peaks. Hydrogen nuclei that are closer to the electronegative atoms such as oxygen and nitrogen, are less shielded by the surrounding electron density, so they experience a greater magnetic field, hence have a higher resonance frequency (Graaf, 2007).

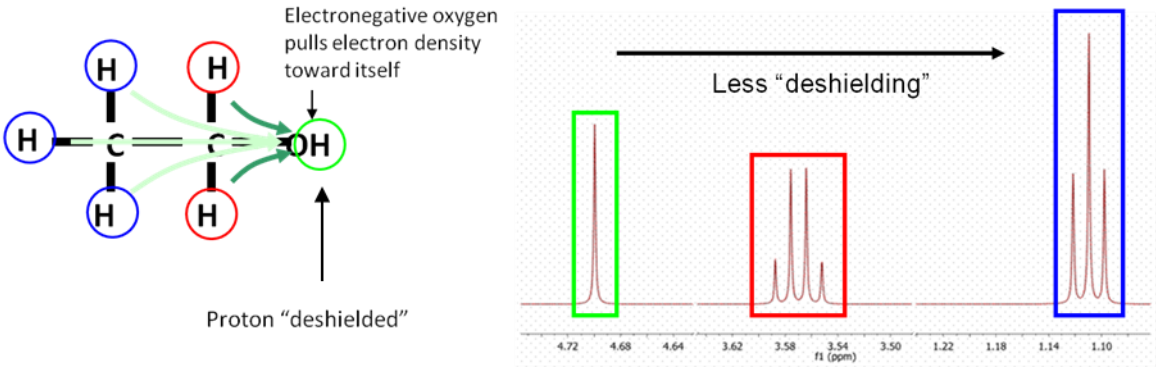

Figure 2.1 Positions and the number of peaks in each compound is unique depending on J-coupling and chemical shifts phenomenon. Electronegative molecules block electron density or magnetic induction effect [figure is adapted from PSIBS courses by Nigel Davies].

Each metabolite has a unique spectrum based on its molecular structure and therefore can be identified. The concentration of each metabolites can be estimated using the MRS spectrum acquisition.

2.3.2 Single-voxel Spectroscopy

The aim of MRS is to quantify metabolite concentrations within the voxel of interest (VOI). The NMR signal is acquired in the time domain and the free induction decay (FID)- the NMR signal generated by non-equilibrium nuclear spin magnetization precessing about the magnetic field- is dependant on the chemicals within the VOI. The time domain FID is Fourier transformed to produce a frequency domain spectrum, in which each peak signal occurs because of the nuclear spin resonance of a particular atom in the molecules; peak amplitude is proportional to the number of atoms in the sample with the same resonance frequency. Molecules containing nucleus of atoms with multiple resonance frequencies have more than one peak. Atomic nuclei in different metabolites with the same resonance frequencies can have peaks that overlap.

Therefore there can be difficulty in distinguishing between spectral peaks associated with different metabolites (Lei et al., 2003, Stagg et al., 2013). This problem can be overcome by increasing magnetic field strength. A stronger magnetic field such as 7T increases sensitivity to detect and distinguish between the spectral signals from different metabolites; but this is not the optimum solution due to limited access to these scanners in addition to several other higher field challenges. Improvement of pulse sequence is another efficient solution which will be explained later in this chapter.

Water concentration (WS) is approximately ~ 50 Molar (M) and water occupies approximately ~ 83% of grey matter (GM) and ~70% of white matter (WM). Although water signals needs to be suppressed in order that smaller concentration metabolites can be detected, water concentration can be used as a reference for quantifying the concentration of other metabolites in healthy brain. Water has a different resonance frequency compared to other metabolites; therefore, by optimising the NMR pulse sequence, it can be suppressed. Differing pulse sequences have been developed to suppress water. VAriable pulse power and Optimized Relaxation delays (VAPOR) -- utilising several RF pulses and different timing interpulses -- is one of the most complex but effective techniques (Tkac et al., 1999b).

One common pulse sequence used for MRS is Point-RESolved Spectroscopy (PRESS), which enables us to detect metabolites such as N-acetyl aspartate (NAA), Creatine (Cr), Choline (Cho), Myo Inositol (Ins) and GLX, which is a combination of glutamate (Glu) and Glutamine (Gln). PRESS sequence is consisting of three slice selective pulses in orthogonal planes (90° pulse followed by two 180° pulses); signals originate from the intersection of the three planes.

Metabolites with overlapped frequencies and lower concentrations such as Gamma aminobutyric acid (GABA) cannot be detected by the conventional PRESS sequence at 3T and spectral editing needs to be performed. A selective editing pulse known as MErcher-GArwood (MEGA) PRESS enables us to detect GABA with 3T magnetic fields.

GABA with the structure ($C_4H_9NO_2$) can be measured by H-MRS due to six nuclear NMR protons in three methylene groups (-CH_2).; two triplet resonances for CH_2 at 3.01 part per million (ppm) and 2.28 ppm and a quintet peak from CH_3 appears at 1.89 ppm. GABA concentration in the human cortex is approximately 1mM (~ 40,000 times less than water molecule) (Puts and Edden, 2012). After suppressing the water signal, GABA still cannot be detected because the GABA spectrum is obstructed with higher concentration metabolites such as NAA at 2 ppm, creatine at 3 ppm and glutamate and glutamine at 2.3 ppm (Figure 2.2). Therefore, GABA measurement is only possible by utilising either a stronger magnetic field (improve signal to noise and seperate the peaks in the spectrum) (Puts and Edden, 2012) or editing the pulse technique.

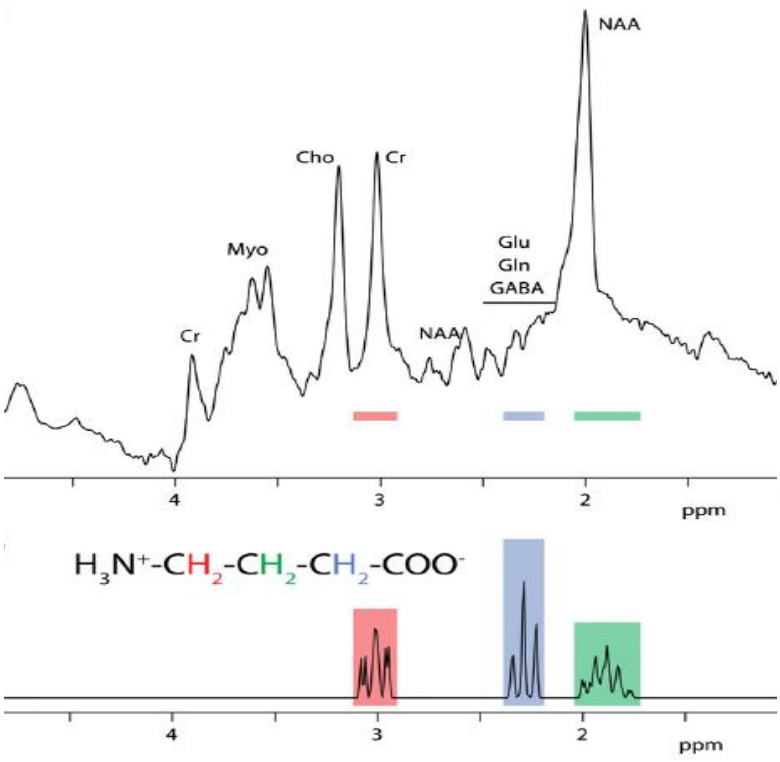

Figure 2.2 GABA can be discerned in three different groups correspond to the three methylene groups; three peaks are separated due to shielding (shown in different colours) and all of the peaks are obstructed with higher concentration metabolites such as NAA at 2 ppm, Creatine at 3 ppm and Glutamate and Glutamine at 2.3 ppm [figure is adapted from PSIBS courses by Nigel Davies].

MEGA-PRESS incorporates frequency selective refocusing pulses into a PRESS pulse sequence. Double banded Gaussian radio frequency pulses can be simultaneously applied for both water suppression and spectral editing. The water suppression band set to 4.68 ppm and editing pulse alternating between 1.9 ppm and 8.4 (or 1.5) ppm. First frequency applies on 1.9 ppm affects J-coupled hydrogen atoms with GABA at 3 ppm (edit On), but as the editing pulse is not sharp enough, it affects lysine - macro molecule at 1.7 ppm too. The second pulse can be applied to 8.4 ppm (edit Off), which is far from all metabolite resonate frequencies, Thus, by subtracting edit On and edit Off, we end up with GABA+MM (Figure 2.3).

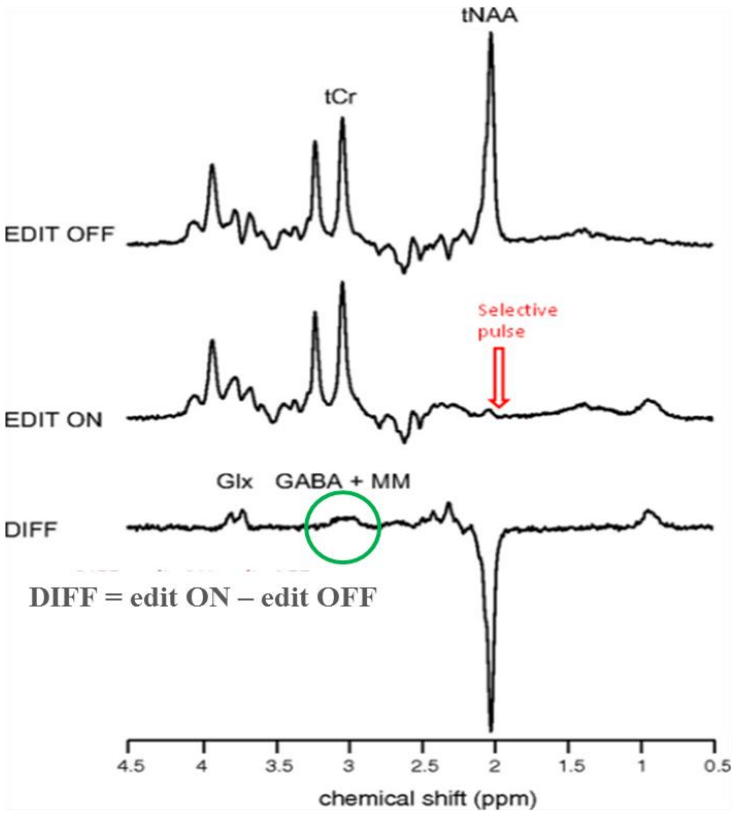

Figure 2.3 Detection of GABA with MEGA-PRESS. Editing pulse alternating between 1.9 ppm and 8.4 ppm. First frequency applies on 1.9 ppm affects J-coupled hydrogen atoms with GABA at 3 ppm, but as the editing pulse is not sharp enough, it affects lysine - macro molecule (MM) at 1.7 ppm too. The second pulse can be applied to 8.4 ppm, which is far from all metabolite resonate frequencies, Thus, by subtracting edit On and edit Off, we end up with GABA+MM.

However, if we apply the second RF pulse on 1.5 ppm (instead of 8.4 ppm) we affect Lysine at 1.7 ppm once more, and GABA without MM can be determined following subtraction (Henry et al., 2001).

Theoretically, hydrogen atoms of water molecules precess in 3T at a frequency of ~127 MHz; therefore we expect to detect a single spectral line at this resonance frequency. However, in practice, due to magnetic field imperfections, participant motion and other factors, the spectral line will broaden, which cause a less distinct spectrum peak. Line broadening occurs for all other metabolites, which makes quantification more difficult and lessens accuracy. Therefore, full width at half maximum (FWHM) is one of the most fundemental assessments of the quality of spectrum acquisition. (FWHM < 10 mm is ususally acceptable)

The area under each peak is proportional to the concentration of a particular chemical compound. The peak area measurements can be calibrated using signals with known metabolite concentrations. With additional acquisition of non-suppressed water signals, for example, water can be used as a reference for calibrating the peak intensity measurements from the spectrum.

Metabolite concentrations should be in the range of milimolar to exceed signal noise level in order to be reliably quantified; The signal to noise ratio (SNR). SNR can be improved by repetition of the experiment (with the penalty of increasing the total scanning time) and determining the average. Signal grows linearly, but noise grows by the square root of the number of samlples. The number of repetitions (dynamic scans) is usually 128 or 256. Therefore, it is important to carefully optimise the MRS method, so that necessary metabolites can be measured without requiring very long acquisition sessions.

2.4 Materials and Methods

2.4.1 Modifying RF pulse for cerebellar stimulation study:

In order to measure GABA for this study, original MEGA-PRESS sequences that had been set on the scanner from a previous unrelated study needed to be modified (table 2.3 for the details). First, the original pulse was optimised to collect signal from a relative large voxel 3x3x3 cm^3. The voxel had to be fitted in the region of interest-posterior cerebellum- far enough from the cerebrospinal fluid (CSF) to avoid artefact or noisy spectra. However, the original voxel was too large for our region of interest. Second, for the tDCS study I ideally wanted to measure GABA without any macromolecule (MM) contamination because the effect of stimulation on different molecules is not completely understood; so removing Lysine as the overlapped MM with GABA could provide additional power to measure any small change in GABA.

The advantages and disadvantages of each pulse sequence are described in table 2-1.

Table 2-1 *Pros and cons of each pulse sequence*

Pulse sequence	**Advantage**	**Disadvantage**
Original	Larger voxel and therefore higher SNR	GABA contaminated by macromolecule Low resolution (where the GABA is coming from) Larger voxel and therefore worse shimming
Modified	GABA without MM contamination Voxel could be fit in our ROI Better shimming	lower SNR

In order to modify the pulse sequence, several phantom studies were performed prior to in-vivo acquisition; by making the voxel smaller, less GABA could be collected and therefore signal to noise ratio (SNR) dropped significantly. MM suppression made this detection even more difficult as peaks were even smaller and the shape of GABA peak was not stable. To compensate for these changes, the effective number of signal averages (NSA) was increased (Effective NSA = dynamic scans x NSA).

2.4.2 Phantom Study

I performed several phantom studies in order to modify the RF pulse sequence for my study. All phantoms were made in 250 ml round bottom flasks.

- Two phantoms included only GABA with 2 mM and 20 mM to detect the GABA signals.
- Several brain phantoms included an equal amount of human brain metabolites (NAA, Cr, Cho, Glu, Gln, Lactate) with different amounts of GABA in each. GABA added to brain phantoms with the following concentrations: 2 mM, 4 mM, 20 mM, 40 mM. Knowing all concentrations, we could quantify measured GABA in the MRS spectra.

All metabolites were dissolved in distilled water and PH were adjusted according to the brain (PH = 7 ± 0.1) using phosphate buffer mono and dibasic; sodium azide was used as an anti –fungal agent. The concentrations of GABA in three phantoms are higher than what would be found in the brain in-vivo to produce larger signals so that scanning time could be reduced for the sequence testing and optimisation (table 2.2).

Table 2-2 Phantom – with brain metabolites concentrations

Abbreviation	Chemical name	Concentration (mM)
GABA	Gamma-aminobutyric acid	2, 4, 20, 40
NAA	N-acetyl-L-aspartic acid	13
Cr	Creatine	10
Cho	Choline Chloride	3
Ins	Myo-Inositol	8
Glu	L-glutamic acid	13
Glutamin	L-Glutamine	6
Lac	C3H5NaO3	5

The study of brain phantoms provided us with the confidence to:

1. Detect GABA and validate it
2. Optimise MEGA-PRESS sequence parameters
3. Check reproducibility of the GABA signal detection,

Phantoms were kept out of the refrigerator in the scanner room for 24 hours prior to scanning, in order to avoid spectrum shifting due to temperature. Scanning commenced 15 min after final positioning of the phantoms to minimise fluid movements and inhomogeneity.

This study began with MEGA-PRESS and then, by adding Henry method (Henry et al., 2001), I could detect pure GABA in 3 ppm. The editing pulse optimised for our scanner was in a form of a Gaussian function and applied for 16.5 ms. The small SNR was roughly compensated for by adding additional dynamic scans.

The details of the final modified/developed pulse sequence are provided in table 2.3.

Table 2-3 The details of both sequences are shown in table below for comparison

	Original (St)	**Developed (Dp)**
Channel coil	8	32
Voxel size (mm^3)	30x30x30	20x20x20
Second pulse sequence	8.5	1.5
NSA/value	8	1
Num of steps	-	8
Editing pulse	MEGA	MEGA
Pulse duration (s)	14	16.5
Water frequency (ppm)	4.68	4.68
pulse freq 1 (ppm)	7.46	1.5
pulse freq 2 (ppm)	1.9	1.9
TR/TE (Savic et al.)	1800/68	2000/68
NSA	8	4
Dynamic study	individual	individual
Dynamic scans	32	128
Start-up acquisition	0	1
dummy scans	0	4
Shifted metabolites displayed	non	H2O
PNS/level	60%	52%
Scan duration	15 min	25 min

Some phantom studies were performed prior to applying in-vivo:

Two phantoms containing GABA were scanned in order to simply detect peaks from GABA without contributing any other metabolites. The next step was to detect and measure GABA from a wide range of metabolites in the human brain (table 2.2). To do so, several brain phantoms containing all main human brain metabolites and different percentages of GABA concentration (2, 4, 20, 40 mM) were scanned and measured.

2.4.3 In vivo GABA measurements

After optimising the MEGA-PRESS sequence, five participants were scanned pre- during and post- tDCS with both protocols for comparison. Data was collected from the posterior cerebellum underneath the electrode (Figure 2.4).

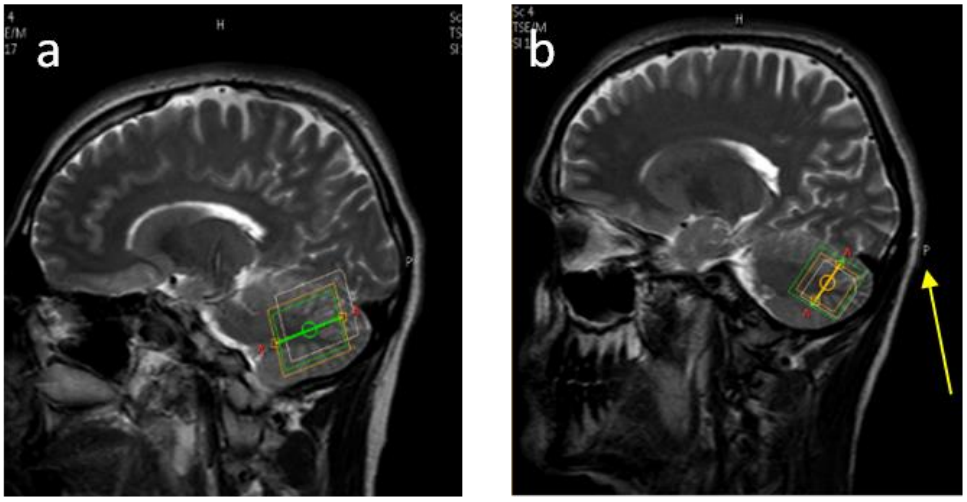

Figure 2.4 One subject in two measurements (a) 3x3x3 voxel size from original pulse sequence and (b) 2x2x2 voxel size from modified pulse sequence. Voxel was located in the posterior part of the right cerebellum underneath the anode. A cod liver oil tablet was placed on the top left edge of the electrode (yellow arrow). Data was collected pre- during and post- cerebellar tDCS.

2.4.4 Data Analysis

Data was analysed by TARQUIN (Total Automatic Robust QUantitation In NMR) (Wilson et al., 2011). Raw data were Fourier-transformed to a spectrum 2048 data points (1024 for phantom), the signal was smoothed by a 3 Hz Lorentzian filter, phased and referenced to water signal at 4.7 ppm. A Lorentzian-Gaussian (Voigt) line shape model (Reynolds et al., 2006) fitted to the data.

A basis set predefined in TARQUIN was initially constructed based on known peak positions. This basis set was fit to the average spectrum allowing peak amplitudes, widths, and frequencies to be optimized (Wilson et al., 2011). To detect GABA, all edit-On and edit-Off spectra were averaged separately and then subtracted from each other.

TARQUIN quantifies the metabolite concentration ratios by calculating the relative amplitudes of each spectrum based on prior knowledge of the approximate in-vivo metabolites, macromolecules, and lipids. The measured spectrum is compared with a linear combination of basis set. Most of the metabolites have several peaks with fixed relative intensity and frequencies. In other words, when a metabolite with three peaks changes (e.g GABA), all the relevant peaks change proportionally while their relative frequencies and intensities remain unchanged. This is the basis of measuring the concentration of metabolites even when they are overlapped.

2.5 Results

In order to modify the pulse sequence from the original one, I changed some of the main parameters and verified the spectrum mostly based on the quality of spectrum.

2.6 Phantom study

2.6.1 Detect and validate:

The first two scans were performed using phantoms including only GABA to reliably detect the signal. Then four brain phantoms with different concentrations of GABA were scanned to validate the sensitivity of our measurements by showing strong linear correlations (Pearson's r=0.99) between measured GABA signal amplitude and the actual concentration in the phantom (Figure 2.5). The pulse sequence utilised in these scans did not suppress MM.

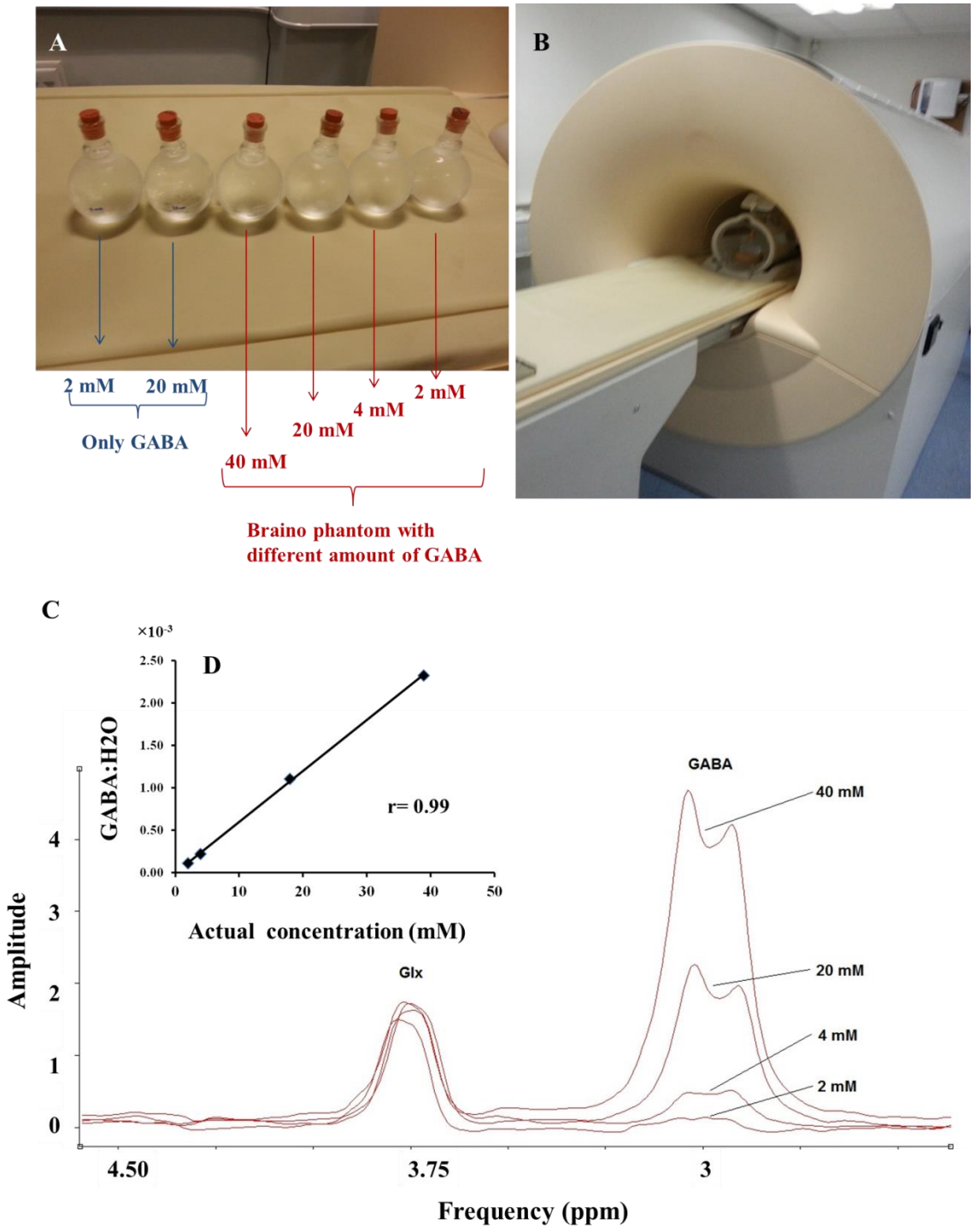

Figure 2.5 Two phantoms contained only GABA without any other metabolites to detect GABA, four brain phantoms were made to validate their sensitivity. Linear correlation between GABA signal amplitude and phantom concentrations. The pulse sequence utilised in these scans did not suppress MM.

2.6.2 Effects of MM suppression RF pulse on GABA peak

One phantom contained 20 mM GABA and was scanned with both sequences in order to assess whether applying the RF=1.5 ppm pulse affect GABA signal (in addition to Lysine). As shown in Figure 2.6, two spectrums are overlapped. The blue arrow is pointed to the spectrum which is acquired by the RF pulse with frequency 2 applied on 8.46 (no MM suppression; $GABA^{+}$) and is compared with the spectrum pointed by green in which the spectrum is acquired by when frequency 2 were applied on 1.5 ppm (MM suppression: GABA). GABA concentrations have been measured and compared: ($GABA^{+}$:H_2O= $(0.84\pm0.02)\times10^{-3}$; Figure 2.6A, GABA:$H_2O$= $(0.56\pm0.03)\times10^{-3}$; Figure 2.6B). This comparison indicated that the modified sequence was less efficient in detecting GABA.

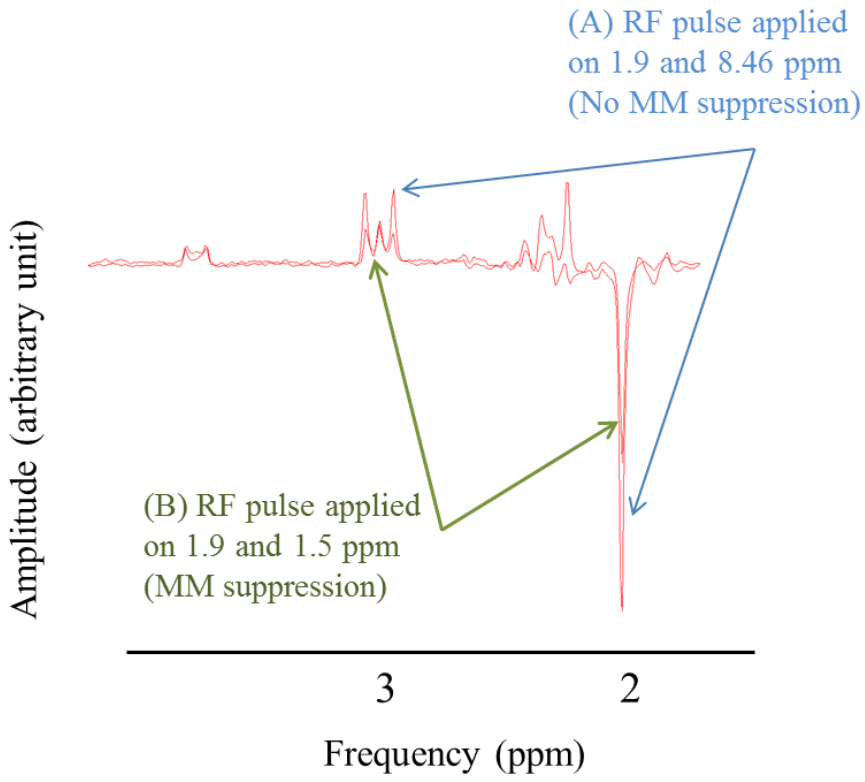

Figure 2.6 Phantom 20 mM (A) MM is not suppressed, (B) MM is suppressed. This shows that the shape of GABA peaks in 3ppm is affected by the applied RF pulse on the 1.5 ppm to suppress MM.

2.6.3 Coil

The original sequence was initially set for 8-channel coil; while 32-channel coil had to be used. Therefore, 2mM phantom was scanned with both coils, but spectrums from two acquisitions were completely overlapped with similar concentration 1. GABA:H_2O = $(0.87\pm0.058)\times10^{-4}$ & 2. GABA:H_2O = $(0.79\pm0.55)\times10^{-4}$, which suggested that the coil did not have a considerable effect on acquisition (Figure 2.7).

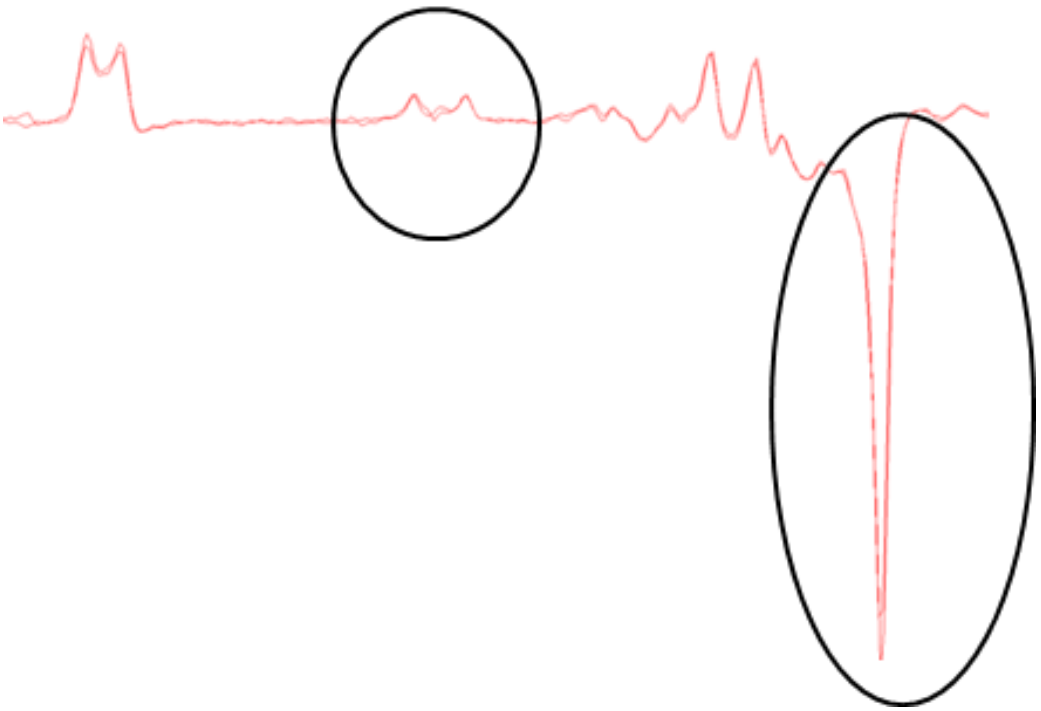

Figure 2.7 Comparison between 8-channel and 32-channel coil. Both average spectrums are completely overlapped.

2.6.4 Reproducibility

The planned study required three subsequent scans to measure GABA pre- during and post- tDCS in a single voxel. Therefore, I investigated the stability of the scanner across three scans to clarify if the GABA measurement was temporally stable. To do so, I scanned the 40 mM phantoms 3 times using optimised sequence parameters (32 channel coil, voxel size = 2×2×2 cm^3, frequency1= 1.9 ppm, frequency 2= 1.5 ppm). The results did not show any imperfections either qualitatively or quantitatively between three scans. All spectrums were aligned and the measured concentration from all three scans were similar: GABA:H2O= mean ± standard deviation = (1.35±0.15) $\times 10^{-3}$. Two sample spectrums with their measurements are shown in figure 2.8 A and B.

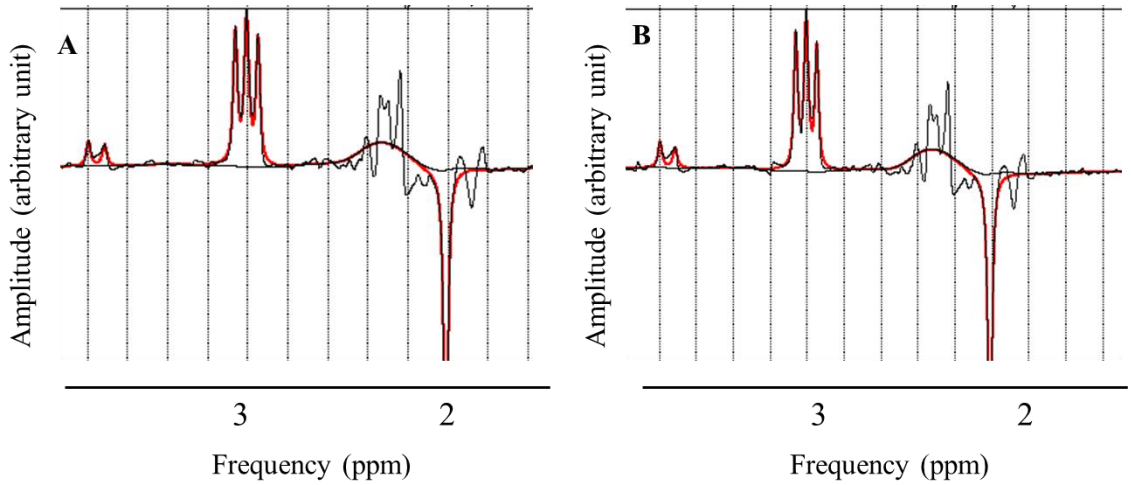

Figure 2.8 Two sample spectrums for stability check. Phantom including 40 mM GABA was scanned twice with the modified pulse sequence and showed very similar concentrations: (A) GABA:H2O=(1.35 ± 0.1) $x10^{-3}$, (B) GABA:H2O=(1.36 ±0.3) $x10^{-3}$

2.6.5 Quality assurance:

As quality assurance, 2mM phantom were scanned 7 times, but two of them showed some major artefacts (Figure 2.9). The sources of this artefact are regarded as the subtraction artefacts from the misalignment of the edit-on and edit-off spectra. In order to improve the editing efficiency of GABA, a post-processing correction step can be used to minimize the misalignment artefact (Evans et al., 2013). Therefore, the TARQUIN version was updated (only for in-vivo) for correcting this misalignment by aligning all the water peaks (Figure 2.10).

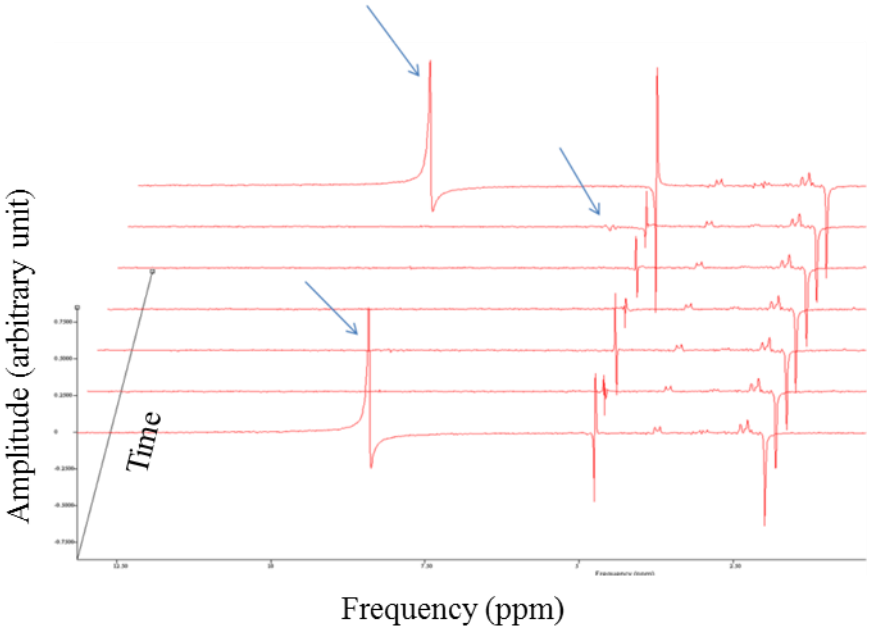

Figure 2.9 Phantom 2 mM were scanned 7 times. (A) In two of 7 acquisitions, water signal did not suppressed completely because of scanner instability. Residual of water suppression has been denoted by blue arrow.

2.6.6 Data acquisition timing

Finally, the 2mM phantom was scanned when the scanner had just warmed up at the beginning of the day and once at the end of the day after many heavy fMRI scans, after which the scanner might be more unstable. The spectrums from both acquisitions were compared and they were completely aligned. This finding suggested that data acquisition did not require any specific timing.

2.7 In vivo

2.7.1 Pilot study

Five participants (mean age = 22 ± 3) were scanned pre- during and post- cerebellar tDCS (the detail of cerebellar tDCS attachment is discussed in chapter 3) with both RF pulse sequences to identify whether/how voxel size and MM suppression affect the detection of GABA change in response to tDCS. The concentration of GABA:H2O has been analysed and averaged across five participants and compared in Figure 2.11 for during/pre and in figure 2.12 for post/pre. As demonstrated, the pattern of GABA change in response to stimulation was similar in both protocols in terms of decrease or increase. However, the developed sequence showed a larger effect size than the standard sequence (Figure 2.11 and 2.12), which suggested that in large voxel we might have measured noise. Therefore, in order to detect subtle changes in GABA, the developed sequence seemed to work more sensitively to allow detection of changes in GABA due to cerebellar tDCS.

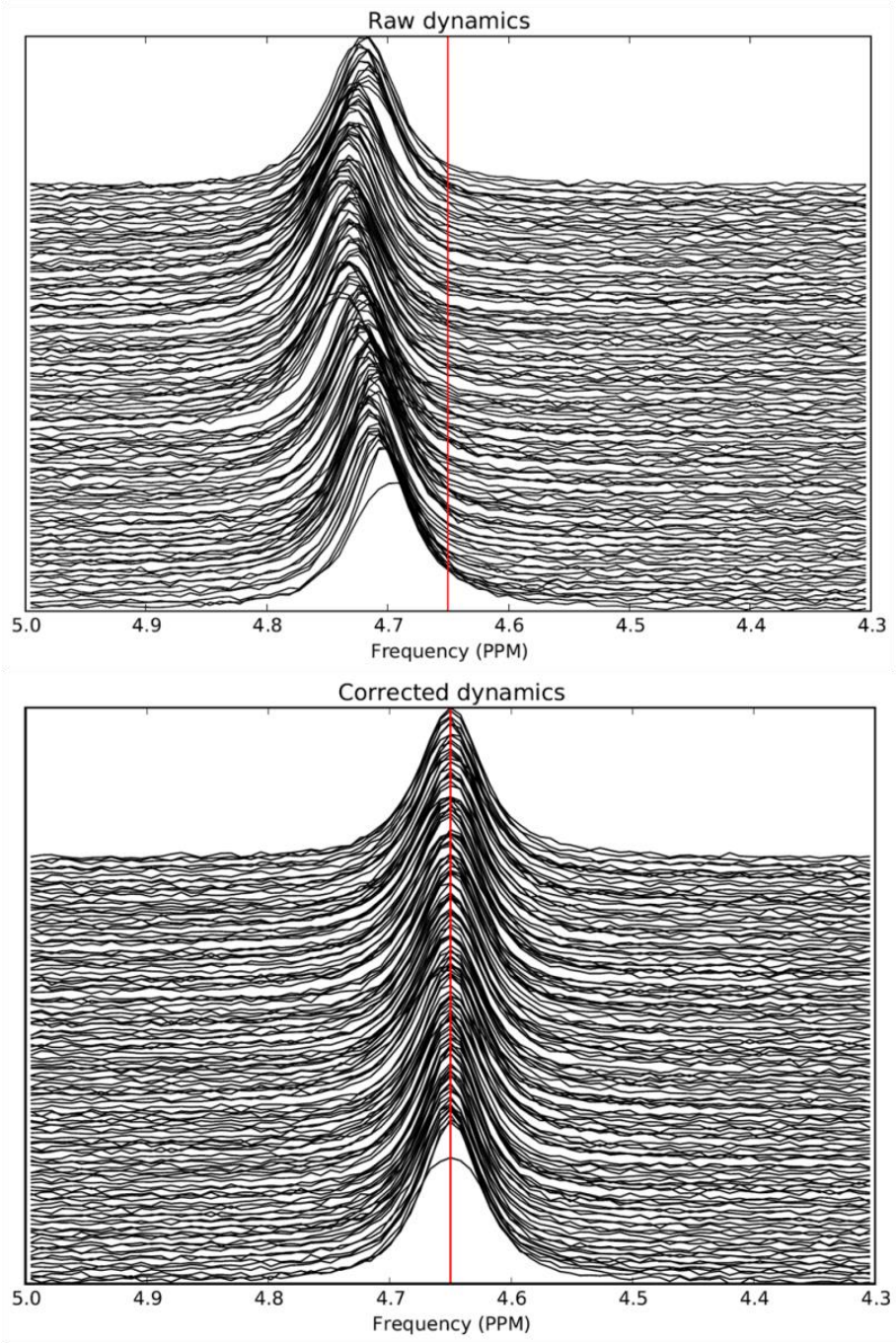

Figure 2.10 Spectrums have been drifted over time because of magnet imperfection.

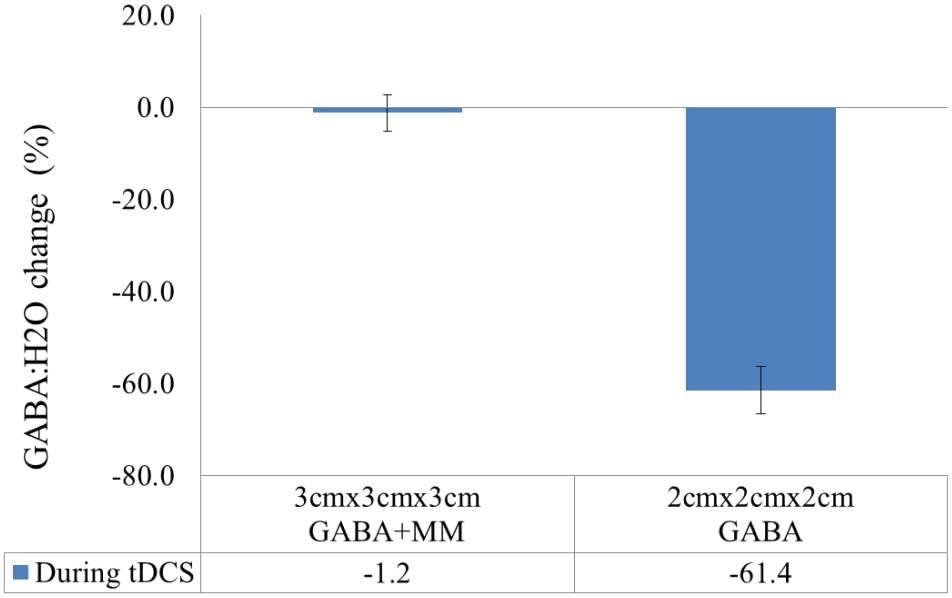

Figure 2.11 GABA percentage changes comparison between two RF pulse sequences during tDCS compare to pre. The effect size is larger with the modified RF pulse sequence. Error bars are standard error of the means.

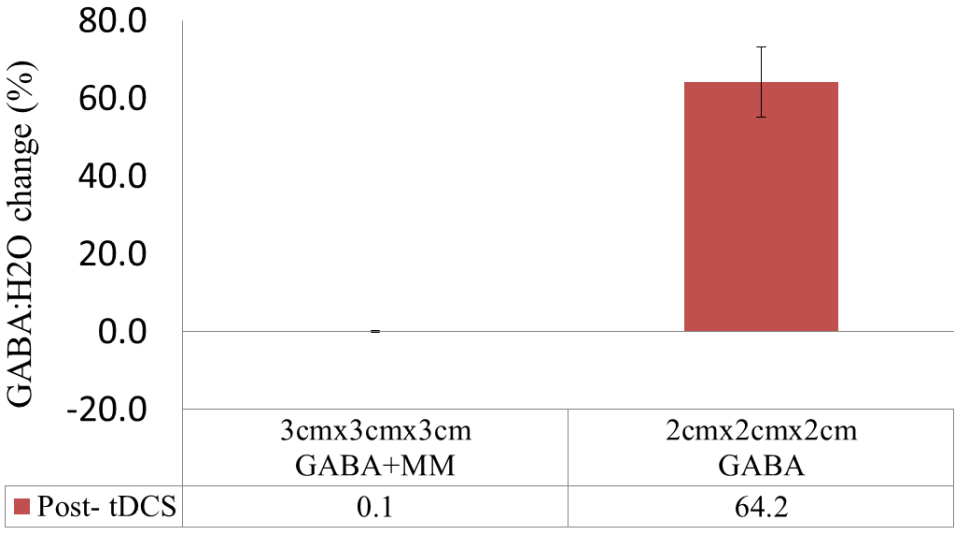

Figure 2.12 GABA percentage changes comparison between two RF pulse sequences post cerebellar tDCS compare to pre. The effect size is larger with the modified RF pulse sequence. Error bars are standard error of the means.

2.7.2 MR compatible tDCS set up

Dozens of scans were also carried out to optimise the MR-compatible tDCS in order to avoid artefact in MRS acquisition. The finalised set up is written as an instruction manual on the Birmingham university imaging centre (BUIC) website (Appendix I). (Link: https://www.buic.bham.ac.uk/wiki/index.php/Stimulus_Equipment)

2.8 Conclusion

In conclusion, I optimised the MRS pulse sequence so that I was able to detect and measure GABA confidently within the cerebellum. The pulse modification entailed several phantom studies that enabled me to make the voxel size small enough to fit in the right posterior cerebellum and to measure GABA without MM contamination. The modified sequence was tested in-vivo and displayed a more sensitive response to changes in GABA relative to the original RF pulse sequence.

3 NEURAL CHANGES ASSOCIATED WITH CEREBELLAR TDCS USING MRS

3.1 Introduction

Numerous studies have shown the facilitatory effect of anodal cerebellar transcranial direct current stimulation (tDCS) on both motor and cognitive behavioural tasks (Galea et al., 2009, Grimaldi et al., 2014, Cantarero et al., 2015). For instance, Galea et al., (2011) applied anodal cerebellar tDCS during visuomotor adaptation. They found that anodal cerebellar tDCS led to faster adaptation, relative to either primary motor cortex (M1) anodal tDCS or sham tDCS. This effect on motor adaptation/learning has been replicated in visuomotor adaptation (Block and Celnik, 2013), force-field adaptation (Herzfeld et al.), locomotor adaptation (Jayaram et al., 2012). As a result, it has been suggested that cerebellar tDCS is not only a useful tool to understand cerebellar function but also as a possible clinical technique to restore cerebellar function in patients suffering cerebellar-based disorders (Grimaldi et al., 2014). However, there are also inconsistencies regarding the impact of cerebellar tDCS with several studies reporting cerebellar tDCS having no effect on motor learning (Conley et al., 2016, Minarik et al., 2016) or large variability between- and within-subjects across sessions (Dyke et al., 2016). Therefore, understanding the underlying causes of this variability is essential.

Previous work has investigated the neural changes associated with primary motor cortex (M1) anodal tDCS using a range of MRI techniques (Stagg et al., 2011, Kim et al., 2014, Antal et al., 2011, Hunter et al., 2015, Kunze et al., 2016). For example, magnetic resonance spectroscopy (MRS) revealed that M1 anodal tDCS caused a decrease in gamma-aminobutyric acid (GABA), with the magnitude of this decrease being correlated with improvements in both sequence learning (Stagg et al., 2011), force-field adaptation (Kim et al., 2014), and impairments in tactile discrimination (Puts et al., 2011b). In addition, MRS has revealed detectable levels of GABA and glutamate (Glu) within the cerebellum (Waddell et al., 2011).

In addition, it has previously been shown using transcranial magnetic stimulation (TMS) that anodal cerebellar tDCS was associated with an increase in excitability between the cerebellar cortex and primary motor cortex (Galea et al., 2009). As the

Purkinje cells, the only output cells of the cerebellar cortex, are GABAergic (Ruigrok and Voogd, 1995), it is possible that the beneficial effects of anodal tDCS on cerebellar function are a result of local decreases in GABA.

To test this prediction, I measured the neural changes associated with concurrent cerebellar tDCS using MRS. With MRS, the changes in GABA and other metabolites were quantified within the right cerebellar cortex directly underneath the anodal electrode to examine whether tDCS induced change in any of the metabolites could predict individual differences in the effect that cerebellar tDCS had on visuomotor adaptation.

3.2 Materials and methods

3.2.1 Participants

34 healthy young individuals participated in this study (mean age: 22 ± 2 years; 11 male) and were divided into two groups of 17: anodal (23 ± 5 years; 8 male) and sham (19 ± 2 years; 3 male). All were naïve to the task, self-assessed as right handed, had normal/corrected vision, and reported to have no history of any neurological condition. The study was approved by the Ethical Review Committee at the University of Birmingham and was in accordance with the declaration of Helsinki. Written informed consent was obtained from all participants. Participants were recruited through online advertising and received monetary compensation. At the end of the behavioural session, participants were asked to report their attention, fatigue, and quality of sleep using a questionnaire with a scale from 1-7. They also reported whether they believed they had received active or placebo stimulation, and their hours of sleep during the previous night (table 3.1). After completing the behavioural task, those 17 participants from the anodal group underwent two sessions of MRS and resting state fMRI separated by one week (due to limitation of scanning hours, sham participants were not MRI scanned). Both MRI sessions performed during resting state because performing the visuomotor

learning task in the scanner was not possible. Participants in all three sessions were the same. The resting state fMRI data will be discussed in the next chapter.

3.2.2 Transcranial direct current stimulation (tDCS)

For the behavioural session, anodal tDCS (DC-Stimulator, NeuroConn, Germany) was delivered through a pair of rubber electrodes (4 x 4 cm^2) within two 5 x 5 cm^2 pads soaked in a saline solution. The anodal electrode was placed over the right cerebellar cortex, 3 cm lateral to the inion. The cathodal electrode (reference) was placed over the right buccinator muscle (Galea et al., 2011). At the onset of stimulation, current was increased in a ramp-like fashion over a period of 10 seconds. For the behavioural study, in the anodal group, a 2 mA current (current density J=0.08 A/cm2) was applied for up to 25 minutes. In the sham group, tDCS was ramped up over period of 10 seconds, remained on for 10 seconds before being switching off. Participants were blinded as to whether anodal or sham was applied (table 3.1).

For the MR sessions, 1.8 mA anodal tDCS was delivered (J=0.07 mA/cm2) through a pair of rubber electrodes (5 x 5 cm2). The electrodes were attached to each participant's head using EEG paste and Coban self-adhesive tape (in the same position as behavioural session). Electrodes were connected to an MR-compatible tDCS machine (DC-Stimulator-MR, NeuroConn, Germany). Ideally 2 mA stimulation would have been used; however high impedance (>55 kΩ) using the MRI-compatible tDCS equipment meant this was not possible. To avoid MR image artefacts, the tDCS current was set to 0 mA for pre-and post-stimulation data acquisition. This was because the tDCS device employed two filters for the magnetic field that were only activated when stimulation was turned on even at 0 mA. tDCS was ramped up over 10 seconds, with the scan starting immediately after the current reached 1.8 mA and remained on for 25 minutes and then was ramped down over 1 second.

3.2.3 Behavioural protocol

Participants were seated behind a table, with their chin supported by a rest (figure 3.1A), in front of a computer monitor (30-inch; 1280×1024 pixel resolution; 105 cm from chin rest). A Polhemus motion tracking sensor (Colchester, VT, USA) was attached to their right index finger and their arm was placed underneath a horizontally suspended wooden board, which prevented direct vision of the arm (Figure 3.1A). The visual display consisted of a 1cm-diameter starting box, a green cursor (0.25cm diameter) representing the position of the subject's index finger, and a circular white target (0.33cm diameter). Targets appeared in 1 of 8 positions (45˚ apart) arrayed radially at 8 cm from the central start position. Targets were selected pseudo-randomly so that every set of 8 consecutive trials (an "epoch") included 1 movement towards each target position. Participants controlled the green cursor on the screen by moving their right index finger across the table top (Figure 3.1A). At the beginning of each trial, participants were asked to move their index finger to the start position and a target then appeared. Participants were instructed to make a fast 'shooting' movement through the target such that online corrections were effectively prevented. At the moment the cursor passed through the invisible boundary circle (an invisible circle centred on the starting position with an 8 cm radius), the cursor was hidden and the intersection point was marked with a static yellow circle to denote the terminal (endpoint) error. In addition, a small square icon at the top of the screen changed colour based on movement speed. If the movement was completed within 100-300ms, then it remained white. If the movement was slower than 300ms, then the box turned red (too slow) and if the movement was faster than 100ms, then the box turned green (too fast). Importantly, the participants were reminded that spatial accuracy was the main goal of the task. After each trial, subjects moved back to the central start position, with the cursor only reappearing once they were within 2cm of its location.

3.2.3.1 Visuomotor adaptation

The aim of this experiment was to replicate the findings of Galea et al., (2011). Therefore, participants were exposed to 8 blocks of 96 trials (12 repetitions of the 8 targets). The first 2 blocks acted as baseline and consisted of veridical feedback with (pre1) and without (pre2) online visual feedback (Figure 3.1B). During the no visual feedback trials, participants were instructed to continue to strike through the visible target, but received no visual feedback either during or at the end of their movement. Following this, participants were exposed to 3 blocks (adapt 1-3) of trials in which an abrupt 30° counter clockwise (CCW) visual rotation was applied. Finally, to assess retention, three blocks (post-1-3) were performed without visual feedback. tDCS was applied from the start of pre2 throughout the adaptation blocks and lasted for approximately 25 minutes (Figure 3.1B).

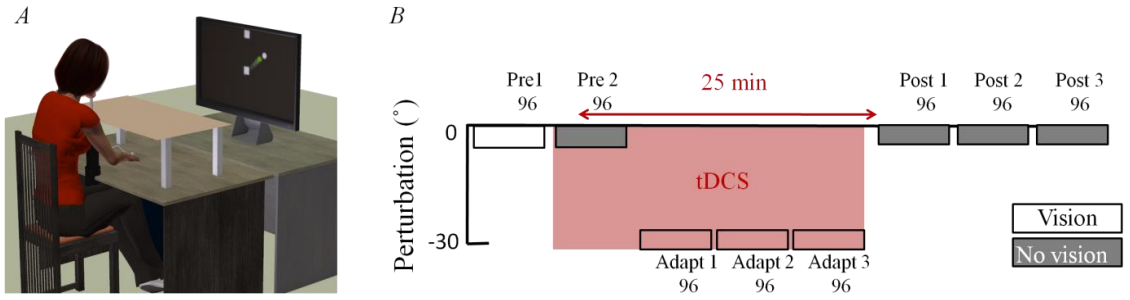

Figure 3.1 Visuomotor adaptation task. (A) Experimental set up; participants sat behind a table facing a vertically- orientated screen placed 105 cm in front of them. (B) Task protocol: Following 2 baseline blocks (each 96 trials: pre 1-2), an abrupt 30˚ VR was applied to the screen cursor and was maintained across 3 blocks (adapt 1-3). Cerebellar tDCS (anodal/sham) was applied from pre 2 until adapt 3 (pink). Following this, retention was examined by removing visual feedback (grey) for the final 3 blocks (post 1-3).

3.2.4 Magnetic resonance acquisition

The anodal stimulation group also participated in two MRS sessions with the order of the sessions counterbalanced across subjects (all sessions were interleaved by one week apart). In both MR sessions, data were acquired pre-, during and post 25 minutes of cerebellar tDCS on a Philips Achieva 3T system (Philips Medical Systems, Best, The Netherlands) with a 32-channel radio frequency coil.

3.2.4.1 MRS (MEGA-PRESS) acquisition

The aim of this session was to measure tDCS-induced changes in GABA and Glutamate (Glu) concentrations within the cerebellum. Three orthogonal T2-weighted scans (34 slices, 4 mm thickness, and 1 mm gap, voxel size= 0.8 x 1.1 mm2, 40 seconds duration) were collected to allow precise manual localisation of the 2 cm x 2 cm x 2 cm MRS single voxel on the posterior part of the cerebellum underneath the electrode. A cod liver oil capsule was placed on the top right corner of the electrode. As this could be seen in the images, it was used as an additional marker to aid the localisation of the MRS voxel (Figure 3.4 A).

A GABA signal was measured from the proton spin coherence resonance at 3.0 ppm, accomplished by J-difference editing after scanning using a MEscher-GArwood-Point RESolved Spectroscopy (MEGA-PRESS) (Mescher et al., 1998) sequence with a pulse repetition time (TR) of 2000 ms, echo time (TE) of 68ms and total duration ~25 minutes. We produced an average GABA spectrum from a total of 512 spectral acquisitions each with a bandwidth of 2150 Hz, sampled at 2048 data points, and with prior water suppression using variable power radio-frequency pulses with optimized relaxation delays (VAPOR) at 4.68 ppm (Tkac et al., 1999a).

To achieve an edited GABA spectral signal without contamination from macromolecules (MM), the two frequency selective 180° RF pulses (Gaussian pulses with duration of 16.5 ms) in the MEGA-PRESS sequence were applied with the centre

of the frequency band interleaving between 1.9 ppm (edit-On) and 1.5 ppm (edit-Off) (Henry et al., 2001), across the 512 spectral acquisitions. The edit-Off spectra were subtracted from the edit-On spectra resulting in a spectrum with an unequivocal GABA signal (Figure 3.2). The acquired edit-Off spectra were also separately analysed to obtain measurements in other metabolites including GLX (Glu + Glutamine (Gln)) and additional unsuppressed water scans were also acquired to allow corrected metabolite signal quantification.

MRS data were collected pre-, during and post-tDCS, with three scans (lasting 25 mins each) performed sequentially within the same individually localised voxel (Figure 3.2).

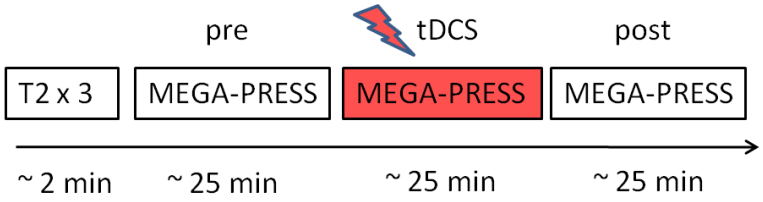

Figure 3.2 Graphical representation of MRS session using MEGA-PRESS pulse sequence. Data was acquired pre-, during, and post- tDCS.

3.2.4.2 MRS (PRESS) acquisition

I also acquired MRS scans using a Point RESolved Spectroscopy (PRESS) (Bottomley et al., 1983) sequence (TR/TE = 2000/32ms, 128 averages, 2048 data points sampled over a spectral bandwidth of 2000 Hz, with water suppression using VAPOR. The PRESS scan voxel size was 2 cm x 2 cm x 2 cm, which was localised in the posterior part of the cerebellum underneath the electrode. The PRESS scans lasted 10 minutes and were acquired pre-, during and post- tDCS (Figure 3.3). This enabled quantification of signals from metabolites including N-acetyl aspartate (NAA), Creatine (Cr), Choline

(Cho) and myoInositol (Ins). In this session, BOLD signal was also measured following each of these MRS scans (pre, during, post), but the details will be explained in the next chapter.

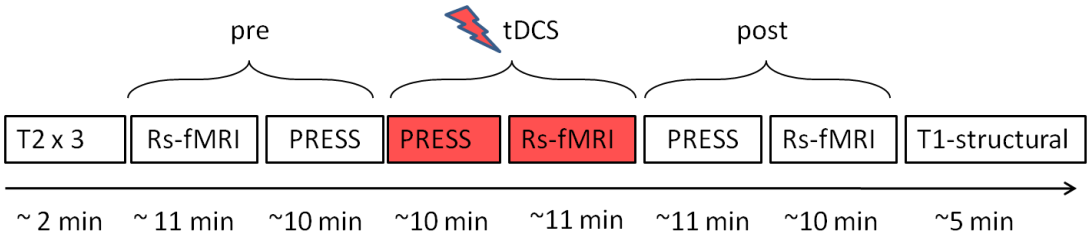

Figure 3.3 Graphical representation of resting state fMRI & MRS session (using PRESS pulse sequence). Details of resting state fMRI are discussed in chapter 4. Data was acquired pre-, during, and post- cerebellar tDCS.

3.2.5 Data analysis

3.2.5.1 Visuomotor task

Data and statistical analysis was performed using MATLAB (The Math Works, USA) and SPSS (IBM, USA). Index finger position (X & Y position) data was collected at 120 Hz. For each trial, angular hand direction (°) was calculated as the difference between the angular hand position and angular target position at the point when the cursor intersected the 8 cm invisible circle centred on the starting position. During veridical feedback block (pre1, Figure 3.1B), the goal was for hand direction to be 0°. However, with the visuomotor transformation (adapt 1-3), hand direction had to compensate; that is, for the −30° (CCW) visuomotor rotation, a hand direction of +30° relative to the target was required. Positive values indicate a CW direction, whereas negative values indicate a CCW direction. In addition, reaction time (RT: difference between the target appearing and the participant moving out of the start position) and movement time (MT: difference between reaction time and movement end) were

calculated for each trial. We removed any trial in which hand direction, RT or MT exceeded 2.5 standard deviations above the group mean. This accounted for 1.22 % of trials. Epochs were created by binning 8 consecutive movements, 1 towards each target.

The hand direction (°) of anodal and sham groups was compared for each block of baseline using separate 2-tailed independent t-tests. For adaptation and retention, separate repeated-measures ANOVAs compared groups (anodal/sham) across adaptation blocks (Adapt 1-3). Finally, for reaction time (RT) and movement time two separate repeated-measures ANOVAs compared groups (anodal/sham) across all 8 blocks (Pre 1-2, Adapt 1-3, Post 1-3). The threshold for all statistical comparisons was $P<0.05$. Effect sizes are reported as partial eta squared for ANOVA and Cohen's d for t-tests. All data presented as mean ± standard error of the mean, unless otherwise specified.

3.2.5.2 MRS analysis

Spectroscopy data was analysed using TARQUIN version 4.3.4 (Wilson et al., 2011). First, pre-processing was carried out including inspection and removal of corrupted spectra arising from motion or technical problems. Then, raw data were Fourier-transformed to a spectrum of 2048 data points, the signal was smoothed by a 3 Hz Lorentzian filter, phased and referenced to water signal at 4.7 ppm. Random drift due to scanner instability or subject motion was corrected by aligning the water peak before fitting a Lorentzian-Gaussian (Voigt) line shape model. The amount of drift was plotted and used to assess the quality of acquisition. Scans with less than 10 Hz drift were taken to have acceptable spectra. However, high drift was not the only criterion used to remove data; all the spectra were visually inspected in all acquisitions and abnormal spectrums were excluded from the study. This accounted for 9% of the averaged spectra; three subjects were removed from analysis due to an unreliable spectrum in one of the three acquisitions (pre-, during, or post-tDCS).

A basis set predefined in TARQUIN was initially constructed based on known metabolite peak positions (Voigt function). This basis set was fit to the average spectrum allowing peak amplitudes, widths, and frequencies to be optimized (Wilson et al., 2011). The basis set was then updated with the newly determined frequencies and peak widths and this process of basis set refinement was repeated until fitting resulted in negligible adjustment to the basis set. To detect GABA, all edit-On and edit-Off spectra were averaged separately and then subtracted from each other (Figure 3.4B), but GLX (Glu+Gln) was measured from the average of edit off spectra and Glu extracted from GLX using the predefined basis set in TARQUIN.

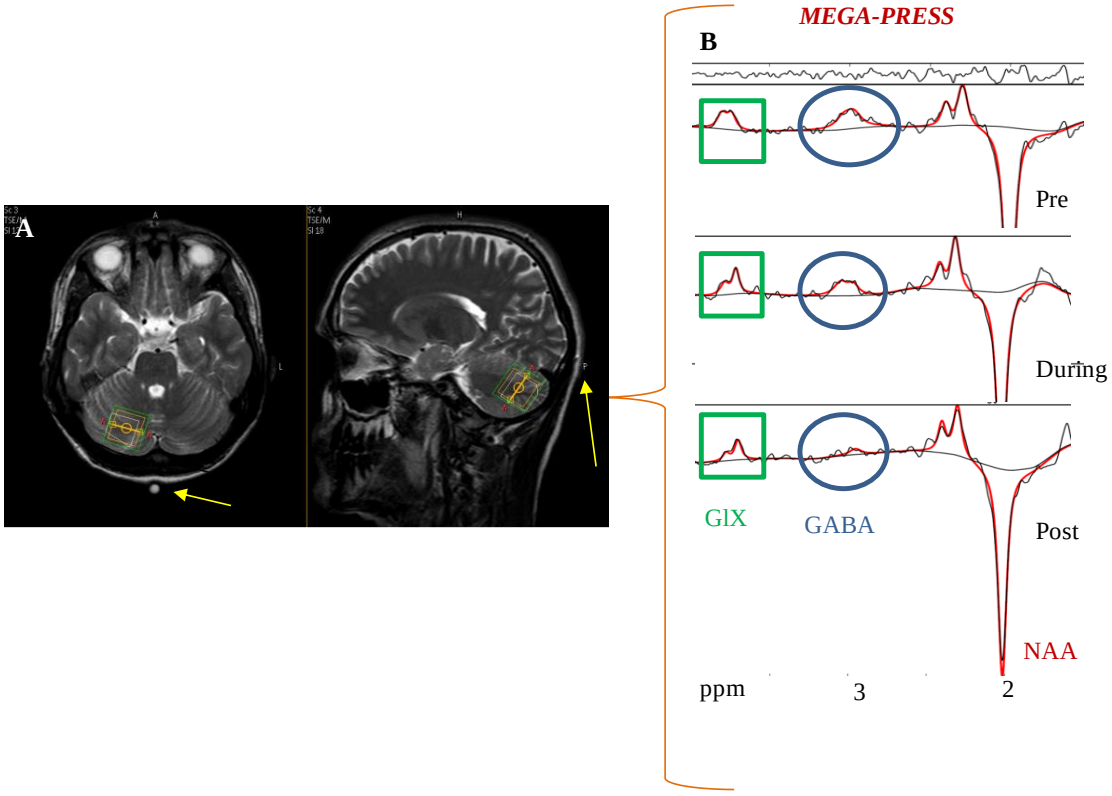

Figure 3.4 MRS voxel localisation. (A) A single 2x2x2 cm voxel size was located manually in the posterior part of the right cerebellum underneath the anodal electrode. A cod liver oil capsule (yellow arrow) was situated at the top left edge of the electrode to assist with voxel localisation. (B) Three sets of data were acquired: pre-, during and post- cerebellar tDCS.

Next, a T1-image of each participant was co-registered to their T2-image using Statistical Parametric Mapping (SPM) (Friston et al., 1989) and the quality of registration was checked by plotting joint histograms of co-registered T1 vs. T2 images, and by inspection of land marks (specifically on the cerebellum). Then segmentation of the T1 image was carried out using the FMRIB automated segmentation tool (FAST) (Zhang et al., 2001) to calculate the relative volume of each tissue type; grey matter , white matter (WM) and cerebral spinal fluid (CSF) within the voxel. The amplitude of GABA, GLX, and Glu were corrected for the proportion of GM volume in the voxel by multiplying by $\frac{GM}{GM+WM+CSF}$. Other metabolites such as total NAA (tNAA) and total Cr (tCr) were corrected for the proportion of both GM and WM volumes in the voxel by multiplying by $\frac{GM+WM}{GM+WM+CSF}$ (Stagg et al., 2011, Kim et al., 2014). Finally, the percentage change ratios for all metabolites for pre- versus during-tDCS, and pre- versus post-tDCS scans were calculated by (100 x (during-pre)/pre) and (100 x (post-pre)/pre) respectively (Stagg et al., 2011).

To assess the modulation of metabolites in response to cerebellar tDCS, a one-way ANOVA was performed to compare concentration of each metabolite pre-, during, and post- tDCS. The threshold for all statistical comparisons was $P<0.05$. All data are presented as mean ± standard error of the mean, unless otherwise specified.

3.3 Results

3.3.1 Visuomotor task

The performance of 17 anodal and 17 sham participants were compared across all blocks. Both groups behaved similarly during baseline with no significant differences in hand direction, relative to target, between groups during either pre1 (anodal: 1.20 ± 0.22, sham 1.83 ± 0.32; $t_{(32)}$= -1.4, p=0.1, d= 0.08; Figure 3.5) or pre2 (anodal: 2.24 ±

0.33, sham: 1.53 ± 0.34; $t_{(32)}$= 0.9, p=0.4, d=0.2). For adaptation, we found no significant differences between the anodal and sham groups. Specifically, there was a significant main effect for blocks ($F_{(2, 32)}$= 205.6, p< 0.005, $\eta 2$= 0.86), but no significant main effect for group ($F_{(1, 32)}$ = 2.3, p=0.14, $\eta 2$= 0.07) or block-group interaction ($F_{(1,32)}$ = 0.63, p=0.43, $\eta 2$= 0.02; Figure 3.5). Based on these results (total adaptation: anodal = 20.84 SD = 2.3, sham =19.44 SD = 2.98), a power analysis revealed (d = 0.53, power =0.8) that group sizes of 45 participants would be required to observe a significant result. For retention, I found an unexpected difference between groups whereby the anodal group retained significantly more than the sham group. Specifically, there was a significant main effect for blocks ($F_{(2, 32)}$= 114.9, p< 0.005, $\eta 2$=0.78) and group ($F_{(1,32)}$= 4.7, p= 0.037, $\eta 2$=0.13), but no significant block-group interaction ($F_{(1, 32)}$= 0.6, p= 0.44, $\eta 2$=0.02). For RT, there were no significant main effect for group (anodal: 0.43 ± 0.04, sham: 0.39 ± 0.05; $F_{(1, 32)}$= 2.02, p= 0.2, $\eta 2$= 0.06), blocks ($F_{(2, 32)}$= 2.5, p=0.1, $\eta 2$= 0.07), or block-group interaction ($F_{(1, 32)}$= 1.2, p= 0.3, $\eta 2$= 0.04). Similarly, for MT there were no significant main effect for group (anodal: 0.22 ± 0.08, sham: 0.24 ± 0.08, $F_{(1, 32)}$= 3.3, p= 0.08, $\eta 2$= 0.09) or block-group interaction ($F_{(1, 32)}$= 0.4, p= 0.8, $\eta 2$= 0.01), but a significant main effect for blocks ($F_{(2, 32)}$ = 9.9 , p < 0.005, $\eta 2$=0.24).

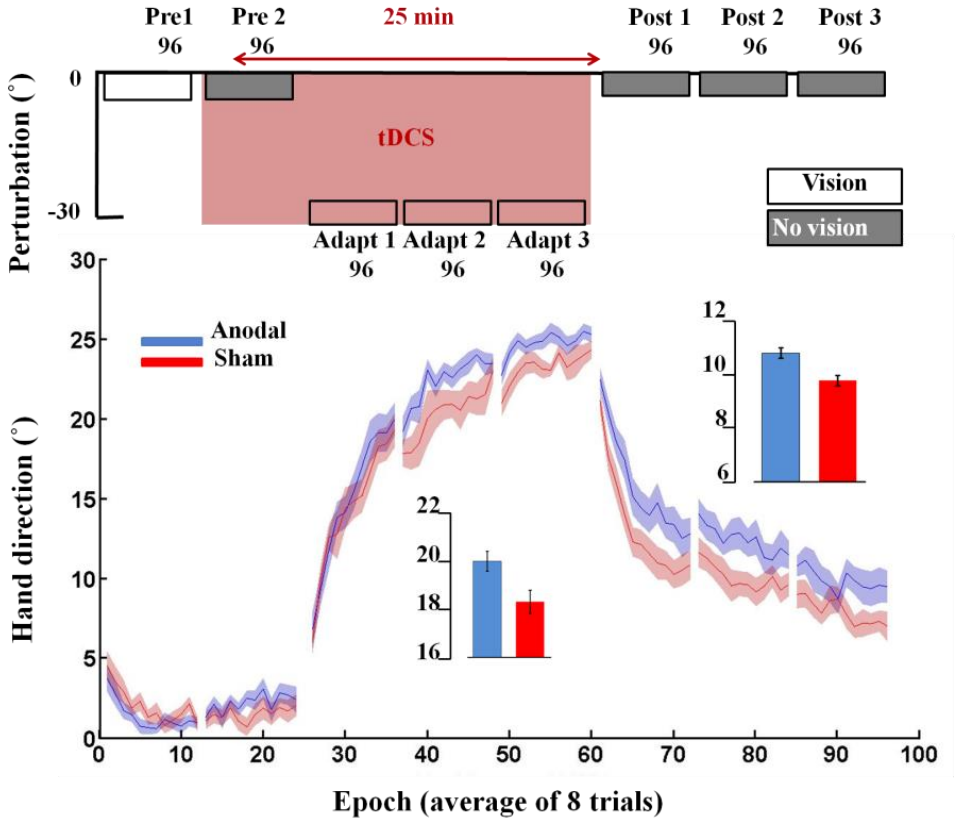

Figure 3.5 Influence of cerebellar tDCS on visuomotor adaptation. Epoch data (average across 8 trials) for angular hand direction (˚) for the 17 anodal (blue) and 17 sham cerebellar tDCS groups. Positive values indicate CW hand direction. The inset bar graphs indicate mean hand direction for the anodal and sham groups during adaptation (adapt 1-3) and retention (post-1-3). Solid lines, mean; shaded areas/error bars, S.E.M.

3.3.2 MRS:

3.3.2.1 tDCS did not consistently modulate metabolites

In the anodal group, I measured metabolites within the right posterior cerebellar cortex underneath the anodal electrode at three time-points: pre-, during and post-25 min of anodal cerebellar tDCS. First, I performed a one-way ANOVA to verify grey matter tissue fraction among individuals and found no significant difference between GM percentage across the three time-points ($F_{(2,39)}$ = 0.3, p = 0.7, $\eta 2$=0.01). My results showed cerebellar tDCS did not have any consistent effect in modulating any of the examined metabolites, while large variability was observed across the participants (e.g. the change in GABA varied from ~90% increase to a 100% decrease; Figure 3.6A). Separate one-way ANOVAs did not reveal any statistically reliable changes across the group; GABA:H2O ($F_{(2,36)}$ = 0.34, p= 0.71, $\eta 2$= 0.02; Figure 3.6A), GLX:H_2O ($F_{(2, 45)}$ = 0.18, p= 0.83, $\eta 2$=0.08; Figure 3.6B), Glu:H2O ($F_{(2,36)}$ = 2.41, p= 0.10, $\eta 2$=0.11; Figure 3.6C), NAA:H_2O ($F_{(2,45)}$ = 1.89, p = 0.16, $\eta 2$=0.08), Cr:H_2O ($F_{(2, 36)}$ = 0.55, p= 0.58, $\eta 2$=0.02), Cho:H_2O ($F_{(2, 45)}$ = 0.26, p= 0.77, $\eta 2$=0.01), and Ins:H_2O ($F_{(2,45)}$ = 0.24, p = 0.79, $\eta 2$=0.01).

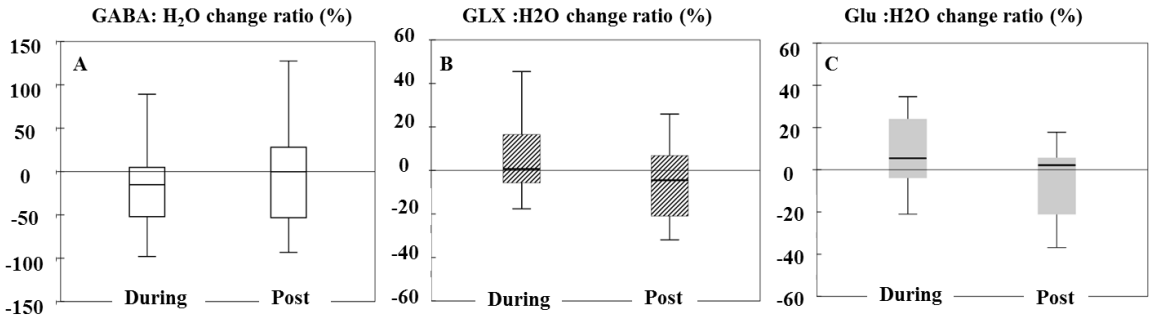

Figure 3.6 Changes in GABA and GLX during and post cerebellar tDCS. Change (%) in (A) GABA:H2O; (B) GLX:H2O; (C) Glu:H2O during and post-cerebellar tDCS relative to baseline (pre-tDCS). The box-plot limits represent the 25th and 75th data percentiles and the middle line represents the median. The error bars represent the range of data.

3.3.2.2 tDCS-induced GABA:H2O and Glu:H2O change are inversely correlated with learning and retention

Given the large between-subject differences in responses (Figure 3.6), I went on to examine whether individual changes in the metabolites could predict visuomotor adaptation. Therefore, Pearson's correlations were carried out between the tDCS-induced alterations in metabolite concentrations and behavioural performance during visuomotor adaptation (adapt1-3). The results demonstrated an increasingly negative correlation across the three blocks, from a non-significant trend in adapt 1 ($r = -0.41$, $p = 0.16$) and adapt 2 ($r = -0.43$, $p = 0.14$) to a significant negative correlation in adapt 3 ($r = -0.59$, $p = 0.04$; Figure 3.7A). This correlation was specific to GABA and not any other metabolites (all $p>0.05$) (Figure 3.7B). These results suggest that participants whose GABA:H_20 ratio decreased more than 50% from pre-tDCS to during-tDCS also showed greater visuomotor adaptation with cerebellar tDCS (Figure 3.7A). Finally, as it is assumed that the GABA peak is mostly derived from grey matter (Stagg et al., 2011), the fraction of grey matter in the MRS voxel was also assessed. A Pearson's correlation was performed between GM percentage and visuomotor adapt3; however, no significant correlation was found ($r = 0.006$, $p = 0.98$).

Surprisingly, there was also a significant negative correlation between Glu:H2O (change from pre-tDCS to during tDCS) and behavioural performance at every block of retention: retention 1 ($r = -0.60$, $p = 0.04$) , retention 2 ($r = -0.77$, $p = 0.002$), retention 3 ($r = -0.72$, $p = 0.006$), and total retention (post1-3; $r = -0.74$, $p = 0.004$; Figure 3.7C). As Glu was measured from GLX (Glutamate + Glutamine), the same correlation was also observed between GLX:H2O and total retention ($r= -0.64$, $p=0.01$). This correlation was specific to changes in GLX/Glu concentration from baseline to during tDCS. For example, changes in GLX/Glu from baseline to post-tDCS, and changes in all other metabolites, were not correlated with retention (all $p > 0.05$).

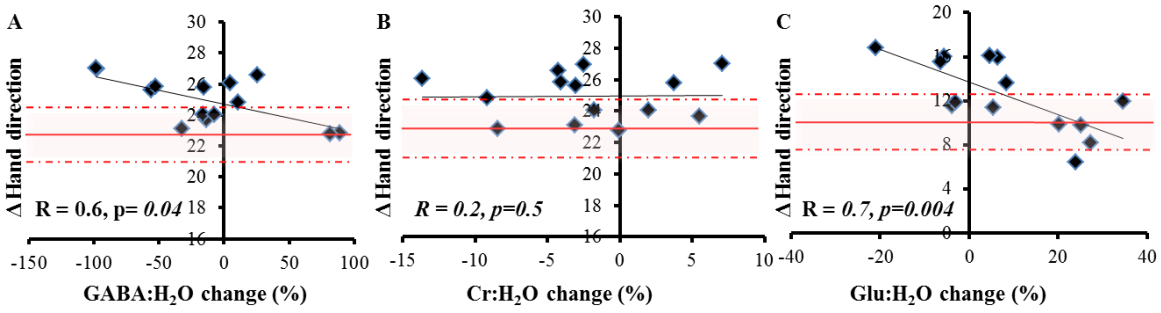

Figure 3.7 Correlations between MRS and visuomotor adaptation. (A) A negative correlation was observed between changes in GABA during cerebellar tDCS and behavioural performance during adaptation (adapt 3). This indicates a cerebellar tDCS decrease in GABA was associated with a greater amount of adaptation. The red line represents the sham group's mean performance during adapt 3 (shaded area = SD across group). (B) The significant correlation was specific to GABA and not observed with any other metabolite such as Cr:H_2O. (C) A negative correlation was also observed between changes in Glu:H_2O during cerebellar tDCS and total retention. This suggests a cerebellar tDCS dependent decrease in Glu was associated with a greater amount of retention.

3.3.3 Self-reported ratings of attention, fatigue, and sleep

There were no significant differences between groups across all experiments for the self-reported ratings of attention, fatigue and quality of sleep (Table 3.1).

Table 3-1 Self-reported rate of attention, fatigue, quality of sleep (1 is poorest and 7 is the maximal), perceived tDCS as active (1) or placebo (0) and sleep hours. All the values are averaged and compared using independent t-test across the whole experiments and presented as mean ± standard deviation.

Visuomotor task	**attention**	**Fatigue**	**Sleeping hours**	**Quality of sleep**	**Active or placebo**
Anodal	5.3 ± 1.1	3.7 ± 1.5	7.2 ± 1.2	5.1 ± 1.4	0.8 ± 0.3
Sham	4.6 ± 1.1	3.7 ± 1.5	7.2 ± 1.6	4.7 ± 1.7	0.6 ± 0.5
T-test	$t_{(27)}$= 1.6, p= 0.1	$t_{(27)}$= 0.03, p= 0.9	$t_{(27)}$=0.04, p= 0.9	$t_{(27)}$= 0.6, p= 0.5	$t_{(27)}$ = 1.4, p= 0.2

3.4 Discussion

This study revealed that the effects of cerebellar tDCS on visuomotor adaptation were correlated with a decrease in GABA, and individual differences in retention were correlated with a decrease in Glu.

3.4.1 Cerebellar tDCS did not significantly enhance visuomotor adaptation

Although participants showed a clear ability to adapt to the novel visuomotor rotation, the expected significant enhancement of adaptation by anodal cerebellar tDCS, that had been shown in various studies (Galea et al., 2011, Hardwick and Celnik, 2014, Block and Celnik, 2013), was not observed here. Despite our sample size being in the same range of previously published tDCS papers, a recent study indicates this could be significantly under powered (Minarik et al., 2016). Minarik et al (2016) showed that with a suggested tDCS effect size of 0.45, the likelihood of observing a significant result with 14 participants per group was approximately 20%. In fact, a power analysis based on our results revealed that I achieved an effect size of 0.53, suggesting group sizes of 45 participants would have been required to observe a significant difference between the anodal and sham tDCS groups. Nevertheless, my work indicates that there is substantial variation in the behavioural effect of cerebellar tDCS across participants. I therefore examined whether this could be explained by between-subject differences in the neural effect tDCS had on the cerebellum.

3.4.2 Online cerebellar tDCS reduction in GABA was correlated with motor adaptation

Similar to the behavioural results, there was no consistent group effect of tDCS on GABA or any other metabolite measured within the cerebellum either during or after

stimulation. This is in contrast to several previous studies that have shown tDCS to cause a significant decrease in GABA within M1 (Stagg, 2014, Stagg et al., 2014, Stagg et al., 2011, Kim et al., 2014, Bachtiar et al., 2015).

However, our findings demonstrated a correlation between a tDCS-induced reduction in GABA and greater adaptation to a visuomotor rotation with cerebellar tDCS. As this correlation was specific to GABA, and not any other metabolites, it suggests a crucial role for GABA in the online effects of cerebellar tDCS. This finding is similar to the results observed in M1 where a reduction in GABA was correlated with improvements in sequence learning (Stagg et al., 2011) and force-field adaptation (Kim et al., 2014). The relationship between cell-type activity and MRS-detected changes within the cerebellum is currently unknown, and therefore it is difficult to determine the cellular origin of a decrease in GABA as several cerebellar cortical interneurons are known to be GABAergic (Purkinje cells, stellate and basket cells, and Golgi cells). However, it is possible that a decrease in GABA reflects a reduction in Purkinje cell activity akin to the long-term depression (LTD) observed with cerebellar learning. Interestingly, it has previously been shown that visuomotor adaptation was associated with a decrease in cerebellar-cortical excitability (Schlerf et al., 2012). This work supports the view that a tDCS-dependent decrease in GABA may enhance visuomotor adaptation through a reduction in Purkinje cell activity/output.

3.4.3 Online cerebellar tDCS-induced reduction in GLX/Glu was correlated with motor retention

Surprisingly, this study also showed that a tDCS-induced reduction in both Glu and GLX had a strong negative correlation with subsequent visuomotor retention. At present, it is difficult to explain this correlation between changes in Glu/GLX and retention. One possibility is that a decrease in Glu/GLX reflects a decrease in glutamatergic input into the cerebellar cortex (from mossy fibres and/or granule cells) and reduced activity of Purkinje cells. This would reduce cerebellar brain inhibition

(CBI) and enhance M1 function. It is known that excitation of M1 facilitates retention, potentially retaining or consolidating what has been learnt by the cerebellum (Galea et al., 2011, Sami et al., 2014). However, there are still many unanswered questions regarding these results. For instance, it is not known why the cerebellar tDCS-dependent changes in GABA and Glu/GLX were not correlated across participants. In addition, I was unsure why cerebellar tDCS led to a significant increase in retention within this study whereas previous studies have not reported this effect (Hardwick and Celnik, 2014, Block and Celnik, 2013).

3.5 Conclusion

In conclusion, this study provided a novel insight into the neurophysiology underpinning cerebellar tDCS. I found that the positive effects of cerebellar tDCS on visuomotor adaptation were correlated with a decrease in cerebellum GABA levels and visuomotor retention were correlated with a decrease in cerebellum Glu levels, with these relationships being neuro-chemically specific.

4 RESTING STATE FUNCTIONAL CONNECTIVITY CHANGE ASSOCIATED WITH CEREBELLAR TDCS

4.1 Introduction

As discussed in chapter 3, unlike cerebellar tDCS the neural changes associated with M1 anodal tDCS have been studied extensively using a range of MRI techniques (Stagg et al., 2011, Kim et al., 2014, Antal et al., 2011, Hunter et al., 2015, Kunze et al., 2016). For example, resting state functional magnetic resonance imaging (fMRI) has shown anodal M1 tDCS to cause an increase in functional connectivity within the motor network (Stagg et al., 2014). However, the M1 tDCS-dependent decreases in GABA and increases in functional connectivity were found not to be correlated across participants (Bachtiar et al., 2015), suggesting they may be driven by distinct underlying mechanisms.

Numerous studies have used resting state fMRI to examine human cerebellar-cerebral pathways. For example, resting state fMRI has revealed that the cerebellar cortex contains zones that have distinct functional connections. Two parts of the cerebellum was found to be functionally connected to the sensorimotor parts of the cerebral cortex, whilst the other regions of the cerebellum are connected to non- motor areas of the cerebral cortex (Buckner et al., 2011). The posterior portion of the cerebellar cortex in particular was functionally connected to the frontal and parietal cortices (O'Reilly et al., 2010).

Anodal cerebellar tDCS has been associated with an increase in excitability between the cerebellar cortex and primary motor cortex, as assessed with TMS (Galea et al., 2009). As the Purkinje cells, the only output cells of the cerebellar cortex, are GABAergic (Ruigrok and Voogd, 1995) it is possible that the beneficial effects of anodal tDCS on cerebellar function are a result of local decreases in GABA and increases in connectivity between the cerebellum and distant brain regions.

To test this prediction, in addition to measuring GABA using MRS (in the previous chapter), I also measured the neural changes in functional connectivity associated with concurrent cerebellar tDCS using resting state fMRI.

In the previous chapter, I found the tDCS-induced changes in GABA within the right cerebellar cortex were correlated with improvements in visuomotor adaptation. In this chapter, the changes in functional connectivity between the right cerebellar cortex and other visuomotor-related brain regions were measured using resting state fMRI to examine whether the neural changes could predict individual differences in the effect cerebellar tDCS had on visuomotor adaptation.

4.2 Materials and Methods

4.2.1 Participants

From 17 healthy individuals who participated in the behavioural session (described in chapter 3), one withdrew from the study and 16 participated successfully, and underwent resting state fMRI (8 female, mean age = 26 ± 8 years). All were assessed to be eligible for MR scanning session. The study was approved by Ethical Review Committee of the University of Birmingham and was in accordance with the declaration of Helsinki. Written informed consent was obtained from all participants.

4.2.2 Transcranial direct current stimulation (cerebellar tDCS)

In this MR session, 1.8 mA anodal tDCS (DC-Stimulator, NeuroConn, Germany) was delivered (J=0.07 mA/cm2) through a pair of rubber electrodes (5 x 5 cm2). The

electrodes were attached to each participant's head using EEG paste and Coban self-adhesive tape (in the same position as behavioural session). Electrodes were connected to an MR-compatible tDCS machine (DC-Stimulator-MR, NeuroConn, Germany). Ideally 2 mA stimulation would have been used (same as behavioural session); however high impedance (>55 kΩ) in the MRI-compatible tDCS equipment meant this was not possible. To avoid MR image artefacts, the tDCS current was set to 0 mA for pre-and post-stimulation data acquisition. This was because the tDCS device employed two filters for the magnetic field that were only activated when stimulation was turned on. TDCS was ramped up over 10 seconds, with the scan starting immediately after the current reached 1.8 mA and remained on for 25 minutes and then was ramped down over 1 second.

4.2.3 Magnetic resonance acquisition

The anodal group also participated in two MR sessions (MRS, fMRI) with the order of the sessions counterbalanced across subjects. In both MR sessions, data were acquired pre-, during and post- 25 minutes of cerebellar tDCS on a Philips Achieva 3T system (Philips Medical Systems, Best, The Netherlands) with a 32-channel radio frequency head receive-coil.

4.2.3.1 Resting state functional connectivity

The aim of this session was to measure tDCS-induced changes in resting state rs-functional connectivity between the cerebellum and other visuomotor-related brain areas. Rs-fMRI data were acquired using a whole brain echo planar imaging (EPI) sequence using the following parameters; field-of-view (FOV) = 240 mm x 240 mm, in plane voxel resolution = 2.5 mm x 2.5 mm, slice thickness 3 mm, TR/TE = 2500/34ms, flip angle = 84˚, EPI factor = 51, slices = 41, number of dynamics = 250, total scan

duration approximately = 10 minutes; Figure 4.1). At the end, high resolution T1-weighted acquired sagittal, 175 slices, voxel size 1×1×1 mm, TR/TE= 8.4/3.8 ms, NSA=1, total scan time 10.40 min.

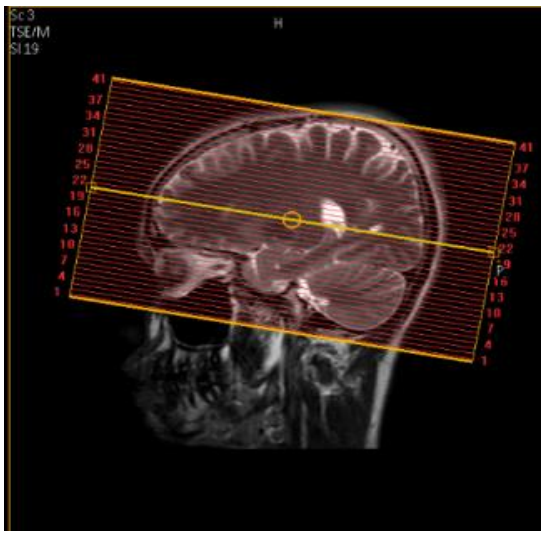

Figure 4.1 BOLD signal was acquired from the whole brain using Echo planar imaging (EPI) in ascending order.

Participants were consistently given the same instruction before starting each scan to keep their eyes open, not to think about anything in particular, and stay as still as possible. tDCS current was set at 0 mA for the pre and post scan and 1.8 mA for the during stimulation scan (Figure 4.2). No control study was performed for fMRI and all received anodal stimulation with a within-participants design in which resting state fMRI was measured pre-, during, and post- tDCS. Participants remained in the scanner between the three scans; all participants were aware of stimulating ON and OFF. In addition to each of the EPI scan, I also acquired MRS scans using a Point RESolved Spectroscopy (PRESS), which was explained in the previous chapter.

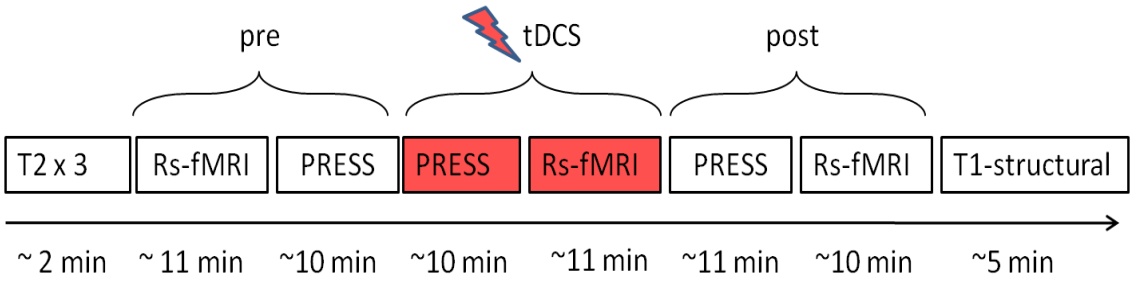

Figure 4.2 Graphical representation of rs-fMRI & MRS session (PRESS)

4.2.4 Data analysis

All fMRI data was analysed using FMRIB Software Library v5.0 (FSL) (Jenkinson et al., 2012) and custom in-house MATLAB software. Data analysis was performed in 4 main steps: 1) Anatomical pre-processing, 2) Functional pre-processing, 3) Functional connectivity, 4) Statistics.

4.2.4.1 Anatomical pre-processing

Pre-processing of anatomical image was performed in three main steps:

a) **Rotation** of T1-structural image to the same orientation as functional data using fslswapdim. This tool is an advanced tool that re-orders the data storage to permit changes between axial, sagittal and coronal slicing.

b) **Brain extraction** to remove the skull and extract the skull-stripped brain image using Brain Extraction Tool (BET) (Smith, 2002, M. Jenkinson, 2005). This tool takes the anatomical image as input and, based on the tissue segmentation, identifies the boundary between the brain and non-brain tissue. Results were observed to check if the skull-off output was precise and robustly worked for all the data (i.e. the skull removed completely without removing part of the brain).

c) **Segmentation** to grey matter, white matter (WM) and cerebrospinal fluid (CSF) using FMRIB's Automated Segmentation Tool (FAST). The output was three binary masks (Zhang et al., 2001).

4.2.4.2 Functional pre-processing

Functional pre-processing included

a) **Motion correction (MC)** was carried out by Motion Correction FMRIB's Linear Image Registration Tool MCFLIRT tool (Jenkinson et al., 2002). MCFLIRT reduces the misalignment and correct for bulk motion by lining up every functional image to the reference image (middle image) (Jenkinson et al., 2002).

b) **Slice timing correction** regulated all the slices based on image acquisition from bottom (cerebellum) to the top of the brain. The reason for this correction is due to the assumption we made that all the slices in each volume are acquired at the same time; however in reality there is small difference between all slice acquisitions (equal to RT). Therefore, by adding a statistical model including temporal derivatives acquired from the pulse sequence utilised in the study (here regular ascending), the impact of slice timing difference can be reduced (Smith, 2002).

c) **Registration to the brain extracted anatomical image**

Each fMRI image was registered to the individual subject's brain-extracted T1-weighted anatomical image with 7 degrees of freedom (DOF); 2 degree of translation, 2 scale, 1 skew, 1 rotation, and 1 DOF to compensate for global scale.

d) **Spatial smoothing** was performed with a Gaussian kernel of 5 mm full-width at half maximum (FWHM). Noise level or random variation in image intensity is usually between 0.5 to 1 % of the average intensity. Spatial smoothing was therefore performed to increase the SNR, with the penalty of reducing the spatial resolution. Twice the voxel

dimension is generally recommended to be a reasonable value for smoothing (Russel 2011).

e) **fMRI registration**

Then, all the registered fMRI images were registered to the standard MNI152-1mm template image using FMRIB's Linear Image Registration Tool (FLIRT) (Jenkinson et al., 2002). MNI152 is an average image acquired from the MRI data of 152 healthy subjects (mean age 25 years) (Ashburner et al., 1997). The registration was performed with 12 DOF (3 degree of rotation, 3 translation, 3 scale, and 3 skew). After all EPI images were registered, they were visually inspected to ensure the quality of registration; none of the subjects were removed.

f) **High pass temporal filtering** using a Gaussian-weighted filter equivalent to 0.015 Hz was applied to remove low frequency artefacts typically caused by the scanner in the range of 0 and 0.015 Hz.

g) **Geometric unwarping** of EPIs using FUGUE was performed to correct for inhomogeneity caused by air-issue interfaces (Jenkinson, 2003)

h) **Low Pass filtering:** functional data were band pass filtered: 0.015-0.08 Hz. Low pass filter using in-house MATLAB code removed unwanted high frequency from physiological fluctuations like breathing (~ 0.3 Hz) or heartbeat (~1.0 Hz).

4.2.4.3 Functional connectivity

Finally, the following signals were all regressed out of the voxel-wise data: the six realignment parameters of rotation and translation, white matter and cerebrospinal fluid (CSF) signal, and the global brain signal (Fox et al., 2009). We then defined visuomotor-related ROIs in MNI space from 5 different resting-state networks (Figure 4.3) taken from a published atlas (Shirer et al., 2012). According to the study by Halko

et al. 2014, both left and right networks can be modulated in response to cerebellar stimulation:

(a) Bilateral sensorimotor network: anterior cerebellum, thalamus, primary and supplementary motor cortex,

(b) Bilateral basal ganglia network,

(c) Left executive control network: left dorsolateral prefrontal cortex (l-DLPFC), left parietal cortex (lPC), and right posterior cerebellum (rCB),

(d) Right executive control network: right dorsolateral prefrontal cortex (r-DLPFC), right parietal cortex (rPC), and left posterior cerebellum (lCB),

(e) Bilateral visuospatial network: intraparietal sulcus, and frontal eye fields (FEF).

A pre-defined ROI in the right posterior cerebellar cortex (rCB, taken from the left executive control network), underneath the anodal tDCS electrode, was chosen as the seed and registered to individual subject's fMRI data. I calculated correlations between the mean fMRI time series of the seed and the fMRI time series of all other voxels. Significant positively correlated voxels within my pre-defined sensorimotor network masks were counted and utilised later to correlate with the results from visuomotor adaptation task and MRS data (Figure 4.5)

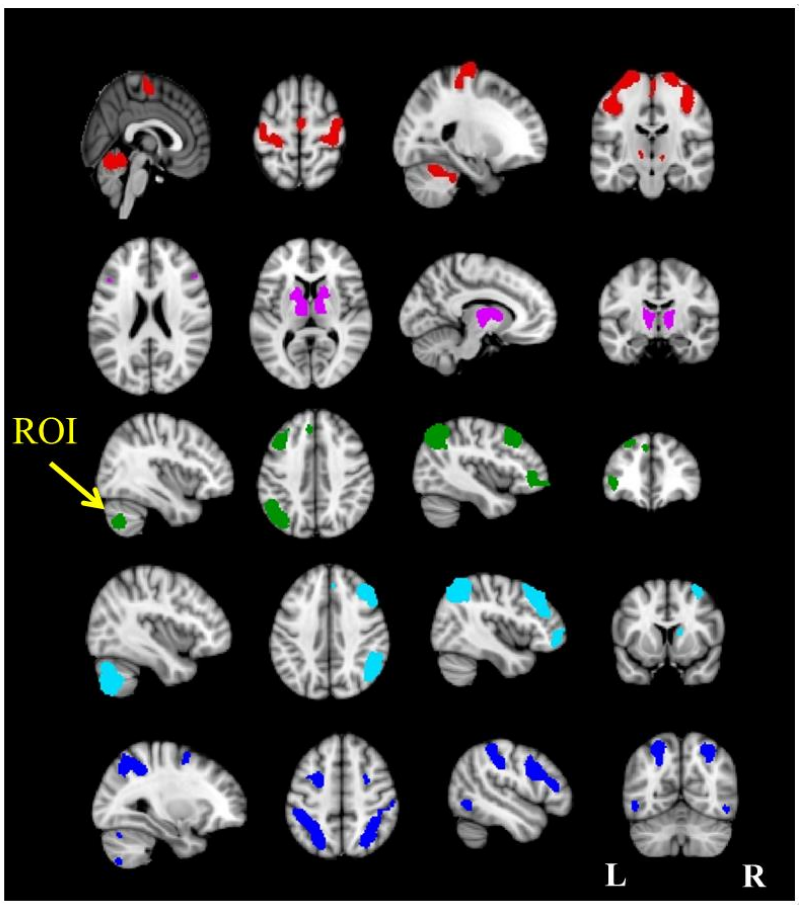

Figure 4.3 Masks utilised for functional connectivity analysis. From top to bottom: Sensorimotor network, Basal ganglia network, left executive control network, right executive control network, visuo-spatial network. A seed ROI was selected on the right posterior cerebellum (rCB) underneath the anodal electrode (pointed with a yellow arrow) and the average time course of the seed ROI was computed. Figure is adapted from (Shirer et al., 2012).

At the first level, statistical analysis was performed using FILM modelling (Woolrich et al., 2001) in FEAT (www.fsl.ox.ac.uk) to calculate individual whole-brain maps of both positive and negative functional connectivity with the cerebellar seed time series, separately for pre-, during and post-tDCS data. Subsequent higher level (mixed-effects FLAME 1+2) group average functional connectivity maps were then calculated. A multiple-comparisons correction was performed using cluster based thresholding ($p<0.05$). In order to assess group-level changes in functional connectivity as a result of

cerebellar tDCS (i.e., the difference between during- versus pre- or post- versus pre-tDCS) separate paired t tests were performed by setting up contrasts in FEAT.

Finally, individual measures of functional connectivity and MRS (GABA, GLX) concentrations or visuomotor performance, were compared using partial correlations, controlling for within-network functional connectivity correlations.

4.3 Results

4.3.1 Resting state functional connectivity and tDCS

I calculated correlations between the mean time series from the right cerebellar cortex seed region under the anodal tDCS electrode and all the pre-defined sensorimotor network masks. Paired t-tests were then carried out for each subject to compare the functional connectivity pre vs. during cerebellar tDCS and pre vs. post-cerebellar tDCS. The results demonstrated a significant decrease in functional connectivity between the right cerebellum (rCB) and right parietal cortex (rPC), and between the rCB and left frontal cortex (lFC) (Figure 4.4 A, B). In addition, there was a significant increase in connectivity between rCB and vermis, within the cerebellum itself (Figure 4.4 C)

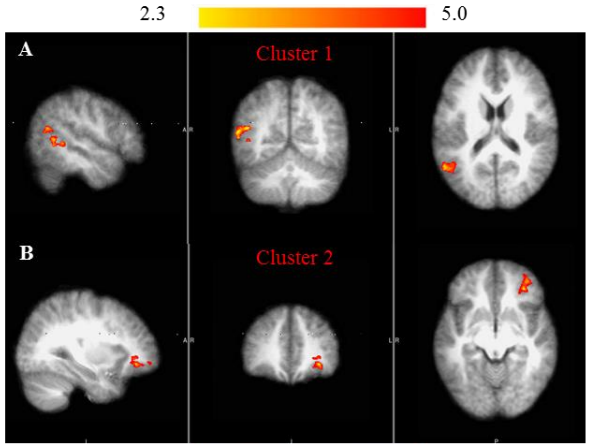

	Voxels	P	z-max	z-max (x-y-z) (mm)
Cluster 1	1874	0.047	5.01	-32, 40, -8
Cluster 2	2193	0.019	3.6	59, -58, 16

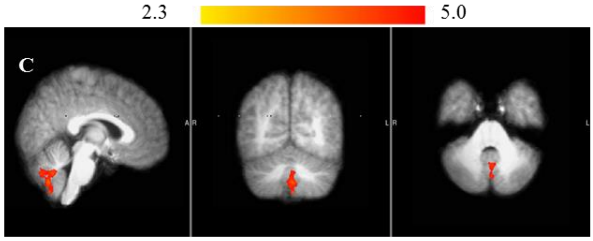

	Voxels	P	z-max	z-max (x-y-z) (mm)
Cluster 3:	1891	0.043	3.44	-2, -66, -45

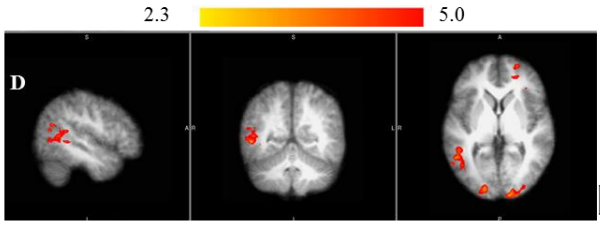

	Voxels	P	z-max	z-max (x-y-z) (mm)
Cluster 4:	4920	0.039	4.13	39, -27, 54

Figure 4.4 Changes in functional connectivity due to cerebellar tDCS. Cerebellar tDCS significantly decreased functional connectivity between a seed in the right cerebellum and two clusters; **(A)** Cluster 1: Right parietal cortex including angular gyrus, lateral occipital, superior division **(B)** Cluster 2: Left inferior frontal gyrus. Cerebellar tDCS also caused an increase in functional connectivity between the right cerebellum and **(C)** Cluster 3: vermis VIII, Left VIII, Left IX. **(D)** Cluster 4: To verify if the reduction in connectivity to rPC was directly influenced by rCB, or indirectly via lFC, another seed was located on lFC. Increased activation was observed in right postcentral and precentral gyrus, but not in Cluster 2. This suggests that the functional connectivity from the right cerebellum to rPC was not driven by an indirect pathway, rCB-lFC-rPC.

One would not expect right parietal cortex to be directly influenced by right cerebellum, as anatomical connections are crossed. To verify if the reduction in connectivity to rPC was directly influenced by rCB, or indirectly via lFC, I placed another seed on lFC and calculated maps of the voxel-wise group functional connectivity, using FEAT methods described previously. (Figure 4.4D). The connectivity between lPC and rPC increased during tDCS, but not in the same region of the previous cluster. In other words, this confirmed that cerebellar tDCS resulted in independent reductions of functional connectivity between rCB and both lFC and rPC.

4.3.2 Relationship between functional connectivity-GABA & functional connectivity-motor learning

Next, I wanted to examine whether the cerebellar tDCS induced changes in functional connectivity were correlated with performance during the visuomotor adaptation task across participants. Therefore, I calculated partial volume correlations between functional connectivity change and the performance in the late phase of adaptation, correcting for within networks correlations. There was only one significant positive correlation after this correction which was between performance in adapt 3 and the change in functional connectivity between rCB-left parietal cortex (lPC) (Pearson's r =+0.6, p= 0.03; Figure 4.5A). This suggests that those who performed better in the visuomotor adaptation task during cerebellar tDCS stimulation also showed stronger tDCS-induced changes in rCB-lPC functional synchronisation. Interestingly, no correlation was found between learning and either rCB-lFC (r=0.2, p=0.36) or rCB-rPC (r=0.4 , p=0.14), which were significantly altered by tDCS across all participants.

Finally, I investigated the relationship between tDCS-induced changes in GABA within the rCB and the changes in functional connectivity of rCB- left parietal cortex in 14 subjects (two subjects had to be removed from MRS due to unreliable spectrum). There was a strong trend towards a significant correlation between these two physiological changes (r=0.58, p=0.06; Figure 4.5B). However, this was driven by three participants

who exhibited a substantial decrease in GABA (>50%) and increase in functional connectivity between rCB-lFC (>100%) during cerebellar tDCS. These 3 participants (responders) also showed greater visuomotor adaptation compared to the rest of the anodal group (Figure 4.5C).

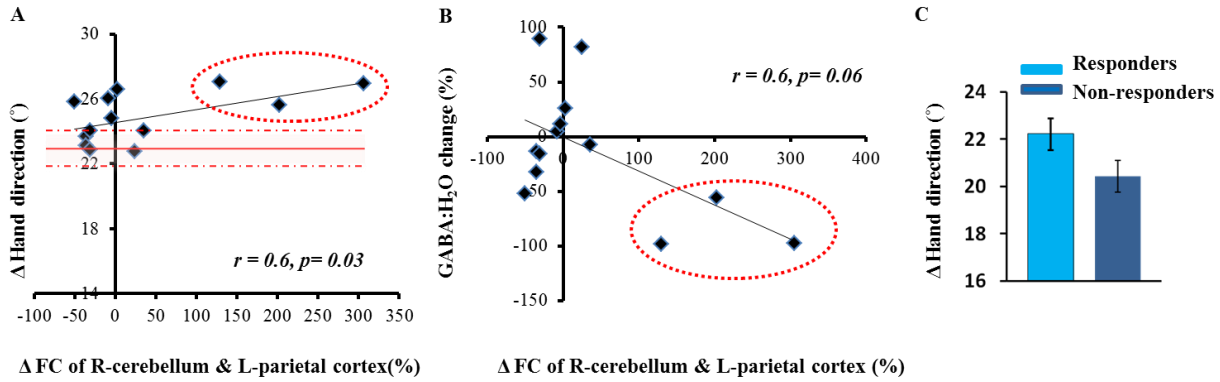

Figure 4.5 Individual differences in participant's response to cerebellar tDCS. (A) A correlation was observed between cerebellar tDCS-induced changes in functional connectivity between rCB-lPC and performance during late adaptation. (B) A weak correlation was observed between cerebellar tDCS-induced changes in GABA and the functional connectivity changes between rCB-lPC. However, both correlations were driven by three participants who showed a large decrease in GABA (>50%) and large increase in functional connectivity between rCB-lPC (>100%) (red circle). (C) These 3 participants (responders: light blue) also showed greater adaptation (adapt 3) compared to the rest of the anodal group (non-responders: dark blue).

4.4 Discussion

The results from chapter 3 and 4 revealed that the effects of cerebellar tDCS on visuomotor adaptation were correlated with a decrease in GABA and increase in connectivity between the cerebellar cortex and parietal cortex. However, these changes were only observed in approximately 21% of the participants suggesting an 'all-or-nothing' type effect of cerebellar tDCS.

4.4.1 Online cerebellar tDCS changes the functional connectivity between the cerebellum with frontal and parietal cortex

Cerebellar tDCS caused a significant decrease in resting-state connectivity between the cerebellum, left frontal cortex and right parietal cortex; however, this change was not correlated with participant's visuomotor adaptation performance. Recently, it has been shown that transcranial magnetic stimulation (TMS) over the lateral or midline cerebellum separately modulates the default network and dorsal attention network, respectively (Halko et al., 2014). My results support this work and suggest cerebellar tDCS could lead to changes in multiple resting state networks.

4.4.2 'All or nothing' type effect of cerebellar tDCS

Interestingly, I found that the only connectivity change in functional connectivity, which was correlated with participant's visuomotor adaptation performance, was an increase in connectivity between the cerebellum and left parietal cortex. Although not significant, there was also a strong trend for this increase in connectivity to be correlated with the decrease in GABA caused by cerebellar tDCS. However, these relationships were primarily driven by 3 participants who displayed a strong response to cerebellar tDCS across the 3 sessions; enhanced visuomotor adaptation, large reduction

in GABA (greater than 50%) and a large increase in connectivity between the cerebellum and left parietal cortex (greater than 100%). A decrease in GABA within the cerebellar cortex could reflect a decrease in Purkinje cell activity. Hypothetically, this may lead to reduced inhibition of the deep cerebellar nuclei and an increase in connectivity between the cerebellum and left parietal cortex. In addition, this explanation may also fit with models of motor learning that posit communication between the cerebellum and parietal cortex being crucial for successful visuomotor adaptation (Shadmehr and Krakauer, 2008). According to this model, the cerebellum predicts the motor command, whilst the posterior parietal cortex compares this prediction with the actual sensory (visual) feedback. This indicates that cerebellar tDCS may have an all-or-nothing type effect on individual participants with 21% showing substantial online changes in GABA and resting connectivity. These results could provide some explanation regarding the inconsistency of cerebellar tDCS in behavioural tasks (Conley et al., 2016, Minarik et al., 2016, Dyke et al., 2016) as significant differences between anodal and sham groups would be heavily dependent on the proportion of 'responders' within the anodal group. Being responder/ non-responder needs to be studied further, but it might be due to the genetics, the way how the cerebellar cortex is folded, direction of Purkinje cells, and skull thickness.

4.5 Conclusion

This study provides a novel insight into the neurophysiology underpinning cerebellar tDCS. These findings indicate an all-or-nothing type effect of cerebellar tDCS with a strong physiological and behavioural response being observed in 21% of participants. This provides a possible explanation why cerebellar tDCS is associated with between participant variability when applied to behavioural tasks.

5 NO CONSISTENT EFFECT OF CEREBELLAR TDCS ON VISUOMOTOR ADAPTATION

5.1 Introduction

The main part of chapter 5 has been accepted by Journal of Neurophysiology as an original article.

As explained in chapter 1, motor adaptation is a specific form of motor learning, which refers to the error reduction that occurs in response to a novel perturbation (Krakauer, 2009, Shadmehr and Mussaivaldi, 1994). Specifically, when we make a movement with a defined goal, i.e. reaching to a visual target, the brain compares the actual and predicted sensory outcome of the executed movement. A sensory prediction error can be induced by a systematic perturbation such as a visual rotation or force-field. This perturbation induces prediction errors that inform the brain of an environmental change (Miall and Wolpert, 1996, Wolpert et al., 1998). To return to accurate performance, the brain gradually updates its prediction, and resulting motor commands, so that it accounts for the new dynamics of the environment (Yamamoto et al., 2006, Tseng et al., 2007).

Patients with cerebellar lesions show a pronounced impairment in their ability to adapt to novel perturbations (Yamamoto et al., 2006, Criscimagna-Hemminger et al., 2010, Diedrichsen et al., 2005, Martin et al., 1996, Maschke et al., 2004, Rabe et al., 2009, Smith and Shadmehr, 2005, Weiner et al., 1983, Donchin et al., 2012). Specifically, they are often unable to reduce the movement error induced by the visual rotation or force-field. This suggests that the cerebellum is crucial during the feedforward process required for successful motor adaptation. Although patient studies can provide us with a good insight regarding cerebellar function, there is a scarcity of patients with isolated cerebellar lesions. In addition, testing patients leaves the possibility that some changes, or the lack of them, are due to long-term compensation by other brain areas.

An alternative approach to investigate cerebellar function is to use non-invasive brain stimulation such as transcranial direct current stimulation (tDCS) in healthy participants. As mentioned previously, Galea et al., (2011) applied tDCS over the cerebellum during adaptation to a visual rotation (visuomotor adaptation). It was found

that anodal cerebellar tDCS led to faster adaptation, relative to either primary motor cortex (M1) anodal tDCS or sham tDCS (Galea et al., 2011). Such positive effects of cerebellar tDCS on cerebellar function have been replicated in visuomotor adaptation (Galea et al., 2011, Cantarero et al., 2015, Hardwick and Celnik, 2014, Block and Celnik, 2013), force-field adaptation (Herzfeld et al., 2014), saccade adaptation (Panouilleres et al., 2015, Avila et al., 2015), motor skill learning (Cantarero et al., 2015), and language prediction tasks (Miall et al., 2016). As a result, it has been suggested that cerebellar tDCS is a possible clinical technique to restore cerebellar function in patients suffering cerebellar-based disorders (Grimaldi et al., 2014). However, the number of studies reporting inconsistencies regarding the impact of cerebellar tDCS or having no effect on motor learning is increasing. These contradictory findings may call into question the validity of using cerebellar tDCS within a clinical context where a robust and consistent effect across behaviour is required (Mamlins et al., 2016, Steiner et al., 2016).

Therefore, in this chapter, I examined the influence of anodal cerebellar tDCS on visuomotor adaptation across a range of different task parameters. Specifically, I examined whether cerebellar tDCS produced a reliable behavioural effect when manipulating task parameters such as screen orientation, tDCS machine type, tDCS timing, tool-use, tDCS montage, and the perturbation schedule.

5.2 Materials and methods

5.2.1 Participants

218 healthy young individuals participated in this study (40 male, 25 ± 5 yrs). Each participated in one of nine experiments and received either anodal or sham cerebellar tDCS. All were blinded to the stimulation, naïve to the task, self-assessed as right handed, had normal/corrected vision, and reported to have no history of any

neurological condition. The study was approved by Ethical Review Committee of the University of Birmingham and was in accordance with the declaration of Helsinki. Written informed consent was obtained from all participants. Participants were recruited through online advertising and received monetary compensation upon completion of the study. At the end of the session, participants were asked to report their attention, fatigue, and quality of sleep using a questionnaire with a scale from 1-7, and also reported their perceived tDCS as active (1) or placebo (0), and their hours of sleep in the previous night (Table 5.1). These self-reports were collected from 192 participants, excluding one from experiments 1 and 2, thirteen (either anodal or sham) from experiment 7 and all 13 sham participants from experiment 9.

5.2.2 Experimental Procedure

Participants were seated, with their chin supported by a rest, in front of a computer monitor (30-inch; 1280×1024 pixel resolution; 105 cm from chin rest). A Polhemus motion tracking system (Colchester, VT, USA) was attached to their pronated right index finger and their arm was placed underneath a horizontally suspended wooden board, which prevented direct vision of the arm (Figure 5.1A). This was unlike the original Galea et al., (2011) study where participants used a digitised pen and wore goggles to prevent vision of their hand. The visual display consisted of a 1cm-diameter starting box, a green cursor (0.25cm diameter) representing the position of their index finger, and a circular white target (0.33cm diameter). For all experiments, targets appeared in 1 of 8 positions (45˚ apart) arrayed radially at 8 cm from the central start position. Targets were displayed pseudo-randomly so that every set of 8 consecutive trials (an "epoch") included 1 movement towards each target position. Participants controlled the green cursor on the screen by moving their right index finger across the table (Figure 5.1A). At the beginning of each trial, participants were asked to move their index finger to the start position and a target then appeared. Participants were instructed to make a fast 'shooting' movement through the target such that online corrections were

effectively prevented. At the moment the cursor passed through the invisible boundary circle (an invisible circle centred on the starting position with an 8 cm radius), the cursor was hidden and the intersection point was marked with a yellow square to denote the terminal (endpoint) error. In addition, a small square icon at the top of the screen changed colour based on movement speed. If the movement was completed within 100-300 msec, then it remained white. If the movement was slower than 300 msec, then the box turned red (too slow). Importantly, the participants were reminded that spatial accuracy was the main goal of the task. After each trial subjects moved back to the start, with the cursor only reappearing once they were within 2cm of the central start position.

5.2.3 Transcranial direct current stimulation (tDCS)

Anodal tDCS was delivered (NeuroConn, Germany; Figure 5.3A) through two 5 x 5 cm^2 electrodes soaked in a saline solution unless otherwise specified. The anodal electrode was placed over the right cerebellar cortex, 3 cm lateral to the inion. The cathodal electrode (reference) was placed over the right buccinator muscle (Galea et al., 2011) unless otherwise specified. At the onset of stimulation, current was increased in a ramp-like fashion over 1 second. In the anodal groups, a 2 mA current (current density 0.08 A/cm2) was applied for up to 25 minutes. As adaptation involved additional trials, cerebellar tDCS was applied for ~8 minutes longer than in the original study (Galea et al., 2011). In the sham groups, tDCS was applied for 10 seconds before being ramped down over 1 second turned off. Participants were blinded to whether anodal or sham was applied (Table 5.1).

5.2.4 Experiment 1: Vertical screen

The aim of experiment 1 was to replicate the findings of Galea et al., (2011). However, unlike the original Galea et al., (2011) study, participants did not use a digitising pen

and did not wear goggles to prevent vision of their hand. 28 participants (8 male, 21 ± 4 yrs) were exposed to 8 blocks of 96 trials (12 repetitions of the 8 targets) during a reaching task in which the computer screen was placed in a vertical position (Figure 5.1B). The first 2 blocks acted as baseline and consisted of veridical feedback with (pre 1) and without (pre 2) online visual feedback. During no visual feedback trials, the target was visible, but once the subjects had moved out of the starting position the cursor indicating their hand position was hidden. In addition, subjects did not receive terminal feedback. Participants were instructed to continue to strike through the target. Following this, participants were exposed to 3 blocks (adapt 1-3) of trials in which an abrupt 30° counter clockwise (CCW) visual rotation (VR) was applied. Finally, to assess retention, three blocks (post 1-3) were performed without visual feedback. TDCS was applied from the start of pre 2 until the end of adapt 3 and lasted for approximately 25 minutes (Figure 5.1B).

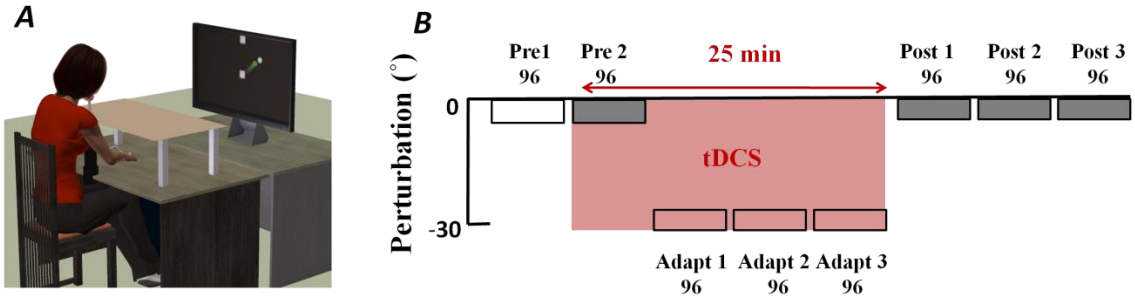

Figure 5.1 Experiment 1: (A) Participants sat behind a table facing a vertically-orientated screen 105 cm from their face with their chin supported on a chin rest and sensor was attached to their right index finger. The visual transformation between hand trajectory and cursor was similar to a computer mouse. (B) Abrupt counter-clockwise 30˚ counter-clockwise VR protocol: Following 2 baseline blocks (96 trials: pre 1-2), an abrupt 30˚ visual rotation (VR) was applied to the screen cursor and was maintained across 3 blocks (adapt 1-3). Cerebellar tDCS (anodal/sham) was applied from pre 2 until adapt 3 (pink area). Following this, retention was examined by removing visual feedback (grey) for the final 3 blocks (post 1-3).

5.2.5 Experiment 2: Horizontal screen

A large proportion of motor learning studies are performed whilst the visual feedback is provided in the same plane as the movement (Shabbott and Sainburg, 2010). Therefore, experiment 2 investigated whether the positive influence of cerebellar tDCS on visuomotor adaptation was observed when the screen orientation was flipped to a horizontal position (Figure 5.2B). 20 participants (5 male, 22 ± 4 yrs) were split into two groups (anodal/sham; 10 in each group) and experienced an identical experimental protocol as in experiment 1 (Figure 5.1B), except now the participants pointed with their semi-pronated right index finger underneath a horizontally suspended mirror. The mirror prevented direct vision of the hand and arm, but showed a reflection of a computer monitor mounted above that appeared to be in the same plane as the finger (Figure 5.2B). Once again, participants controlled a cursor on the screen by moving their finger across the table.

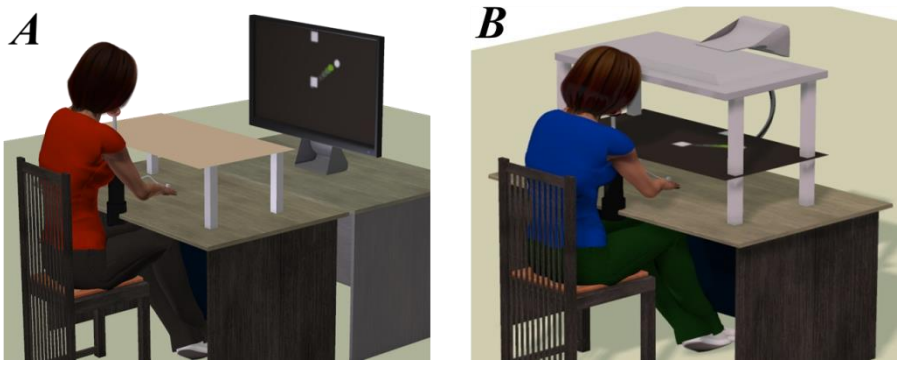

Figure 5.2 Experiment 2: **(A)** Vertical set up; participants sat behind a table facing a vertically-orientated screen 105 cm from their face with their chin supported on a chin rest and sensor was attached to their right index finger. The visual transformation between hand trajectory and cursor was similar to a computer mouse. **(B)** Horizontal screen set up; participants sat in front of a horizontally suspended mirror. The mirror prevented direct vision of the hand and arm, but showed a reflection of a computer monitor mounted above that appeared to be in the same plane as the hand.

5.2.6 Experiment 3: tDCS machine

Several studies with significant effect of cerebellar tDCS on motor adaptation used Phoresor machine (Chattanooga, USA) (Galea et al., 2009, Galea et al., 2011, Herzfeld et al., 2014, Cantarero et al., 2015). Therefore, in experiment 3, I used the Phoresor machine. As a result, this was a closer replication of the experiment that used in Galea et al., (2011). 14 participants (1 male, 22 ± 5 yrs) experienced anodal cerebellar tDCS with an identical experiment protocol as experiment 1, and compared with the sham group of experiment 1 (Figure 5.3 B).

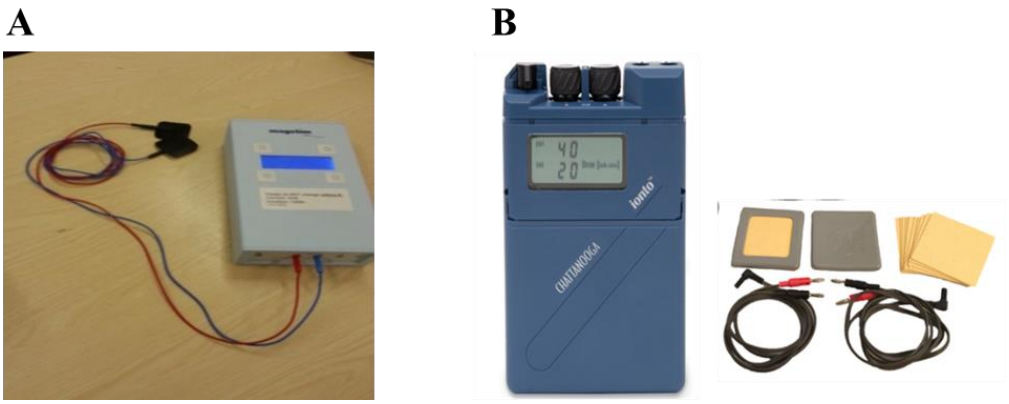

Figure 5.3 Experiment **3: (A)** NeuroConn tDCS device passed 0.08mA/cm2 through the skull. The stimulator did not start working until getting the skin low enough impedance (<55 kΩ). **(B)** Phoresor tDCS device was adjusted to pass 0.08mA/cm2 through the skull, automatic ramping up and down.

The current density was 0.08 mA/cm^2 for both machines, However, NeuroConn did not start working until skin impedance is low enough (<55 kΩ), whereas the Phoresor always worked regardless of skin impedance level. Current in NeuroConn was adjusted to ramp up and down (e.g. 1 sec), but for Phoresor, it ramped up and down automatically in 30 sec.

5.2.7 Experiment 4: Tool use

Several visuomotor studies have required participants to hold a digitising pen instead of a sensor attached to their finger (Figure 5.4A) (Galea et al., 2011, Schlerf et al., 2012). Therefore, in experiment 4, we changed the motion tracking arrangement so that the Polhemus sensor was attached to the bottom of a pen shaped tool (Figure 5.4B). As a result, this was a closer replication of the task design used in Galea et al., (2011) than experiment 1. However, unlike Galea et al., (2011) participants did not wear goggles that restricted vision of the hand. 27 subjects (2 male, 21 ± 4 yrs) were split into two groups (14 anodal/13 sham) and experienced an identical experimental protocol as experiment 1 (Figure 5.1B) except that now participants controlled the cursor on the screen by holding the 'pen' and moving it across the surface of the table (Figures 5.1A & 5.4B).

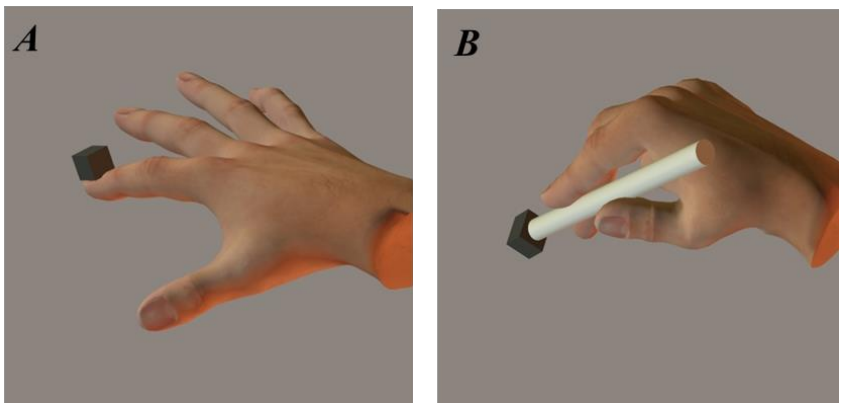

Figure 5.4 Experiment **4: (A)** Finger; Initial experiment started with the Polhemus sensor attached to the right index finger. **(B)** Pen tool; Sensor was attached to a pen-shape tool. Participants were asked to hold the top part of the pen.

5.2.8 Experiment 5: Montage

Modelling studies have suggested that altering the position of the reference (cathode) electrode leads to substantial changes in the neural effects of tDCS (Mehta et al., 2015). As several other studies have used a different reference electrode position for cerebellar tDCS (Benussi et al., 2015, Sebastian et al., 2016), I investigated whether the beneficial effects of anodal tDCS on visuomotor adaptation was maintained when using this alternative reference electrode position (placed on the right deltoid muscle ; Figure 5.5B). Therefore, 14 participants (2 male, 19 ± 1 yrs) were tested with anodal tDCS and experienced an identical experimental protocol as experiment 1 (Figure 5.1B) to compare with the sham group in experiment 1.

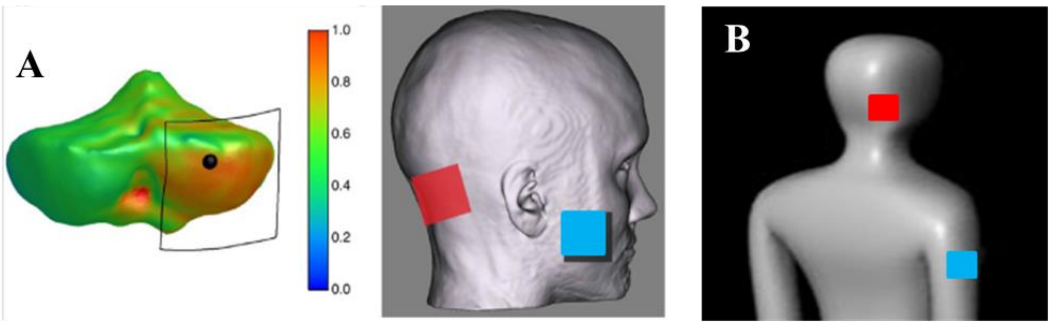

Figure 5.5 Experiment **5: (A)** Unilateral hemispheric montage with reference on the face was mainly used to target the anterior and posterior of the cerebellum with the least drift to the neighbouring areas. Modified from Rampersad et al. (2014). **(B)** Unilateral hemispheric montage with reference on the unilateral shoulder was used to target the posterior of the cerebellum. Modified from: http://www.ehw.ieiit.cnr.it/?q=emfmed

5.2.9 Experiment 6: Offline cerebellar tDCS

Previous works have applied anodal cerebellar tDCS during rest and found both physiological and behavioural changes after the cessation of stimulation (Galea et al., 2009, Pope and Miall, 2012). This indicates that anodal cerebellar tDCS applied during rest (offline tDCS) could have a beneficial effect on visuomotor adaptation tested after the cessation of stimulation. To examine this, 24 participants (7 male, 20 ± 4 yrs) were split into 2 groups (anodal/sham: 12 in each group) and experienced a 25 minute rest period between pre 2 and adapt 1 instead of during adapt (Figure 5.6A). During this time, offline anodal cerebellar tDCS was applied (Figure 5.6B) whilst participants sat quietly and kept their eyes open. In order to maintain a similar overall task length, retention (no visual feedback) was not assessed. All other task parameters (vertical screen, tDCS montage) were identical to experiment 1.

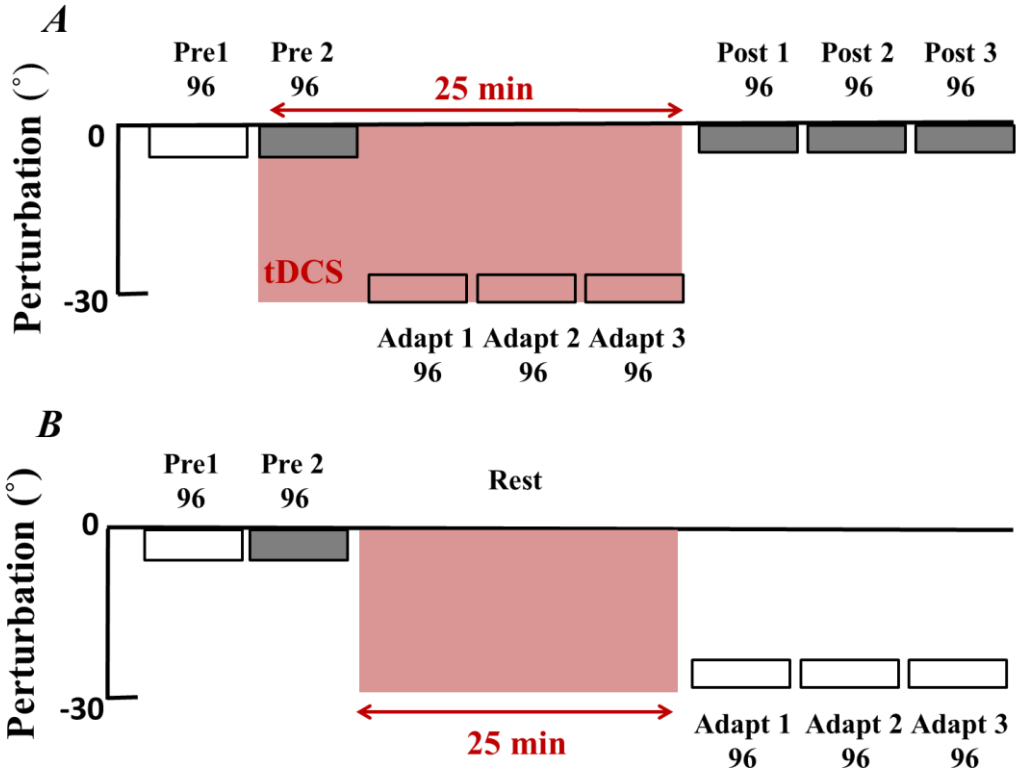

Figure 5.6 Experiment **6: (A)** Online cerebellar tDCS protocol: In all experiments, cerebellar tDCS (anodal/sham) was applied during adapt, from pre 2 until adapt 3 (pink area). Following this, retention was examined by removing visual feedback (grey) for the final 3 blocks (post 1-3). **(B)** Offline cerebellar tDCS protocol: cerebellar tDCS (anodal/sham) was applied for 25 minutes during rest between pre2 and adapt 1. Due to the length of the experiment, retention (no visual feedback blocks) was not examined.

5.2.10 Experiment 7 & 8: Step and gradual perturbation schedules

Visuomotor adaptation involves multiple learning mechanisms whose contribution to performance is determined by task parameters (McDougle et al., 2015). For instance, McDougle suggest that large abrupt visual rotations reduce cerebellar-dependent learning from sensory-prediction errors and enhance strategic learning (development of a cognitive plan). In contrast, smaller gradual visual rotations are thought to bias responses towards sensory-prediction error learning. If true, then cerebellar tDCS should have a particularly beneficial effect on adaptation when the 30˚ visual rotation is introduced either through a multiple small steps (visual rotation is introduced in 3 steps of 10˚; Experiment 7) or a gradual paradigm (visual rotation is introduced gradually by 0.156˚ per trial; Experiment 8).

For experiment 7, 36 participants (1 male, 20 ± 1 yrs) were split into 2 groups (anodal/sham; 18 in each group). Following 2 baseline blocks (64 trials) with (pre 1) and without (pre 2) visual feedback, 3 adaptation blocks (96 trials; adapt 1-3) exposed participants to a 10°, 20°, and 30° CCW visual rotation (Figure 5.7A). To examine the degree of cognitive strategy used by each participant, we included a task developed by Taylor et al., (2014). Specifically, following adapt block 3, participants were asked to verbally report the direction they were aiming towards (explicit). For these trials (16 in total), the target was presented at the centre of a semi-circular arc of numbers displayed at 5º intervals. CW of the target were negative numbers from 1-19, and CCW of the target were positive numbers from 1-19. Participants were asked to report which number they were planning to move their finger towards (Bond and Taylor, 2015, Taylor et al., 2014). Once they had provided this verbal response, the numbers disappeared and the participants performed the reaching movement without visual feedback. If a participant was fully aware of the visual rotation, they would report reaching towards number -6 (30˚ CW). Whereas if they were unaware, participants would report aiming to 0 despite moving their finger 30° CW. Finally, a single block (192 trials) without visual feedback examined retention (post).

For experiment 8, 32 participants (4 male, 19 ± 1 yrs) were split into 2 groups (anodal/sham; 16 in each group). Following 2 baseline blocks (64 trials) with (pre 1) and without (pre 2) visual feedback, 1 long adaptation block (288 trials; adapt 1) involved the 30° CCW visual rotation being applied at rate of 0.156˚ per trial over 192 trials (Figure 5.7B). The rotation was then maintained at 30° for a further 96 trials. Participant's level of cognitive strategy was again assessed (16 trials; explicit) after adaptation. Following this, one block of 192 trials without visual feedback examined retention (post).

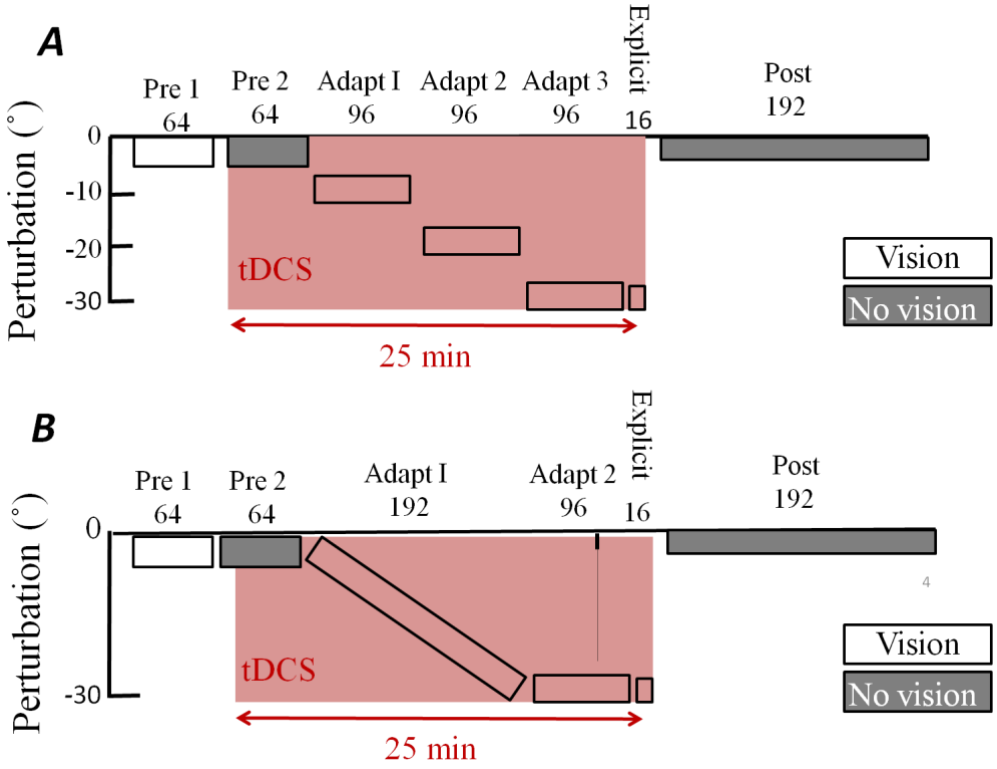

Figure 5.7 Experiment 7 & 8: (A) Step adaptation protocol: Following 2 baseline blocks (64 trials: pre 1-2), a 30˚ VR was applied to the cursor in steps of 10˚ per block (96 trials: adapt 1-3). A short block (16 trials; explicit) followed this in which participants verbally reported their planned aiming direction. This is thought to measure the participant's level of cognitive strategy (Taylor et al., 2014). Finally retention was examined through 1 long block (192 trials) with no visual feedback. (B) Gradual adaptation protocol: A 30˚ VR was applied to the cursor gradually (0.156˚ per trial) across 192 trials. It was then maintained at 30˚ for 96 trials (Adapt).

5.2.11 Experiment 9

Finally, I aimed to validate the results of experiment 1 by using the same task parameters in a new set of participants. Therefore, 26 participants (7 male, 21 ± 4yrs) were split into two groups (anodal/sham; 13 in each group) and exposed to the same protocol as utilised in experiment 1.

5.2.12 Data analysis

The 2-D index finger (X & Y) position data was collected at 120 Hz. For each trial, angular hand direction (°) was calculated as the difference between the angular hand position and angular target position at the point when the cursor intersected an 8-cm invisible circle centred on the starting position. During veridical feedback, the goal was for hand direction to be 0°. However, with a visuomotor rotation and hand direction had to compensate; that is, for a −30° (CCW) visuomotor rotation, a hand direction of +30° relative to the target was required. Positive values indicate a CW direction, whereas negative values indicate a CCW direction. In addition, reaction time (RT: difference between target appearing and the participant moving out of the start position) and movement time (MT: difference between reaction time and movement end) were calculated for each trial. We removed any trial in which hand direction, RT or MT exceeded 2.5 standard deviations above the group mean. This accounted for 7.68 ± 3.54% of trials. One participant in experiment 4 was removed from the study as a result of failing to follow the task instructions.

Epoch averages were created by binning 8 consecutive movements, 1 towards each target. For each participant, average hand direction was calculated for each target position for pre1 (vision baseline) and pre2 (no vision baseline). These values were then subtracted to trial-by-trial performance to that particular target in each visual feedback

condition (Δ hand direction). Specifically, pre1 was subtracted away from adaptation performance and pre2 was subtracted away from retention performance. For baseline, we averaged hand direction across all epochs of pre1 and pre2 and compared the anodal and sham groups' using 2-tailed independent sampled t-tests. For adaptation, I initially compared Δ hand direction in the first trial of adapt 1 to ensure all participants experienced a similar initial error in response to the visuomotor rotation. I then calculated an average across all the epochs of adaptation excluding epoch 1. I believe this best represented the total amount of adaptation expressed by each participant. For retention, I averaged Δ hand direction across all the epochs of retention. For each experiment, the anodal and sham groups were compared using 2-tailed independent sampled t-tests. The threshold for all statistical comparisons was $P < 0.05$. Effect sizes are reported as Cohen's *d*. All data presented represent mean ± standard error of the mean, unless otherwise specified. Data and statistical analysis was performed using MATLAB (The MathWorks, USA) and SPSS (IBM, USA).

5.3 Results

5.3.1 Experiment 1: vertical screen

Despite a slightly different set up from Galea et al., (2011), I showed that anodal cerebellar tDCS led to a greater amount of adaptation relative to sham cerebellar tDCS (Figure 5.8). First, both groups behaved similarly during baseline with there being no significant differences between groups during pre1 or pre 2 (Table 5.2). In addition, when initially exposed to the 30° VR, both groups showed a similar level of performance during the first epoch of adapt 1 (Table 2). However, following this, the anodal group displayed a greater amount of adaptation to the VR compared to the sham group ($t_{(26)} = 2.9$, $p=0.007$, $d=1.17$). Retention in the anodal group appeared to be greater than in the sham group; however this did not reach statistical significance ($t_{(26)}$

=1.2, p=0.24, d=0.4). There were no significant differences between groups for either RT or MT during adaptation or retention (Table 5.3).

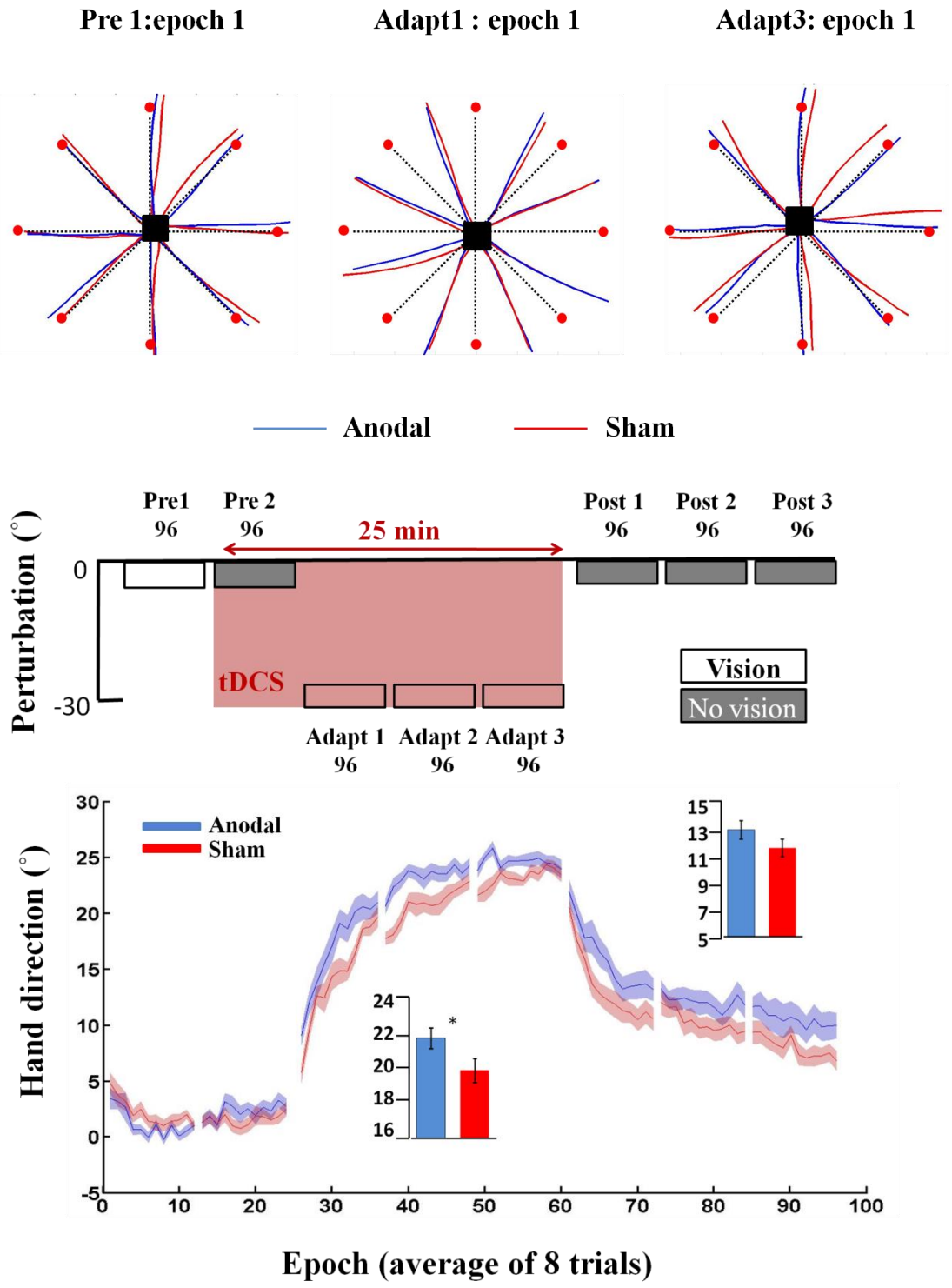

Figure 5.8 **(A)** Kinematic data for two sample participants in experiment 1 (blue = anodal; red = sham). Both participants performed similarly during pre1 (left). In addition, they showed similar initial error when exposed to the 30 degree CCW visual rotation (Middleton and Strick). However, by the end of adaptation the participant in the anodal group displayed a reduced amount of error in their movement trajectories (Sebastian et al.). **(B)** Experiment 1: Vertical screen. Epoch (average across 8 trials) uncorrected angular hand direction (˚) data for the anodal (blue) and sham (red) cerebellar tDCS groups. Positive values indicate CW hand direction. Bar graphs inset indicate mean hand direction for the anodal and sham groups during adaptation (adapt 1-3) and retention (post 1-3). This was determined for each participant by averaging consecutive epochs (see Methods). Independent t-tests compared these values between groups. Solid lines, mean; shaded areas/error bars, S.E.M. There was significant difference between the anodal and sham cerebellar tDCS groups (14 in each group) during adaptation ($t_{(26)}$= 2.9, p=0.007, *d*=1.17).

5.3.2 Experiment 2: Horizontal screen

In experiment 2, an identical stimulation and testing protocol as experiment 1 was used; however now the visual feedback was in the same plane as the movement (horizontal screen). Surprisingly, anodal cerebellar tDCS was no longer associated with greater adaptation (Figure 5.9). First, we found no significant differences between groups for pre 1, pre 2 or the first trial of adapt 1 (Table 5.2). In addition, there were no significant differences between the anodal or sham groups during adaptation ($t_{(18)}$ =-0.005, p=0.9, d=0.002; Figure 5.9) or retention ($t_{(18)}$ =0.39, p=0.69, d=0.14). Finally, there were no significant differences between groups for either RT or MT during adaptation or retention (Table 5.3).

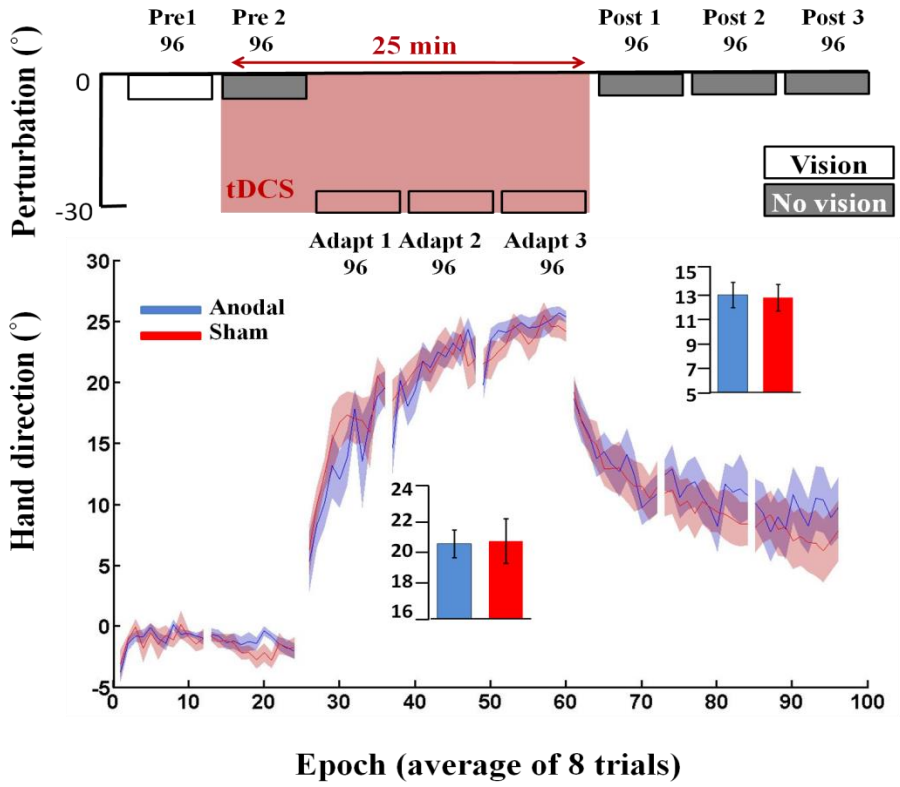

Figure 5.9 Experiment 2: Horizontal screen. Epoch (average across 8 trials) uncorrected angular hand direction (^{0}) data for the anodal (blue) and sham (red) groups. Positive values indicate CW hand direction. Bar graphs inset indicate mean hand direction for the anodal and sham groups during adaptation (adapt 1-3) and retention (post 1-3). This was determined for each participant by averaging consecutive epochs (see Methods). Independent t-tests compared these values between groups. Performance of both groups was identical. Solid lines, mean; shaded areas/error bars, S.E.M. There was no significant difference between the anodal and sham cerebellar tDCS groups (10 in each group) during adaptation ($t_{(18)}$=-0.005, p=0.9, d=0.002).

5.3.3 Experiment 3: tDCS machine

In experiment 3, an identical stimulation and testing protocol as experiment 1 was used; however, the anodal group were stimulated with a Phoresor machine. Their performance was compared with the 14 sham participants of experiment 1. First, I found no significant differences between groups for pre 1, pre 2 or the first trial of adapt 1 (Table 5.2). In addition, there was no significant difference between anodal and sham during adaptaion ($t_{(26)}$=0.09, p=0.93, d=0.22; Figure 5.10) or retention ($t_{(26)}$ =0.20, p=0.84, d=0.08). Finally, there were no significant differences between groups for either RT or MT during adaptation or retention (Table 5.3).

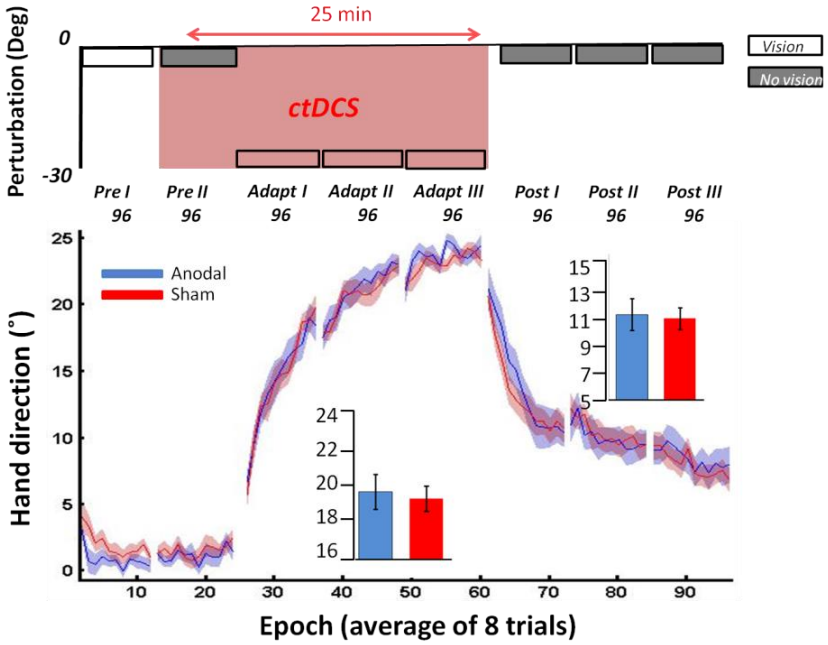

Figure 5.10 Experiment 3: TDCS machine. Epoch (average across 8 trials) uncorrected angular hand direction data for the anodal (blue) and sham (red) groups. Positive values indicate CW hand direction. Bar graphs inset indicate mean hand direction for the anodal and sham groups during adaptation (adapt 1-3) and retention (post 1-3). This was determined for each participant by averaging consecutive epochs (see Methods). Independent t-tests compared these values between groups. No significant difference was observed in any of the blocks (all p>0.05). Solid lines, mean; shaded areas/error bars, S.E.M. There was no significant difference between the anodal and sham cerebellar tDCS groups (14 anodal/13 sham) during adaptation ($t_{(26)}$=0.09, p=0.93, d=0.22).

5.3.4 Experiment 4: Tool use

In experiment 4, participants experienced an identical protocol as experiment 1; however, instead of performing the task with the sensor attached to their index finger, they held a digitising pen. This experimental manipulation led to the anodal and sham cerebellar tDCS groups behaving similarly across all experimental blocks (Figure 5.11). Specifically, there were no significant differences between groups during pre 1, pre 2 or the first trial of adapt 1 (Table 5.2). In addition, no significant differences were observed during adaptation ($t_{(25)}$= -0.28, p=0.78, d=0.09; Figure 5.11) or retention ($t_{(25)}$= -1.15, p=0.13, d=0.6). Finally, there were also no significant differences between groups for either RT or MT during adaptation or retention (Table 5.3).

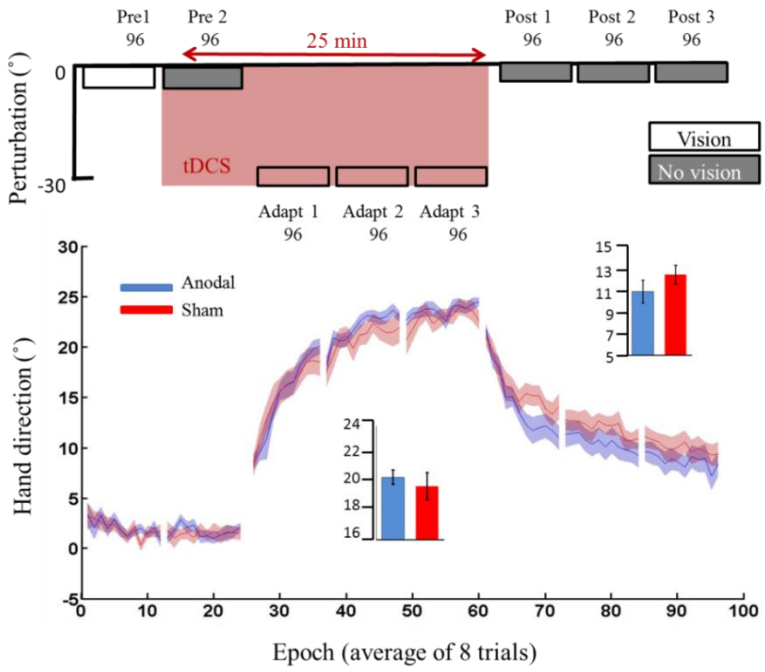

Figure 5.11 Experiment 4: tool. Epoch (average across 8 trials) uncorrected angular hand direction (^{0}) data for the anodal (blue) and sham (red) groups. Positive values indicate CW hand direction. Bar graphs inset indicate mean hand direction for the anodal and sham groups during adaptation (adapt 1-3) and retention (post 1-3). This was determined for each participant by averaging consecutive epochs (see Methods). Independent t-tests compared these values between groups. Solid lines, mean; shaded areas/error bars, S.E.M. There was no significant difference between the anodal and sham cerebellar tDCS groups (14 anodal/13 sham) during adaptation ($t_{(25)}$=- 0.28, p=0.78, d=0.09).

5.3.5 Experiment 5: Montage

Once again, participants experienced an identical protocol as experiment 1; however, this time cerebellar tDCS reference electrode was on their right shoulder. There were no significant differences between groups during pre 1, pre 2 or the first trial of adapt 1 (Table 5.2). In addition, we found no significant differences between the anodal or sham groups during ($t_{(25)}$= 0.80, p= 0.43, d=0.29; Figure 5.12) or retention ($t_{(25)}$= -1.14, p=0.85, d= 0.45). Finally, there were also no significant differences between groups for either RT or MT during adaptation or retention (Table 5.1).

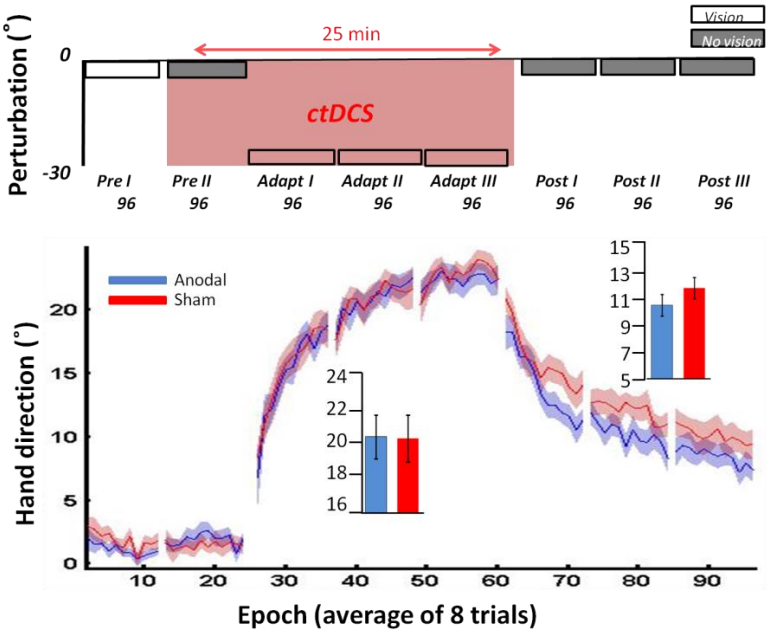

Figure 5.12 Experiment 5: Cerebellar tDCS montage. Epoch (average across 8 trials) uncorrected angular hand direction (°) data for the anodal (blue) and sham (red) groups. Positive values indicate CW hand direction. Bar graphs inset indicate mean hand direction for the anodal and sham groups during adaptation (adapt 1-3) and retention (post 1-3). This was determined for each participant by averaging consecutive epochs (see Methods). Independent t-tests compared these values between groups. Solid lines, mean; shaded areas/error bars, S.E.M. There was no significant difference between the anodal and sham cerebellar tDCS groups (14 anodal/13 sham) during adaptation ($t_{(25)}$=0.80, p=0.43, d=0.29).

5.3.6 Experiment 6: Offline cerebellar tDCS

Next, experiment 6 examined whether cerebellar tDCS applied offline (during 25 mins of rest) had a beneficial effect on subsequent visuomotor adaptation. Contrary to my predictions, offline anodal cerebellar tDCS did not cause greater adaptation relative to offline sham cerebellar tDCS (Figure 5.13). Unfortunately, there was a significant difference between groups during pre 1, suggesting a small variation (approx. 1˚) in baseline performance between groups. However, after correcting the baseline, there was no significant difference between the anodal and sham cerebellar tDCS groups during adaptation when using either hand direction ($t_{(21)}$=0.37, p=0.71, d=0.15). Lastly, there were no significant differences between groups for either RT or MT during adaptation or retention (Table 5.3). Because of the extended rest period prior to the adaptation phase (Figure 5.13), this experiment did not include a retention block.

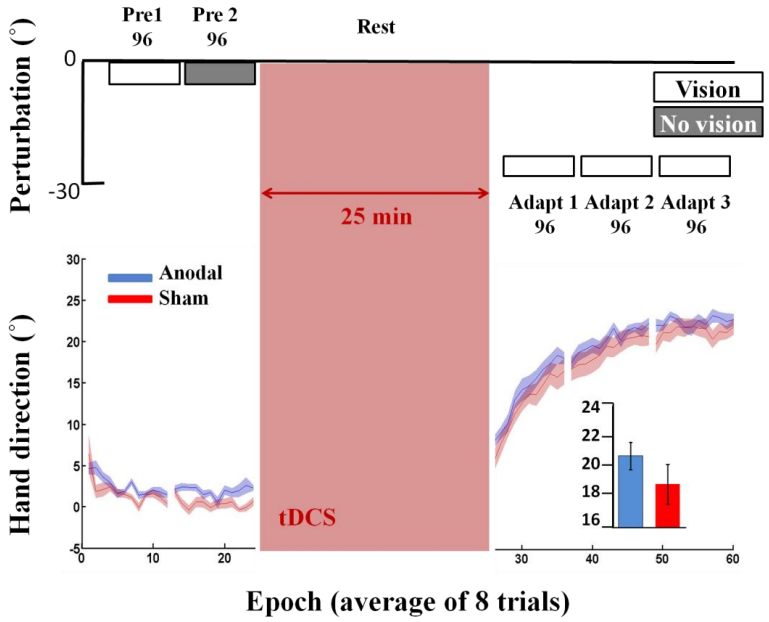

Figure 5.13 Experiment 6: offline cerebellar tDCS. Epoch (average across 8 trials) uncorrected angular hand direction (°) data for the anodal (blue) and sham (red) groups. Positive values indicate CW hand direction. Bar graphs inset indicate mean hand direction for the anodal and sham groups during adaptation (adapt 1-3). This was determined for each participant by averaging consecutive epochs. Independent t-tests compared these values between groups. There was a clear difference between groups during pre 1. However,

there were no significant differences between groups during adaptation when using either hand direction or Δ hand direction (each participant's average hand direction during pre 1 was subtracted from their subsequent performance). Solid lines, mean; shaded areas/error bars, S.E.M. There was no significant difference between the anodal and sham cerebellar tDCS groups (12 anodal/ 11 sham) during adaptation ($t_{(21)}$=0.37, p=0.71, d=0.15).

5.3.7 Experiment 7 & 8: Step and gradual perturbation schedules

Finally, experiments 7 and 8 tested whether anodal cerebellar tDCS was more effective when the 30˚ visual rotation was introduced either with a stepped (visual rotation was introduced in three steps of 10˚; Experiment 7) or gradual paradigm (visual rotation was introduced gradually by 0.156˚ per trial; Experiment 8). However, once again, I found no significant effect of anodal cerebellar tDCS on adaptation (Figures 5.14 and 5.15).

In experiment 7, there were no significant differences between the anodal and sham groups during pre 1, pre 2 or when initially exposed to the 10˚ VR (Table 5.2). In addition, no significant differences were observed across adaptation ($t_{(34)}$=-0.35, p=0.72, d=0.1; Figure 5.14) or retention ($t_{(34)}$=-0.9, p=0.37, d=0.3). To examine the degree of cognitive strategy used by each participant, after adapt 3 I asked participants to verbally report the direction they were aiming towards (Figure 5.14A, explicit). Despite displaying a hand direction of approximately 20-25˚ (Figure 5.14), both groups reported a similar aiming direction towards the target (Anodal explicit report: 1.7 ± 2.1^0, Sham: 1.4 ± 4.1^0, independent t-test $t_{(34)}$=0.47, p=0.64, d=0.09). This indicates that all participants had developed only a minimal cognitive aiming strategy. During this explicit block, although there was no significant difference between groups for Δ hand direction ($t_{(34)}$=-1.8, p=0.07, d=0.61), there did appear to be a trend for the anodal group to display reduced hand direction relative to the sham group (Figure 5.14). In addition, there were no significant differences between groups for either RT or MT during adaptation or retention (Table 5.3).

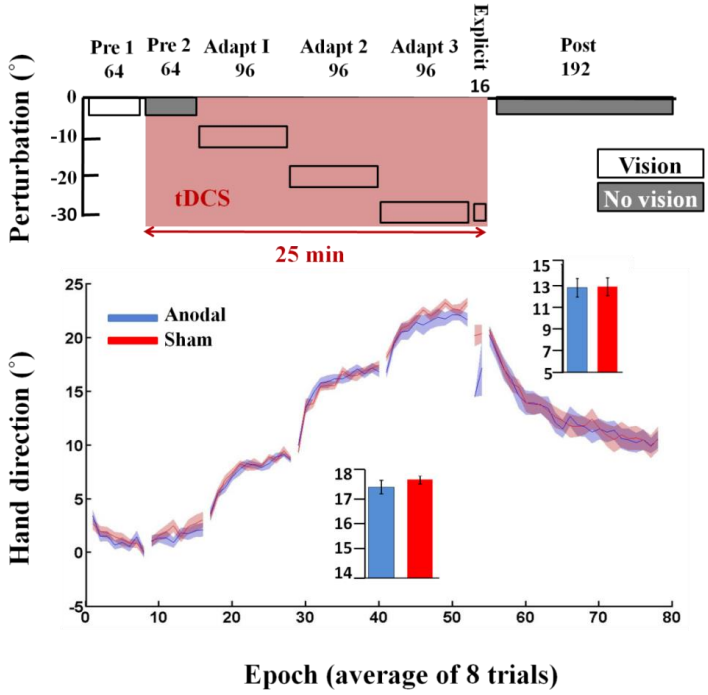

Figure 5.14 Experiment 7: step perturbation schedule. Epoch (average across 8 trials) uncorrected angular hand direction (°) data for the anodal (blue) and sham (red) groups. Positive values indicate CW hand direction. Bar graphs inset indicate mean hand direction for the anodal and sham groups during adaptation (adapt 1-3) and retention. This was determined for each participant by averaging consecutive epochs (see Methods). Independent t-tests compared these values between groups. Performance of the anodal and sham groups was identical throughout the experiment. Solid lines, mean; shaded areas/error bars, S.E.M. There was no significant difference between the anodal and sham cerebellar tDCS groups (18 in each group) during adaptation ($t_{(34)}$=-0.35, p=0.72, d=0.1).

In experiment 8, there was a significant difference between groups during pre 1 (Table 5.2), suggesting a small variation (1°) in baseline performance between groups. Again, to account for these differences, I subtracted each participant's average hand direction during pre1 from their subsequent performance, there was no significant difference between the anodal and sham cerebellar tDCS groups during adaptation ($t_{(30)}$=0.1, p=0.9, *d*=0.004). Similarly to experiment 7, despite displaying a hand direction of approximately 20-25° (Figure 5.15), both groups reported a similar aiming direction

towards the target (Anodal: 0.64±1.5°, Sham: 0.37±0.7°, independent t-test $t_{(30)}$=0.67, p=0.51, d=0.23). This indicates that all participants had developed only a minimal cognitive aiming strategy. During this block, there was also no significant difference between groups for actual hand direction ($t_{(30)}$=0.93, p=0.4, *d*=0.34). There were no significant differences between groups for either RT or MT during adaptation or retention (Table 5.3).

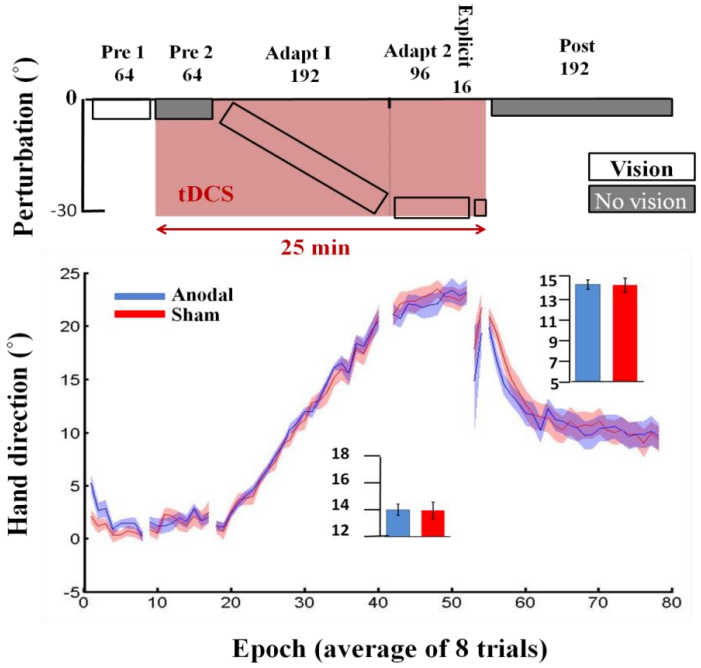

Figure 5.15 Experiment 8: gradual perturbation schedule. Epoch (average across 8 trials) uncorrected angular hand direction (°) data for the anodal (blue) and sham (red) groups. Positive values indicate CW hand direction. Bar graphs inset indicate mean hand direction for the anodal and sham groups during adaptation blocks and retention (post). This was determined for each participant by averaging consecutive epochs (see Methods). Independent t-tests compared these values between groups. Performance of the anodal and sham groups was identical throughout the experiment. Solid lines, mean; shaded areas/error bars, S.E.M. There was no significant difference between the anodal and sham cerebellar tDCS groups (16 in each group) during adaptation ($t_{(30)}$=0.1, p=0.94, d=0.004).

5.3.8 Experiment 9

To validate my only positive result, I repeated experiment 1 with 2 new groups (anodal/sham) of naive participants. Unfortunately, I found no significant difference between the anodal and sham cerebellar tDCS groups. There were no significant differences between groups during pre 1, pre 2 or when initially exposed to the 30˚ VR (Table 5.2). In addition, there were no differences between groups across adaptation ($t_{(24)}$=-2.5, p=0.8, d=0.1; Figure 5.16) or retention ($t_{(24)}$=0.23, p=0.8, d=0.1). Finally, there were no significant differences between groups for either RT or MT during adaptation or retention (Table 5.3).

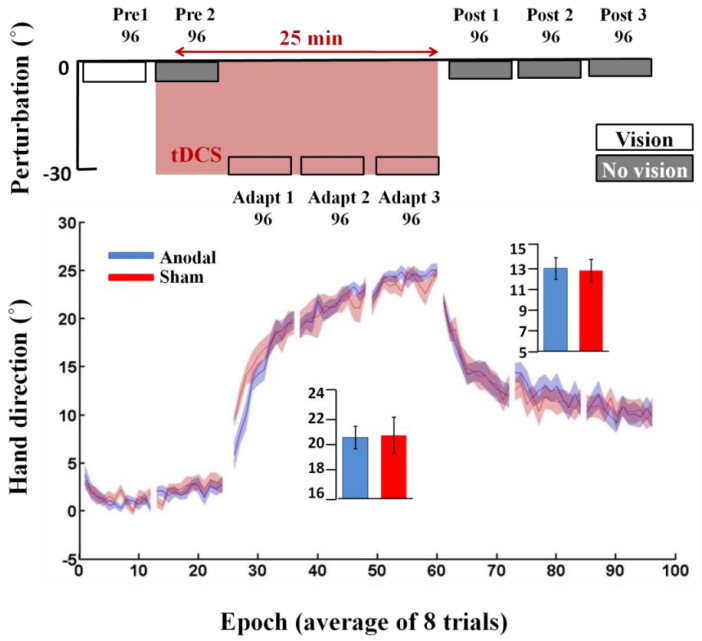

Figure 5.16 Experiment 9: experiment 1 validation. Epoch (average across 8 trials) uncorrected angular hand direction (°) data for the anodal (blue) and sham (red) groups. Positive values indicate CW hand direction. Bar graphs inset indicate mean hand direction for the anodal and sham groups during adaptation blocks and retention (post). This was determined for each participant by averaging consecutive epochs (see Methods). Independent t-tests compared these values between groups. Performance of the anodal and sham groups was identical throughout the experiment. Solid lines, mean; shaded areas/error bars, S.E.M. There was no significant difference between the anodal and sham cerebellar tDCS groups (13 in each group) during adaptation ($t_{(24)}$=-2.5, p=0.8, d=0.1).

Despite the differences between the current experimental set up and Galea et al., (2011), such as number of trials, duration of tDCS and use of tool, I pooled data across experiments 1 and 2 from Galea et al., (2011) and experiments 1, 4 and 9 from the current study. For each participant, I calculated an average Δ hand direction across all adaptation epochs, excluding epoch 1 and performed an independent t-test between the pooled anodal (n=61) and sham (n=60) groups. This pooled data showed a significant difference between anodal (20.1± 2.9) and sham cerebellar tDCS (17.5± 4.1; $t_{(119)}$ =3.9, p=0.0005, d=0.7). Interestingly though, the effect size was substantially smaller than the positive results found in experiment 1.

5.3.9 Self-reported ratings of attention, fatigue, and sleep

There were no significant differences between groups across all experiments for the self-reported ratings of attention, fatigue, and quality of sleep (Table 5.1).

5.4 Discussion

Across all nine experiments, participants showed a clear ability to adapt to the novel visuomotor rotation. In experiment 1, I was able to show that anodal cerebellar tDCS apparently caused a greater amount of adaptation relative to sham tDCS; however, this did not hold when I repeated the same experiment with a new set up participant (experiment 9). Although similar, these experiments differed to the original Galea et al., (2011) study in which participants used a digitised pen and wore goggles to prevent vision of the hand. When manipulating experimental parameters such as screen orientation (experiment 2), different tDCS machine (experiment 3), use of a tool

(experiment 4), different cerebellar tDCS montage (experiment 5), tDCS timing (experiment 6) and the perturbation schedule (experiments 7 and 8), I found anodal cerebellar tDCS to have no reliable effect on visuomotor adaptation.

5.4.1 tDCS did not enhance visuomotor adaptation when using a horizontal screen

Although the facilitatory effect of cerebellar tDCS on motor learning has been shown across visuomotor adaptation (Galea et al., 2011), force-field adaptation (Herzfeld et al., 2014), locomotor adaptation (Jayaram et al., 2012), saccade adaptation (Panouilleres et al., 2015, Avila et al., 2015), motor skill learning (Cantarero et al., 2015) and language prediction tasks (Miall et al., 2016), the sensitivity of this effect to specific task parameters had not been previously documented. As a large proportion of motor learning studies are performed whilst the visual feedback is provided in the same plane as the movement (Shabbott and Sainburg, 2010, Herzfeld et al., 2014), I was first motivated to examine whether the positive influence of tDCS on visuomotor adaptation can be observed when the screen orientation was flipped to a horizontal position. Thus experiment 1 and 2 addressed this issue by first replicating the screen display used in Galea et al. (2011), and then showing that tDCS was not associated with greater adaptation in the more typical in-plane feedback condition. The posterior part of the cerebellum is important for visuomotor adaptation (Rabe et al., 2009) and heavily connected with the posterior parietal cortex (O'Reilly et al., 2010), which is crucial for visuomotor control (Culham et al., 2006). As modelling studies suggest cerebellar tDCS mainly activates the posterior part of the cerebellum (Ferrucci et al., 2012, Parazzini et al., 2014, Rampersad et al., 2014), the increased visuomotor complexity and presumed greater reliance on the posterior cerebellum with a vertical screen orientation may optimise the effects of cerebellar tDCS on visuomotor adaptation.

5.4.2 Phoresor tDCS machine did not enhance visuomotor adaptation

Although several studies have used the Phoresor machine and showed significant facilitatory effect of cerebellar tDCS on visuomotor task (Galea et al., 2009, Galea et al., 2011, Herzfeld et al., 2014, Cantarero et al., 2015), As the Phoresor machine worked in the presence of higher impedance than the Neuroconn machine, it is possible that less current was being passed into the brain. However, as we did not record the level of impedance within each participant this is pure speculation.

5.4.3 tDCS did not improve visuomotor adaptation even when participants used a tool

Next, I was unable to replicate the original Galea et al., (2011) study where participants held a tool/digitizing pen (Galea et al., 2011; Block et al., 2012). Although experiment 4 was a closer replication of Galea et al., (2011) than experiment 1 and 9, participants still did not wear goggles to restrict vision of the hand. While not significant, Figure 5.11 does suggest there was a trend towards the anodal tDCS group adapting by a greater amount.

5.4.4 tDCS did not effective visuomotor adaptation when cerebellar tDCS reference electrode was on the shoulder

I changed the position of the reference electrode from the face to the shoulder to examine if the associated field changes suggested by modelling studies show a beneficial effect of tDCS on visuo motor adaptation (Mehta et al., 2015). However, I failed to show this effect, which suggests that this montage may not alter the physiology of the cerebellum strongly enough to activate the posterior cerebellum.

5.4.5 tDCS after-effect did not affect visuomotor adaptation

It has also been reported that anodal cerebellar tDCS applied during rest can lead to both physiological and behavioural changes over a period of 10-30 minutes after the cessation of stimulation (Galea et al., 2009, Pope and Miall, 2012). This indicates that the after-effect of cerebellar tDCS could have a beneficial effect on visuomotor adaptation. However, following 25 minutes of offline anodal cerebellar tDCS, I found no observable differences between the anodal and sham groups. One significant issue is that despite having neurophysiological evidence regarding the changes associated with offline cerebellar tDCS (Galea et al., 2009), no such published data exists for its online effects except my finding in the previous chapters which showed online tDCS had larger physiological change than post tDCS.

5.4.6 tDCS did not enhance adaptation when the perturbation was applied gradually

The contribution of the cerebellum to abrupt and gradual perturbation paradigms is an area of continued interest within the motor adaptation literature. For example, Criscimagna-Hemminger et al., (2013) showed cerebellar-lesion patients were unable to adapt to abrupt perturbations but preserved the capacity to adapt to gradual perturbations. Similarly, Schlerf et al., (2012) reported modulation of cerebellar excitability for abrupt, but not gradual, visuomotor adaptation (Schlerf et al., 2012). However, Gibo et al., 2013 showed that cerebellar-lesion patients may use non-cerebellar strategic learning to successfully adapt (Gibo et al., 2013). In line with this argument, other recent work suggests that large abrupt visual rotations reduce cerebellar-dependent sensory-prediction error learning and enhance strategic learning, whilst smaller visual rotations bias learning towards sensory-prediction error learning (McDougle et al., 2015, Bond and Taylor, 2015, Taylor et al., 2014). This suggests that cerebellar tDCS may have been more effective with small or gradual perturbation schedules. However, I found that tDCS did not show any significant effect on

adaptation when the perturbation was applied in small steps (experiment 7) or gradually (experiment 8).

5.4.7 The positive effect of cerebellar tDCS in experiment 1 was not replicated

Finally, I wanted to see whether the positive effect of cerebellar tDCS on visuomotor adaptation observed in experiment 1 could be replicated in a new set of naïve participants. Unfortunately, this positive effect was not observed, with experiment 9 showing no significant difference between the anodal and sham tDCS groups during adaptation. This suggests that the positive effects of cerebellar tDCS in experiment 1 were either observed by chance or that the effect size of cerebellar tDCS is significantly smaller than one might imagine. Although my sample sizes (10-15 per group) were in the range of previously published tDCS papers (Galea et al., 2011, Cantarero et al., 2015, Hardwick and Celnik, 2014, Block and Celnik, 2013), a recent study indicates this could be significantly under powered (Minarik et al., 2016). Minarik et al., (2016) showed that with a suggested tDCS effect size of 0.45, the likelihood of observing a significant result with 14 participants (per group) was approximately 20%. To examine this further, I pooled data across experiments 1 and 2 from Galea et al., (2011) and experiments 1, 3 and 7 from the current study. This pooled data showed a significant difference between anodal and sham cerebellar tDCS. However, the effect size was substantially smaller (0.7) than what was initially observed in experiment 1. At present it is difficult to determine a true effect size for not only cerebellar tDCS but tDCS in general due to the clear publication bias in the literature towards positive effects. Through informal discussion with many colleagues, it is clear that researchers are observing null effects with cerebellar tDCS, but have so far been slow to publish these results. Although this is beginning to change (Steiner et al., 2016, Mamlins et al., 2016, Westwood et al., 2016), I believe a more accurate representation of the effect size, and so the required participant numbers, of cerebellar tDCS will only be achieved if null results are published more often.

5.5 Conclusion

In conclusion, I failed to find a consistent effect of cerebellar tDCS on visuomotor adaptation. Although initially replicating previous reports of cerebellar tDCS enhancing visuomotor adaptation, I found this not to be consistent across varying task parameters, nor reproducible in a new group of participants. I believe these results highlight the need for substantially larger group sizes for tDCS studies, and may call into question the validity of using cerebellar tDCS within a clinical context where a robust effect across behaviours would be required.

6 GENERAL DISCUSSION

6.1 Introduction

In this chapter, I would like to summarise the main findings of my work in addition to discuss its limitations and make some suggestions for future research directions. Cerebellar tDCS is known to enhance motor adaptation. Although promising, the neural mechanism underpinning the effects of cerebellar tDCS is unknown. Therefore, the objective of my research was to investigate the mechanisms underlying the effect of cerebellar tDCS on motor learning. In this thesis, I investigated the neurobiological changes associated with cerebellar tDCS through visuomotor adaptation, MRS and resting state fMRI in addition to assessing the consistency of cerebellar tDCS on visuomotor adaptation across a range of varying task parameters. The major finding of this work was that there appeared to be an 'all-or-nothing' type effect of cerebellar tDCS whereby ~20% of participants showed a strong neurobiological response to cerebellar tDCS. The results imply that cerebellar tDCS only produced measurable neural changes in a subset of participants, providing a possible explanation why

cerebellar tDCS causes variable results across participants when used with behavioural tasks (Steiner et al., 2016, Mamlins et al., 2016, Westwood et al., 2016).

6.2 Summary of results

The three of four experimental chapters (chapter 2 explained the MRS techniques), all investigated different aspects of cerebellar tDCS. In chapter 3, I compared the level of adaptation and retention between two groups while they received either anodal or sham cerebellar tDCS. The anodal group then underwent two sessions of MRS (chapter 3) and fMRI (chapter 4) for further physiological assessment. Using MRS, I measured metabolites in a localised voxel within their right posterior cerebellum pre-, during and post– cerebellar tDCS. In contrast to the previous studies that have demonstrated tDCS to cause a significant decrease in GABA within M1 (Stagg, 2014, Stagg et al., 2014, Stagg et al., 2011, Kim et al., 2014, Bachtiar et al., 2015), I found cerebellar tDCS caused a large variability across the participants (~90% increase to a 100% decrease). However, similar to the results observed in M1 tDCS where a reduction in GABA was correlated with improvements in sequence learning (Stagg et al., 2011) and force-field adaptation (Kim et al., 2014), I found cerebellar tDCS-induced reduction in GABA was correlated with improvement in visuomotor adaptation. According to the previously shown finding that visuomotor adaptation was associated with a decrease in cerebellar-cortical excitability (Schlerf et al., 2012), my finding supports the view that a tDCS-dependent decrease in GABA may enhance visuomotor adaptation through a reduction in Purkinje cell activity and related to the long-term depression (LTD) observed with cerebellar learning.

The next finding of this work was tDCS-induced reduction in both Glu/GLX was associated with better visuomotor retention. This result is difficult to explain because not only the mechanism of retention in the human cerebellum, but also the relationship

between cell-type activity and MRS-detected changes within the cerebellum is still unknown. One possibility is that a decrease in Glu/GLX reflects a decrease in glutamatergic input into the cerebellar cortex and reduced activity of Purkinje cells. This would reduce CBI and enhance M1 function. It is known that excitation of M1 facilitates retention, potentially retaining or consolidating what has been learnt by the cerebellum (Galea et al., 2011, Sami et al., 2014). To explain this result, the MRS data should have ideally been collected while M1 is activated, which entailed performing the task.

In chapter 4, I studied the effect of cerebellar tDCS on functional connectivity between the right cerebellum (rCB) and other component of the visuomotor related network and found a significant decrease in FC between the rCB and right parietal cortex (rPC) and between rCB and left frontal cortex (lFC). This change was not correlated with participant's visuomotor adaptation performance. However, this result supports the recently published work that has been shown that TMS over the lateral or midline cerebellum separately modulates multiple resting state networks; default mode network and dorsal attention network (Halko et al., 2014). As tDCS electrode cover both lateral and part of midline of the cerebellum, therefore it is not unexpected to affect multiple network simultaneously. There was also a significant increase in connectivity between rCB and Vermis, within the cerebellum itself, which could be related to the reduction of inhibitory output of GABAergic cerebellar cortex.

In chapter 4, I also found an increase in functional connectivity between the cerebellum and left parietal cortex was correlated with greater participant's visuomotor adaptation. This finding fits the model suggested by Shadmehr and Krakauer in 2008, the cerebellum predicts the motor command, whilst the posterior parietal cortex compares this prediction with the actual sensory (visual) feedback. Therefore, this network is known to be crucial in successful visuomotor adaptation (Shadmehr and Krakauer, 2008). Anatomically, this might be reflecting the effect of tDCS on decreasing GABAergic Purkinje cell activity within the cerebellar cortex and reduction of the deep cerebellar nuclei that may lead to an increase in connectivity between the cerebellum and left parietal cortex. By correlating the change in GABA and functional connectivity,

I found this relationship was essentially driven by 21% of participant which may suggest the small percentage of responsive people to stimulation.

In addition to the physiological assessment, in chapter 5, I also investigated the consistency of the cerebellar tDCS effects on a visuomotor adaptation task across a wide range of task parameters, which were systematically varied. In this chapter, I initially showed anodal cerebellar tDCS caused a greater amount of adaptation relative to sham tDCS as previously reported (Galea et al., 2011). However, this did not hold when I repeated the same experiment with a new group of participants or after any unique feature of the task was altered such as position of the monitor, tDCS machine, offline tDCS, use of a tool, tDCS montage, and perturbation schedule. Therefore, I failed to find a consistent effect of cerebellar tDCS on visuomotor adaptation. This inconsistency in behavioural experiment supports both of my physiology finding and increasingly published data regarding the inconsistency of cerebellar tDCS in behavioural tasks (Conley et al., 2016, Minarik et al., 2016, Dyke et al., 2016) as significant differences between anodal and sham groups would be heavily dependent on the proportion of 'responders' within the anodal group.

In conclusion, this study provided a novel insight into the neurophysiology underpinning cerebellar tDCS, which indicates that cerebellar tDCS may have an all-or-nothing type effect on individual participants with approximately 21% showing substantial online changes in GABA (decrease of between 50% -100%) and resting connectivity (increase of more than 100% between rCB-left parietal cortex) were responsive to cerebellar tDCS.

6.3 Limitations of the research

The main limitation of my work was the small sample sizes used. The results from chapter 3 and 4 both indicated that greater sample sizes were needed in order to confirm

whether 3 responders (21%) to cerebellar tDCS really reflected the sensitivity rate within the population as a whole. In addition, my visuomotor adaptation chapter suffers from the limitation of a between-subject design. Previous work has shown large inter-individual variation in motor learning rates (Stark-Inbar et al., 2017), implementation of motor learning processes (Christou et al., 2016) and responsivity to stimulation (Wiethoff et al., 2014). These factors may have all negatively affected my ability to observe consistent between-subject tDCS differences in visuomotor. Although a within-subject design would overcome many of these issues, this is also problematic as it introduces the substantial problem of carry-over effects being observed with visuomotor adaptation weeks after initial exposure (Krakauer, 2009).

6.4 Future direction

My results indicate that for cerebellar tDCS to become an effective tool, technical advances must be identified that improve the strength and consistency of its effect on functional tasks. For example, the common assumption is to that currents of 1-2mA are effective (Woods et al., 2016). However, previous work has used currents of up to 5mA on other brain areas (Furubayashi et al., 2008, Hammerer et al., 2016, Bonaiuto and Bestmann, 2015), suggesting greater current intensities are possible with cerebellar tDCS. Alternatively, there is exciting work suggesting high-definition tDCS combined with computational modelling of the brain's impedances can lead to more exact predictions regarding the behavioural results associated with tDCS. It is possible that using high-definition tDCS along with computational modelling to optimise electrode placement could enhance the magnitude and reliability of the tDCS effect on the cerebellum (Kuo et al., 2013). Finally, it would be very informative to investigate the neurobiological change underneath cerebellar tDCS while motor learning is happening instead of during rest.

7 REFERENCES

ALBUS, J. S. 1971. A theory of cerebellar function. *Mathematical bioscience,* 10**,** 25-61.

ANTAL, A., POLANIA, R., SCHMIDT-SAMOA, C., DECHENT, P. & PAULUS, W. 2011. Transcranial direct current stimulation over the primary motor cortex during fMRI. *Neuroimage,* 55**,** 590-596.

AVILA, E., VAN DER GEEST, J. N., KAMGA, S. K., VERHAGE, M. C., DONCHIN, O. & FRENS, M. A. 2015. Cerebellar Transcranial Direct Current Stimulation Effects on Saccade Adaptation. *Neural Plasticity*.

AZEVEDO, F. A. C., CARVALHO, L. R. B., GRINBERG, L. T., FARFEL, J. M., FERRETTI, R. E. L., LEITE, R. E. P., JACOB, W., LENT, R. & HERCULANO-HOUZEL, S. 2009. Equal Numbers of Neuronal and Nonneuronal Cells Make the Human Brain an Isometrically Scaled-Up Primate Brain. *Journal of Comparative Neurology,* 513**,** 532-541.

BACHTIAR, V., NEAR, J., JOHANSEN-BERG, H. & STAGG, C. J. 2015. Modulation of GABA and resting state functional connectivity by transcranial direct current stimulation. *Elife,* 4.

BENUSSI, A., KOCH, G., COTELLI, M., PADOVANI, A. & BORRONI, B. 2015. Cerebellar transcranial direct current stimulation in patients with ataxia: A double-blind, randomized, sham-controlled study. *Mov Disord,* 30**,** 1701-5.

BERNARD, J. A., SEIDLER, R. D., HASSEVOORT, K. M., BENSON, B. L., WELSH, R. C., WIGGINS, J. L., JAEGGI, S. M., BUSCHKUEHL, M., MONK, C. S., JONIDES, J. & PELTIER, S. J. 2012. Resting state cortico-cerebellar functional connectivity networks: a comparison of anatomical and self-organizing map approaches. *Frontiers in Neuroanatomy,* 6.

BITSCH, A., BRUHN, H., VOUGIOUKAS, V., STRINGARIS, A., LASSMANN, H., FRAHM, J. & BRUCK, W. 1999. Inflammatory CNS demyelination: Histopathologic correlation with in vivo quantitative proton MR spectroscopy. *American Journal of Neuroradiology,* 20**,** 1619-1627.

BLOCK, H. & CELNIK, P. 2013. Stimulating the Cerebellum Affects Visuomotor Adaptation but not Intermanual Transfer of Learning. *Cerebellum,* 12**,** 781-793.

BONAIUTO, J. J. & BESTMANN, S. 2015. Understanding the nonlinear physiological and behavioral effects of tDCS through computational neurostimulation. *Computational Neurostimulation,* 222**,** 75-103.

BOND, K. M. & TAYLOR, J. A. 2015. Flexible explicit but rigid implicit learning in a visuomotor adaptation task. *J Neurophysiol,* 113**,** 3836-49.

BOTTOMLEY, P. A., HART, H. R., EDELSTEIN, W. A., SCHENCK, J. F., SMITH, L. S., LEUE, W. M., MUELLER, O. M. & REDINGTON, R. W. 1983. NMR imaging/spectroscopy system to study both anatomy and metabolism. *Lancet,* 2**,** 273-4.

BRAND, A., RICHTERLANDSBERG, C. & LEIBFRITZ, D. 1993. Multinuclear Nmr-Studies on the Energy-Metabolism of Glial and Neuronal Cells. *Developmental Neuroscience,* 15**,** 289-298.

BUCKNER, R. L., KRIENEN, F. M., CASTELLANOS, A., DIAZ, J. C. & YEO, B. T. T. 2011. The organization of the human cerebellum estimated by intrinsic functional connectivity. *Journal of Neurophysiology,* 106**,** 2322-2345.

CANTARERO, G., SPAMPINATO, D., REIS, J., AJAGBE, L., THOMPSON, T., KULKARNI, K. & CELNIK, P. 2015. Cerebellar Direct Current Stimulation Enhances On-Line Motor Skill Acquisition through an Effect on Accuracy. *Journal of Neuroscience,* 35**,** 3285-3290.

CASTILLO, M., SMITH, J. K. & KWOCK, L. 2000. Correlation of myo-inositol levels and grading of cerebral astrocytomas. *AJNR Am J Neuroradiol,* 21**,** 1645-9.

CHRISTOU, A. I., MIALL, R. C., MCNAB, F. & GALEA, J. M. 2016. Individual differences in explicit and implicit visuomotor learning and working memory capacity. *Sci Rep,* 6**,** 36633.

CONLEY, A. C., FULHAM, W. R., MARQUEZ, J. L., PARSONS, M. W. & KARAYANIDIS, F. 2016. No Effect of Anodal Transcranial Direct Current Stimulation Over the Motor Cortex on Response-Related ERPs during a Conflict Task. *Frontiers in Human Neuroscience,* 10.

CRISCIMAGNA-HEMMINGER, S. E., BASTIAN, A. J. & SHADMEHR, R. 2010. Size of Error Affects Cerebellar Contributions to Motor Learning. *Journal of Neurophysiology,* 103**,** 2275-2284.

CULHAM, J. C., CAVINA-PRATESI, C. & SINGHAL, A. 2006. The role of parietal cortex in visuomotor control: what have we learned from neuroimaging? *Neuropsychologia,* 44**,** 2668-84.

DE ZEEUW, C. I., SIMPSON, J. I., HOOGENRAAD, C. C., GALJART, N., KOEKKOEK, S. K. & RUIGROK, T. J. 1998. Microcircuitry and function of the inferior olive. *Trends Neurosci,* 21**,** 391-400.

DIEDRICHSEN, J., & BASTIAN, A. J. 2014. *Cerebellar Function,* Cambridge, MA, MIT press.

DIEDRICHSEN, J., HASHAMBHOY, Y., RANE, T. & SHADMEHR, R. 2005. Neural correlates of reach errors. *Journal of Neuroscience,* 25**,** 9919-9931.

DONCHIN, O., RABE, K., DIEDRICHSEN, J., LALLY, N., SCHOCH, B., GIZEWSKI, E. R. & TIMMANN, D. 2012. Cerebellar regions involved in adaptation to force field and visuomotor perturbation. *Journal of Neurophysiology,* 107**,** 134-147.

DUARTE, J. M., LEI, H., MLYNARIK, V. & GRUETTER, R. 2012. The neurochemical profile quantified by in vivo 1H NMR spectroscopy. *Neuroimage,* 61**,** 342-62.

DYKE, K., KIM, S., JACKSON, G. M. & JACKSON, S. R. 2016. Intra-Subject Consistency and Reliability of Response Following 2 mA Transcranial Direct Current Stimulation. *Brain Stimulation,* 9**,** 819-825.

EDDEN, R. A., POMPER, M. G. & BARKER, P. B. 2007. In vivo differentiation of N-acetyl aspartyl glutamate from N-acetyl aspartate at 3 Tesla. *Magn Reson Med,* 57**,** 977-82.

EVANS, C. J., PUTS, N. A. J., ROBSON, S. E., BOY, F., MCGONIGLE, D. J., SUMNER, P., SINGH, K. D. & EDDEN, R. A. E. 2013. Subtraction Artifacts and Frequency (Mis-)Alignment in J-Difference GABA Editing. *Journal of Magnetic Resonance Imaging,* 38**,** 970-975.

FERRUCCI, R., GIANNICOLA, G., ROSA, M., FUMAGALLI, M., BOGGIO, P. S., HALLETT, M., ZAGO, S. & PRIORI, A. 2012. Cerebellum and processing of negative facial emotions: Cerebellar transcranial DC stimulation specifically enhances the emotional recognition of facial anger and sadness. *Cognition & Emotion,* 26**,** 786-799.

FLOYER-LEA, A. & MATTHEWS, P. M. 2005. Distinguishable brain activation networks for short- and long-term motor skill learning. *Journal of Neurophysiology,* 94**,** 512-518.

FOX, M. D., ZHANG, D. Y., SNYDER, A. Z. & RAICHLE, M. E. 2009. The Global Signal and Observed Anticorrelated Resting State Brain Networks. *Journal of Neurophysiology,* 101**,** 3270-3283.

FRISTON, K. J., PASSINGHAM, R. E., NUTT, J. G., HEATHER, J. D., SAWLE, G. V. & FRACKOWIAK, R. S. J. 1989. Localization in Pet Images - Direct Fitting of the Intercommissural (Ac-Pc) Line. *Journal of Cerebral Blood Flow and Metabolism,* 9**,** 690-695.

FURUBAYASHI, T., TERAO, Y., ARAI, N., OKABE, S., MOCHIZUKI, H., HANAJIMA, R., HAMADA, M., YUGETA, A., INOMATA-TERADA, S. & UGAWA, Y. 2008. Short and long duration transcranial direct current stimulation (tDCS) over the human hand motor area. *Experimental Brain Research,* 185**,** 279-286.

GALEA, J. M., JAYARAM, G., AJAGBE, L. & CELNIK, P. 2009. Modulation of Cerebellar Excitability by Polarity-Specific Noninvasive Direct Current Stimulation. *Journal of Neuroscience,* 29**,** 9115-9122.

GALEA, J. M., VAZQUEZ, A., PASRICHA, N., DE XIVRY, J. J. O. & CELNIK, P. 2011. Dissociating the Roles of the Cerebellum and Motor Cortex during Adaptive Learning: The Motor Cortex Retains What the Cerebellum Learns. *Cerebral Cortex,* 21**,** 1761-1770.

GAZZANIGA, M. S., IVRY, R. B. & MANGUN, G. R. 2014. *Cognitive neuroscience : the biology of the mind,* New York, W. W. Norton & Company, Inc.

GIBO, T. L., CRISCIMAGNA-HEMMINGER, S. E., OKAMURA, A. M. & BASTIAN, A. J. 2013. Cerebellar motor learning: are environment dynamics more important than error size? *Journal of Neurophysiology,* 110**,** 322-333.

GRAAF, R. A. D. 2007. *In Vivo NMR Spectroscopy*, John Wiley & Sons, Ltd.

GRIMALDI, G., ARGYROPOULOS, G. P., BOEHRINGER, A., CELNIK, P., EDWARDS, M. J., FERRUCCI, R., GALEA, J. M., GROISS, S. J., HIRAOKA, K., KASSAVETIS, P., LESAGE, E., MANTO, M., MIALL, R. C., PRIORI, A., SADNICKA, A., UGAWA, Y. & ZIEMANN, U. 2014. Non-invasive Cerebellar Stimulation-a Consensus Paper. *Cerebellum,* 13**,** 121-138.

HAACKE, E. M., BROWN, R. W., R., M. & THOMPSON, R. V. 1999. *Magnetic Resonance Imaging: Physical Principles and Sequence Design*, Wiley-Blackwell.

HABAS, C. 2010. Functional Imaging of the Deep Cerebellar Nuclei: A Review. *Cerebellum,* 9**,** 22-28.

HALKO, M. A., FARZAN, F., ELDAIEF, M. C., SCHMAHMANN, J. D. & PASCUAL-LEONE, A. 2014. Intermittent Theta-Burst Stimulation of the Lateral Cerebellum Increases Functional Connectivity of the Default Network. *Journal of Neuroscience,* 34**,** 12049-12056.

HALL, K. M., HICKS, R. A. & HOPKINS, H. K. 1970. The effects of low level DC scalp positive and negative current on the performance of various tasks. *Br J Psychiatry,* 117**,** 689-91.

HAMMERER, D., BONAIUTO, J., KLEIN-FLUGGE, M., BIKSON, M. & BESTMANN, S. 2016. Selective alteration of human value decisions with medial frontal tDCS is predicted by changes in attractor dynamics. *Scientific Reports,* 6.

HARDWICK, R. M. & CELNIK, P. A. 2014. Cerebellar direct current stimulation enhances motor learning in older adults. *Neurobiol Aging,* 35**,** 2217-21.

HARRIS, R. K. 1985. Quantitative Aspects of High-Resolution Solid-State Nuclear Magnetic-Resonance Spectroscopy. *Analyst,* 110**,** 649-655.

HENRY, P. G., DAUTRY, C., HANTRAYE, P. & BLOCH, G. 2001. Brain GABA editing without macromolecule contamination. *Magnetic Resonance in Medicine,* 45**,** 517-520.

HERTZ, L. 2004. Intercellular metabolic compartmentation in the brain: past, present and future. *Neurochemistry International,* 45**,** 285-296.

HERZFELD, D. J., PASTOR, D., HAITH, A. M., ROSSETTI, Y., SHADMEHR, R. & O'SHEA, J. 2014. Contributions of the cerebellum and the motor cortex to acquisition and retention of motor memories. *Neuroimage,* 98**,** 147-158.

HIRANO, T. 2013. Long-term depression and other synaptic plasticity in the cerebellum. *Proc Jpn Acad Ser B Phys Biol Sci,* 89**,** 183-95.

HOLMES, G. 1939. The cerebellum of man. *Brain,* 62**,** 1-30.

HONE-BLANCHET, A., EDDEN, R. A. & FECTEAU, S. 2016. Online Effects of Transcranial Direct Current Stimulation in Real Time on Human Prefrontal and Striatal Metabolites. *Biological Psychiatry,* 80**,** 432-438.

HUNTER, M. A., COFFMAN, B. A., GASPAROVIC, C., CALHOUN, V. D., TRUMBO, M. C. & CLARK, V. P. 2015. Baseline effects of transcranial direct current stimulation on glutamatergic neurotransmission and large-scale network connectivity. *Brain Res,* 1594**,** 92-107.

HWANG, E. J., SMITH, M. A. & SHADMEHR, R. 2006. Dissociable effects of the implicit and explicit memory systems on learning control of reaching. *Exp Brain Res,* 173**,** 425-37.

JANSEN, O. L. J. 1972. The Comparative Anatomy and Histology of the Cerebellum: The Human Cerebellum, Cerebellar Connections, and Cerebellar Cortex. Minnesota University Press; Minnesota Archi edition

JAYARAM, G., TANG, B., PALLEGADDA, R., VASUDEVAN, E. V. L., CELNIK, P. & BASTIAN, A. 2012. Modulating locomotor adaptation with cerebellar stimulation. *Journal of Neurophysiology,* 107**,** 2950-2957.

JENKINS, I. H., BROOKS, D. J., NIXON, P. D., FRACKOWIAK, R. S. J. & PASSINGHAM, R. E. 1994. Motor Sequence Learning - a Study with Positron Emission Tomography. *Journal of Neuroscience,* 14**,** 3775-3790.

JENKINSON, M. 2003. Fast, automated, N-dimensional phase-unwrapping algorithm. *Magnetic Resonance in Medicine,* 49**,** 193-197.

JENKINSON, M., BANNISTER, P., BRADY, M. & SMITH, S. 2002. Improved optimization for the robust and accurate linear registration and motion correction of brain images. *Neuroimage,* 17**,** 825-841.

JENKINSON, M., BECKMANN, C. F., BEHRENS, T. E., WOOLRICH, M. W. & SMITH, S. M. 2012. Fsl. *Neuroimage,* 62**,** 782-790.

JORDAN, M. I. & RUMELHART, D. E. 1992. Forward Models - Supervised Learning with a Distal Teacher. *Cognitive Science,* 16**,** 307-354.

KIM, S., STEPHENSON, M. C., MORRIS, P. G. & JACKSON, S. R. 2014. tDCS-induced alterations in GABA concentration within primary motor cortex predict motor learning and motor memory: a 7 T magnetic resonance spectroscopy study. *Neuroimage,* 99**,** 237-43.

KRAKAUER, J. W. 2009. Motor Learning and Consolidation: The Case of Visuomotor Rotation. *Progress in Motor Control: A Multidisciplinary Perspective,* 629**,** 405-421.

KRAKAUER, J. W., GHILARDI, M. F. & GHEZ, C. 1999. Independent learning of internal models for kinematic and dynamic control of reaching. *Nat Neurosci,* 2**,** 1026-31.

KRIENEN, F. M. & BUCKNER, R. L. 2009. Segregated Fronto-Cerebellar Circuits Revealed by Intrinsic Functional Connectivity. *Cerebral Cortex,* 19**,** 2485-2497.

KUNZE, T., HUNOLD, A., HAUEISEN, J., JIRSA, V. & SPIEGLER, A. 2016. Transcranial direct current stimulation changes resting state functional connectivity: A large-scale brain network modeling study. *Neuroimage,* 140**,** 174-187.

KUO, H. I., BIKSON, M., DATTA, A., MINHAS, P., PAULUS, W., KUO, M. F. & NITSCHE, M. A. 2013. Comparing Cortical Plasticity Induced by Conventional and High-Definition 4 x 1 Ring tDCS: A Neurophysiological Study. *Brain Stimulation,* 6**,** 644-648.

LEHERICY, S., BENALI, H., VAN DE MOORTELE, P. F., PELEGRINI-ISSAC, M., WAECHTER, T., UGURBIL, K. & DOYON, J. 2005. Distinct basal ganglia territories are engaged in early and advanced motor sequence learning. *Proceedings of the National Academy of Sciences of the United States of America,* 102**,** 12566-12571.

LEI, H., ZHU, X. H., ZHANG, X. L., UGURBIL, K. & CHEN, W. 2003. In vivo 31P magnetic resonance spectroscopy of human brain at 7 T: an initial experience. *Magn Reson Med,* 49**,** 199-205.

LIPPOLD, O. C. J. & REDFEARN, J. W. 1964. Mental Changes Resulting from Passage of Small Direct Currents through Human-Brain. *British Journal of Psychiatry,* 110**,** 768-&.

M. JENKINSON, M. P., AND S. SMITH 2005. BET2: MR-based estimation of brain, skull and scalp surfaces. *Eleventh Annual Meeting of the Organization for Human Brain Mapping*.

MAMLINS, A., HULST, T., DONCHIN, O., TIMMANN, D. & CLAAßEN, J. 2016. EP 72. Cerebellar tDCS effects on the adaptation of arm reaching movements to force-field perturbations. *Clinical Neurophysiology,* 127**,** e269.

MANTO, M., BOWER, J. M., CONFORTO, A. B., DELGADO-GARCIA, J. M., DA GUARDA, S. N., GERWIG, M., HABAS, C., HAGURA, N., IVRY, R. B., MARIEN, P., MOLINARI, M., NAITO, E., NOWAK, D. A., OULAD BEN TAIB, N., PELISSON, D., TESCHE, C. D., TILIKETE, C. & TIMMANN, D. 2012. Consensus paper: roles of the cerebellum in motor control--the diversity of ideas on cerebellar involvement in movement. *Cerebellum,* 11**,** 457-87.

MARR, D. 1969. A theory of cerebellar cortex. *J Physiol,* 202**,** 437-70.

MARTIN, T. A., KEATING, J. G., GOODKIN, H. P., BASTIAN, A. J. & THACH, W. T. 1996. Throwing while looking through prisms .1. Focal olivocerebellar lesions impair adaptation. *Brain,* 119**,** 1183-1198.

MASCHKE, M., GOMEZ, C. M., EBNER, T. J. & KONCZAK, J. 2004. Hereditary cerebellar ataxia progressively impairs force adaptation during goal-directed arm movements. *Journal of Neurophysiology,* 91**,** 230-238.

MAZZONI, P. & KRAKAUER, J. W. 2006. An implicit plan overrides an explicit strategy during visuomotor adaptation. *J Neurosci,* 26**,** 3642-5.

MCDOUGLE, S. D., BOND, K. M. & TAYLOR, J. A. 2015. Explicit and Implicit Processes Constitute the Fast and Slow Processes of Sensorimotor Learning. *J Neurosci,* 35**,** 9568-79.

MCROBBIE, D. W., MOORE, E. A., GRAVES, M. J. & PRINCE, M. R. 2003. *MRI from picture to proton*, Canbridge University Press.

MEHTA, A. R., POGOSYAN, A., BROWN, P. & BRITTAIN, J. S. 2015. Montage Matters: The Influence of Transcranial Alternating Current Stimulation on Human Physiological Tremor. *Brain Stimulation,* 8**,** 260-268.

MESCHER, M., MERKLE, H., KIRSCH, J., GARWOOD, M. & GRUETTER, R. 1998. Simultaneous in vivo spectral editing and water suppression. *Nmr in Biomedicine,* 11**,** 266-272.

MIALL, R. C., ANTONY, J., GOLDSMITH-SUMNER, A., HARDING, S. R., MCGOVERN, C. & WINTER, J. L. 2016. Modulation of linguistic prediction by TDCS of the right lateral cerebellum. *Neuropsychologia,* 86**,** 103-109.

MIALL, R. C., WEIR, D. J., WOLPERT, D. M. & STEIN, J. F. 1993. Is the Cerebellum a Smith Predictor. *Journal of Motor Behavior,* 25**,** 203-216.

MIALL, R. C. & WOLPERT, D. M. 1996. Forward models for physiological motor control. *Neural Networks,* 9**,** 1265-1279.

MIDDLETON, F. A. & STRICK, P. L. 2000. Basal ganglia and cerebellar loops: motor and cognitive circuits. *Brain Research Reviews,* 31**,** 236-250.

MILLER, B. L., CHANG, L., BOOTH, R., ERNST, T., CORNFORD, M., NIKAS, D., MCBRIDE, D. & JENDEN, D. J. 1996. In vivo H-1 MRS choline: Correlation with in vitro chemistry histology. *Life Sciences,* 58**,** 1929-1935.

MINARIK, T., BERGER, B., ALTHAUS, L., BADER, V., BIEBL, B., BROTZELLER, F., FUSBAN, T., HEGEMANN, J., JESTEADT, L., KALWEIT, L., LEITNER, M., LINKE, F., NABIELSKA, N., REITER, T., SCHMITT, D., SPRAETZ, A. & SAUSENG, P. 2016. The Importance of Sample Size for Reproducibility of tDCS Effects. *Front Hum Neurosci,* 10**,** 453.

MUTHUKUMARASWAMY, S. D., EDDEN, R. A. E., JONES, D. K., SWETTENHAM, J. B. & SINGH, K. D. 2009. Resting GABA concentration predicts peak gamma frequency and fMRI amplitude in response to visual stimulation in humans. *Proceedings of the National Academy of Sciences of the United States of America,* 106**,** 8356-8361.

NITSCH, R. M., BLUSZTAJN, J. K., PITTAS, A. G., SLACK, B. E., GROWDON, J. H. & WURTMAN, R. J. 1992. Evidence for a Membrane Defect in Alzheimer-Disease Brain. *Proceedings of the National Academy of Sciences of the United States of America,* 89**,** 1671-1675.

O'REILLY, J. X., BECKMANN, C. F., TOMASSINI, V., RAMNANI, N. & JOHANSEN-BERG, H. 2010. Distinct and Overlapping Functional Zones in the Cerebellum Defined by Resting State Functional Connectivity. *Cerebral Cortex,* 20**,** 953-965.

PANOUILLERES, M. T. N., MIALL, R. C. & JENKINSON, N. 2015. The Role of the Posterior Cerebellum in Saccadic Adaptation: A Transcranial Direct Current Stimulation Study. *Journal of Neuroscience,* 35**,** 5471-5479.

PARAZZINI, M., ROSSI, E., FERRUCCI, R., LIORNI, I., PRIORI, A. & RAVAZZANI, P. 2014. Modelling the electric field and the current density generated by cerebellar transcranial DC stimulation in humans. *Clinical Neurophysiology,* 125**,** 577-584.

POLDRACK, R. A., MUMFORD, J. A. & NICHOLAS, T. E. 2011. *Handbook of Functional MRI Data Analysis,* Cambridge University Press.

POPE, P. A. & MIALL, R. C. 2012. Task-specific facilitation of cognition by cathodal transcranial direct current stimulation of the cerebellum. *Brain Stimulation,* 5**,** 84-94.

PROCTOR, W. G. & YU, F. C. 1950. The Dependence of a Nuclear Magnetic Resonance Frequency Upon Chemical Compound. *Physical Review,* 77**,** 717-717.

PUTS, N. A., EDDEN, R. A., EVANS, C. J., MCGLONE, F. & MCGONIGLE, D. J. 2011a. Regionally specific human GABA concentration correlates with tactile discrimination thresholds. *J Neurosci,* 31**,** 16556-60.

PUTS, N. A. J. & EDDEN, R. A. E. 2012. In vivo magnetic resonance spectroscopy of GABA: A methodological review. *Progress in Nuclear Magnetic Resonance Spectroscopy,* 60**,** 29-41.

PUTS, N. A. J., EDDEN, R. A. E., EVANS, C. J., MCGLONE, F. & MCGONIGLE, D. J. 2011b. Regionally Specific Human GABA Concentration Correlates with Tactile Discrimination Thresholds. *Journal of Neuroscience,* 31**,** 16556-16560.

RABE, K., LIVNE, O., GIZEWSKI, E. R., AURICH, V., BECK, A., TIMMANN, D. & DONCHIN, O. 2009. Adaptation to Visuomotor Rotation and Force Field Perturbation Is Correlated to Different Brain Areas in Patients With Cerebellar Degeneration. *Journal of Neurophysiology,* 101**,** 1961-1971.

RAE, C. D., LEE, V. H. C., ORDIDGE, R. J., ALONZO, A. & LOO, C. 2013. Anodal transcranial direct current stimulation increases brain intracellular pH and modulates bioenergetics. *International Journal of Neuropsychopharmacology,* 16**,** 1695-1706.

RAMPERSAD, S. M., JANSSEN, A. M., LUCKA, F., AYDIN, U., LANFER, B., LEW, S., WOLTERS, C. H., STEGEMAN, D. F. & OOSTENDORP, T. F. 2014. Simulating Transcranial Direct Current Stimulation With a Detailed Anisotropic Human Head Model. *Ieee Transactions on Neural Systems and Rehabilitation Engineering,* 22**,** 441-452.

ROBERTS, E. 1956. Formation and utilization of Gamma-aminobutyric acid in brain. *Progress in neurobiology. 1. Neurochemistry***,** 11-25.

ROSSETTI, Y., DESMURGET, M. & PRABLANC, C. 1995. Vectorial coding of movement: vision, proprioception, or both? *J Neurophysiol,* 74**,** 457-63.

RUBIN, D. C. & WENZEL, A. E. 1996. One hundred years of forgetting: A quantitative description of retention. *Psychological Review,* 103**,** 734-760.

RUIGROK, T. J. H. & VOOGD, J. 1995. Cerebellar Influence on Olivary Excitability in the Cat. *European Journal of Neuroscience,* 7**,** 679-693.

SAMI, S., ROBERTSON, E. M. & MIALL, R. C. 2014. The Time Course of Task-Specific Memory Consolidation Effects in Resting State Networks. *Journal of Neuroscience,* 34**,** 3982-3992.

SAVIC, I., LEKVALL, A., GREITZ, D. & HELMS, G. 2000. MR spectroscopy shows reduced frontal lobe concentrations of N-acetyl aspartate in patients with juvenile myoclonic epilepsy. *Epilepsia,* 41**,** 290-6.

SCHEIDT, R. A., REINKENSMEYER, D. J., CONDITT, M. A., RYMER, W. Z. & MUSSA-IVALDI, F. A. 2000. Persistence of motor adaptation during constrained, multi-joint, arm movements. *Journal of Neurophysiology,* 84**,** 853-862.

SCHLERF, J. E., GALEA, J. M., BASTIAN, A. J. & CELNIK, P. A. 2012. Dynamic Modulation of Cerebellar Excitability for Abrupt, But Not Gradual, Visuomotor Adaptation. *Journal of Neuroscience,* 32**,** 11610-11617.

SEBASTIAN, R., SAXENA, S., TSAPKINI, K., FARIA, A. V., LONG, C., WRIGHT, A., DAVIS, C., TIPPETT, D. C., MOURDOUKOUTAS, A. P., BIKSON, M., CELNIK, P. & HILLIS, A. E. 2016. Cerebellar tDCS: A Novel Approach to Augment Language Treatment Post-stroke. *Front Hum Neurosci,* 10**,** 695.

SHABBOTT, B. A. & SAINBURG, R. L. 2010. Learning a visuomotor rotation: simultaneous visual and proprioceptive information is crucial for visuomotor remapping. *Experimental Brain Research,* 203**,** 75-87.

SHADMEHR, R. & KRAKAUER, J. W. 2008. A computational neuroanatomy for motor control. *Experimental Brain Research,* 185**,** 359-381.

SHADMEHR, R. & MUSSAIVALDI, F. A. 1994. Adaptive Representation of Dynamics during Learning of a Motor Task. *Journal of Neuroscience,* 14**,** 3208-3224.

SHADMEHR, R., SMITH, M. A. & KRAKAUER, J. W. 2010. Error Correction, Sensory Prediction, and Adaptation in Motor Control. *Annual Review of Neuroscience, Vol 33,* 33**,** 89-108.

SHEPHERD, G. M. 1994. *Neurobiology,* Oxford University Press.

SHERRINGTON, C. 1924. Problems of muscular receptivity. *Nature,* 113**,** 892-894.

SHIRER, W. R., RYALI, S., RYKHLEVSKAIA, E., MENON, V. & GREICIUS, M. D. 2012. Decoding Subject-Driven Cognitive States with Whole-Brain Connectivity Patterns. *Cerebral Cortex,* 22**,** 158-165.

SMITH, M. A., GHAZIZADEH, A. & SHADMEHR, R. 2006. Interacting adaptive processes with different timescales underlie short-term motor learning. *PLoS Biol,* 4**,** e179.

SMITH, M. A. & SHADMEHR, R. 2005. Intact ability to learn internal models of arm dynamics in Huntington's disease but not cerebellar degeneration. *Journal of Neurophysiology,* 93**,** 2809-2821.

SMITH, S. M. 2002. Fast robust automated brain extraction. *Human Brain Mapping,* 17**,** 143-155.

STAGG, C. J. 2014. Magnetic Resonance Spectroscopy as a tool to study the role of GABA in motor-cortical plasticity. *Neuroimage,* 86**,** 19-27.

STAGG, C. J., BACHTIAR, V., AMADI, U., GUDBERG, C. A., ILIE, A. S., SAMPAIO-BAPTISTA, C., O'SHEA, J., WOOLRICH, M., SMITH, S. M., FILIPPINI, N., NEAR, J. & JOHANSEN-BERG, H. 2014. Local GABA concentration is related to network-level resting functional connectivity. *Elife,* 3.

STAGG, C. J., BACHTIAR, V. & JOHANSEN-BERG, H. 2011. The Role of GABA in Human Motor Learning. *Current Biology,* 21**,** 480-484.

STAGG, C. J., BEST, J. G., STEPHENSON, M. C., O'SHEA, J., WYLEZINSKA, M., KINCSES, Z. T., MORRIS, P. G., MATTHEWS, P. M. & JOHANSEN-BERG, H. 2009. Polarity-Sensitive Modulation of Cortical Neurotransmitters by Transcranial Stimulation. *Journal of Neuroscience,* 29**,** 5202-5206.

STAGG, C. J., KNIGHT, S., TALBOT, K., JENKINSON, M., MAUDSLEY, A. A. & TURNER, M. R. 2013. Whole-brain magnetic resonance spectroscopic imaging measures are related to disability in ALS. *Neurology,* 80**,** 610-615.

STAGG, C. J. & NITSCHE, M. A. 2011. Physiological Basis of Transcranial Direct Current Stimulation. *Neuroscientist,* 17**,** 37-53.

STARK-INBAR, A., RAZA, M., TAYLOR, J. A. & IVRY, R. B. 2017. Individual differences in implicit motor learning: task specificity in sensorimotor adaptation and sequence learning. *J Neurophysiol,* 117**,** 412-428.

STEINER, K. M., ENDERS, A., THIER, W., BATSIKADZE, G., LUDOLPH, N., ILG, W. & TIMMANN, D. 2016. Cerebellar tDCS Does Not Improve Learning in a Complex

Whole Body Dynamic Balance Task in Young Healthy Subjects. *PLoS One,* 11**,** e0163598.

SUMNER, P., EDDEN, R. A., BOMPAS, A., EVANS, C. J. & SINGH, K. D. 2010a. More GABA, less distraction: a neurochemical predictor of motor decision speed. *Nat Neurosci,* 13**,** 825-7.

SUMNER, P., EDDEN, R. A. E., BOMPAS, A., EVANS, C. J. & SINGH, K. D. 2010b. More GABA, less distraction: a neurochemical predictor of motor decision speed. *Nature Neuroscience,* 13**,** 825-827.

TAYLOR, J. A., KRAKAUER, J. W. & IVRY, R. B. 2014. Explicit and Implicit Contributions to Learning in a Sensorimotor Adaptation Task. *Journal of Neuroscience,* 34**,** 3023-3032.

TKAC, I., STARCUK, Z., CHOI, I. Y. & GRUETTER, R. 1999a. In vivo 1H NMR spectroscopy of rat brain at 1 ms echo time. *Magn Reson Med,* 41**,** 649-56.

TKAC, I., STARCUK, Z., CHOI, I. Y. & GRUETTER, R. 1999b. In vivo H-1 NMR spectroscopy of rat brain at 1 ms echo time. *Magnetic Resonance in Medicine,* 41**,** 649-656.

TSENG, Y. W., DIEDRICHSEN, J., KRAKAUER, J. W., SHADMEHR, R. & BASTIAN, A. J. 2007. Sensory prediction errors drive cerebellum-dependent adaptation of reaching. *Journal of Neurophysiology,* 98**,** 54-62.

WADDELL, K. W., ZANJANIPOUR, P., PRADHAN, S., XU, L., WELCH, E. B., JOERS, J. M., MARTIN, P. R., AVISON, M. J. & GORE, J. C. 2011. Anterior cingulate and cerebellar GABA and Glu correlations measured by H-1 J-difference spectroscopy. *Magnetic Resonance Imaging,* 29**,** 19-24.

WATANABE, T., SHIINO, A. & AKIGUCHI, I. 2010. Absolute quantification in proton magnetic resonance spectroscopy is useful to differentiate amnesic mild cognitive impairment from Alzheimer's disease and healthy aging. *Dement Geriatr Cogn Disord,* 30**,** 71-7.

WEINER, M. J., HALLETT, M. & FUNKENSTEIN, H. H. 1983. Adaptation to Lateral Displacement of Vision in Patients with Lesions of the Central Nervous-System. *Neurology,* 33**,** 766-772.

WESTWOOD, S., OLSON, A., MIALL, R., NAPPO, R. & ROMANI, C. 2016. Limits to tDCS effects in language: Failures to modulate word production in healthy participants with frontal or temporal tDCS. *Cortex (in press)*.

WIETHOFF, S., HAMADA, M. & ROTHWELL, J. C. 2014. Variability in response to transcranial direct current stimulation of the motor cortex. *Brain Stimul,* 7**,** 468-75.

WILSON, M., REYNOLDS, G., KAUPPINEN, R. A., ARVANITIS, T. N. & PEET, A. C. 2011. A Constrained Least-Squares Approach to the Automated Quantitation of In Vivo H-1 Magnetic Resonance Spectroscopy Data. *Magnetic Resonance in Medicine,* 65**,** 1-12.

WOLPERT, D. M., MIALL, R. C. & KAWATO, M. 1998. Internal models in the cerebellum. *Trends in Cognitive Sciences,* 2**,** 338-347.

WOODS, A. J., ANTAL, A., BIKSON, M., BOGGIO, P. S., BRUNONI, A. R., CELNIK, P., COHEN, L. G., FREGNI, F., HERRMANN, C. S., KAPPENMAN, E. S.,

KNOTKOVA, H., LIEBETANZ, D., MINIUSSI, C., MIRANDA, P. C., PAULUS, W., PRIORI, A., REATO, D., STAGG, C., WENDEROTH, N. & NITSCHE, M. A. 2016. A technical guide to tDCS, and related non-invasive brain stimulation tools. *Clinical Neurophysiology,* 127**,** 1031-1048.

XU, S., YANG, J. H., LL, C. Q., ZHU, W. J. & SHEN, J. 2005. Metabolic alterations in focally activated primary somatosensory cortex of alpha-chloralose-anesthetized rats measured by H-1 MRS at 11.7 T. *Neuroimage,* 28**,** 401-409.

YAMAMOTO, K., HOFFMAN, D. S. & STRICK, P. L. 2006. Rapid and long-lasting plasticity of input-output mapping. *Journal of Neurophysiology,* 96**,** 2797-2801.

YOON, K. J., LEE, Y. T., CHAE, S. W., PARK, C. R. & KIM, D. Y. 2016. Effects of anodal transcranial direct current stimulation (tDCS) on behavioral and spatial memory during the early stage of traumatic brain injury in the rats. *Journal of the Neurological Sciences,* 362**,** 314-320.

ZHANG, Y. Y., BRADY, M. & SMITH, S. 2001. Segmentation of brain MR images through a hidden Markov random field model and the expectation-maximization algorithm. *Ieee Transactions on Medical Imaging,* 20**,** 45-57.